



Multistability and Transient Dynamics in Networked Systems

Der Fakultät für Mathematik & Naturwissenschaften
der Carl von Ossietzky Universität Oldenburg
zur Erlangung des Grades und Titels
Doktor der Naturwissenschaften (Dr. rer. nat.)
angenommene Dissertation

von

Kalel Luiz Rossi

geboren am 13.10.1997 in Curitiba, Parana, Brasilien

Gutachter: Prof. Dr. Ulrike Feudel

Gutachter: Prof. Dr. Klaus Lehnertz

Tag der Disputation: 24.01.2025

Muss es sein? Es muss sein!

- Ludwig van Beethoven
The Unbearable Lightness of Being, Milan Kundera

At least it's flat and green.

- Popular wisdom
Common motivational mantra

Contents

List of Publications	4
Abstract	6
Zusammenfassung	8
1 Introduction	10
2 Methodology	17
2.1 Basics of dynamical systems theory	17
2.1.1 Dynamical systems and the uniqueness and existence of their solutions	17
2.1.2 The fate of linear dynamical systems	17
2.1.3 The fate of nonlinear dynamical systems I: attractors	18
2.1.4 Formalizing attractors and basins	21
2.1.5 Invariant manifolds: structures that organize state space	22
2.1.6 The fate of nonlinear dynamical systems II: multistability and basins of attraction	25
2.1.7 How to find attractors	25
2.2 Basics of bifurcations	28
2.2.1 Saddle-node bifurcation of equilibria	29
2.2.2 Hopf bifurcation	29
2.2.3 Homoclinic bifurcation	31
2.3 Basics of Network Theory	32
2.4 Basics of Kuramoto oscillators	33
2.4.1 Derivation of the model and transition to synchronization	33
2.4.2 Multistability in homogeneous case: twisted states	35
3 Small changes at single nodes can shift global network dynamics	38
3.1 Introduction	38
3.2 Methodology	40
3.3 Results	42
3.3.1 Introduction to dynamical malleability	42
3.3.2 Comprehensive view of dynamical malleability	44
3.3.3 Unpredictability of dynamical malleability	47
3.3.4 Ratio of short to long-range connections	48
3.3.5 Multistability	49
3.3.6 Distributions of samples	53
3.4 Discussions and conclusions	55
4 Transients versus network interactions give rise to multistability through trapping mechanism	66
4.1 Introduction	66
4.2 Methods	68
4.2.1 Model	68
4.2.2 Numerical algorithms	69
4.3 Results	71

4.3.1	Rich multistability of oscillations with 10 units	71
4.3.2	Emergence of attractors in a two-unit network	74
4.3.3	Bifurcations giving rise to the attractors	75
4.3.4	Emergence of oscillations through reinjection mechanism	77
4.4	Discussions	80
5	Dynamical properties and mechanisms of metastability	87
5.1	Introduction	87
5.2	Short summary of metastability in the brain	88
5.2.1	Observations of metastability	88
5.2.2	Current formulations of metastability	90
5.2.3	The common thread	92
5.3	Metastability in state space	92
5.3.1	Stability and invariance - initial concepts	92
5.3.2	Metastability and almost-invariance - definition	93
5.3.3	Dynamics-based mechanisms for metastability	95
5.3.4	Subtypes of metastability	100
5.4	Conclusions and outlook	100
6	Conclusions	105
Acknowledgments		133

List of Publications

This dissertation is based on the following publications:

Chapter 2.1.7: George Datseris, Kalel L. Rossi, and Alexandre Wagemakers. Framework for global stability analysis of dynamical systems. *Chaos* **33**, 073151 (2023).

Statement of authorship:

George Datseris: Conceptualization (lead); Investigation (equal); Formal analysis (equal); Software (equal); Visualization (lead); Writing – original draft (equal); Writing – review & editing (equal).

Kalel Luiz Rossi: Conceptualization (equal); Formal analysis (equal); Software (equal); Visualization (equal); Writing – original draft (equal); Writing – review & editing (equal).

Alexandre Wagemakers: Conceptualization (equal); Formal analysis (equal); Software (equal); Writing – original draft (equal); Writing – review & editing (equal).

Chapter 3: Kalel L. Rossi, Roberto C. Budzinski, Bruno R. R. Boaretto, Lyle E. Muller, and Ulrike Feudel. Small changes at single nodes can shift global network dynamics. *Physical Review Research* **5**, 013220 (2023).

Statement of authorship:

Kalel Luiz Rossi: Conceptualization (equal); Investigation (lead); Formal analysis (lead); Software (lead); Visualization (lead); Writing – original draft (lead); Writing – review & editing (lead).

Roberto C. Budzinski: Conceptualization (equal); Investigation (equal); Formal analysis (equal); Writing – original draft (equal); Writing – review & editing (equal).

Bruno R. R. Boaretto: Conceptualization (equal); Investigation (equal); Formal analysis (equal); Writing – original draft (equal); Writing – review & editing (equal).

Lyle E. Muller: Conceptualization (equal); Investigation (equal); Formal analysis (equal); Writing – review & editing (equal).

Ulrike Feudel: Conceptualization (equal); Investigation (equal); Formal analysis (equal); Writing – original draft (equal); Writing – review & editing (equal); Supervision (lead).

Chapter 4: Kalel L. Rossi, Everton S. Medeiros, Peter Ashwin and Ulrike Feudel. Transients versus network interactions give rise to multistability through trapping mechanism. In preparation.

Statement of authorship:

Kalel Luiz Rossi: Conceptualization (equal); Investigation (lead); Formal analysis (lead); Software (lead); Visualization (lead); Writing – original draft (lead); Writing – review & editing (lead).

Everton S. Medeiros: Conceptualization (equal); Investigation (equal); Formal analysis (equal); Writing – original draft (equal); Writing – review & editing (equal).

Peter Ashwin: Investigation (supporting); Formal analysis (equal); Writing – review & editing (equal).

Ulrike Feudel: Conceptualization (equal); Investigation (equal); Formal analysis (equal); Writing – original draft (equal); Writing – review & editing (equal); Supervision (lead).

Chapter 5: Kalel L. Rossi, Roberto C. Budzinski, Everton S. Medeiros, Bruno R. R. Boaretto, Lyle E. Muller, and Ulrike Feudel. Dynamical properties and mechanisms of metastability: a perspective in neuroscience. *Physical Review E*. Accepted.

Statement of authorship:

Kalel Luiz Rossi: Conceptualization (equal); Investigation (lead); Formal analysis (lead); Software (lead); Visualization (lead); Writing – original draft (lead); Writing – review & editing (lead).

Roberto C. Budzinski: Conceptualization (equal); Investigation (equal); Formal analysis (equal); Writing – original draft (equal); Writing – review & editing (equal).

Everton S. Medeiros: Conceptualization (equal); Investigation (equal); Formal analysis (equal); Writing – original draft (equal); Writing – review & editing (equal).

Bruno R. R. Boaretto: Conceptualization (equal); Investigation (equal); Formal analysis (equal); Writing – original draft (equal); Writing – review & editing (equal).

Lyle E. Muller: Conceptualization (equal); Investigation (supporting); Formal analysis (supporting); Writing – review & editing (equal).

Ulrike Feudel: Conceptualization (equal); Investigation (equal); Formal analysis (equal); Writing – original draft (equal); Writing – review & editing (equal); Supervision (lead).

On top of these main thesis papers, I have also collaborated in other works, which resulted in two further publications, with me as a co-author. They are not included in this thesis.

- Bruno R. R. Boaretto, Roberto C. Budzinski, Kalel L. Rossi, Thiago L. Prado, Sergio R. Lopes and Cristina Masoller. Temporal Correlations in Time Series Using Permutation Entropy, Ordinal Probabilities and Machine Learning. *Entropy* **23**, 1025 (2021).
- Bruno R.R. Boaretto, Roberto C. Budzinski, Kalel L. Rossi, Cristina Masoller, Elbert E.N. Macau. Spatial permutation entropy distinguishes resting brain states. *Chaos, Solitons and Fractals* **171**, 113453 (2023).

Abstract

Many systems in nature and in theory exhibit emergent behavior, where relatively simple parts interact to create a complex global behavior that is not present in any of the parts alone. Many dynamical systems with emergent behavior can be modeled as networks, in which individual units interact with each other along specified connections. An important phenomenon that can be emergent is multistability, the coexistence of many stable solutions - attractors - in a dynamical system with fixed parameters. Multistability is observed, for instance, in power grids, brain circuits, and ecological networks. This has important consequences: a multistable system operating on a particularly desirable attractor may not be safe, as a perturbation in the state of the system can cause it to switch to another coexisting attractor. On the other hand, coexistence of attractors may be useful for systems performing computations such as memory. Multistability can arise from the interactions of the multiple subunits, but the specific mechanisms that generate it are not fully known. It can also coexist with another emergent phenomenon in networked systems: synchronization, in which the interactions between units cause them to adjust their rhythms toward a collective motion. For instance, frequency synchronization occurs when units with different natural frequencies lock their oscillations onto a common frequency. The phases of their oscillations may also cluster together, in a phenomenon called phase synchronization. Synchronized attractors can coexist with each other and with unsynchronized attractors. In this case, understanding the robustness of the attractors becomes relevant - for instance, the attractor with frequency synchronization is required for proper operation of power grids, and switching to an undesired attractor may correspond to a blackout.

After introducing the fundamental theoretical concepts (Chapter 2), we move to the first work in the thesis (Chapter 3), which studies networks of Kuramoto oscillators with heterogeneous frequencies, a paradigmatic model for studies on synchronization and dynamics of complex networks. By increasing the strength of the inter-unit coupling and by adjusting the topology of connections in the network, these systems display a transition toward phase synchronization. Furthermore, near this transition the networks become highly sensitive to changes in parameters of individual components, such that even changes to single units can alter the dynamics of the entire network. We say that the networks attain a high dynamical malleability and show that this increase in the malleability is due to two effects: increase in sample-to-sample fluctuations near a phase transition and multistability. This work therefore contributes to our understanding of robustness of complex networks, in particular how their malleability and multistability depend on their topology.

In the second work of this thesis (Chapter 4), we focus deeper on mechanisms for multistability, and investigate a network of diffusively coupled excitable neurons. Separately, a unit has only one attractor, a stable equilibrium. Before reaching this attractor, however, some trajectories in the unit's state space must go through long excursions (excitations) along an excitability region. Although the units separately do not have oscillations, we show that a rich variety of stable oscillations can emerge and coexist in the coupled networks. Two coupled units can already have multiple coexisting attractors, with periodic or quasiperiodic oscillations. Going to ten coupled units many more attractors can emerge, including a chaotic attractor. We uncover the bifurcations giving rise to these attractors, and explain the qualitative mechanism behind them. We show that the coupling between the units interacts with the excitability region of their

state space and manages to repeatedly reinject them there, where they stay effectively trapped. This serves as a simple yet powerful mechanism for the creation of multistability in networks, and provides insights into how the topology of networks affects their multistability.

Interestingly, the attractors in the previous case arise due to the interaction with the transient dynamics of the units, in the excitability region. Transient dynamics can also play important roles more broadly. In particular, long-lived transients are a ubiquitous behavior in neural activity. In this context, the third work in this thesis (Chapter 5) provides a general conceptual framework for long-lived transients. Looking at the neuroscience literature, we argue that long-lived transients are the key concept behind metastability, a term that is often used without a clear definition. We use the concept of almost-invariant regions - sets in state space wherein trajectories stay for a long time before leaving - and argue that metastable regimes in time correspond to trajectories visiting an almost-invariant region in state space. With this, we identify general dynamical properties of metastability. Then, we discuss many mechanisms that can generate metastability, and provide a classification of subtypes of metastability, which neatly includes previous works in the literature. Our hope is that this framework aids future research in neuroscience, and even other areas in which metastability occurs, such as climate science.

Finally, this thesis also describes a work (Chapter 2.1.7) developing and implementing state-of-the-art algorithms for finding attractors and their basins of attraction, including the possibility to do so in a continuation scenario over a parameter range. These algorithms were used throughout the thesis, and are available in an efficient open-source package for studying dynamical systems.

Zusammenfassung

Viele Systeme in der Natur und in der Theorie weisen ein emergentes Verhalten auf, bei dem relativ einfache Teile interagieren, um ein komplexes Gesamtverhalten zu erzeugen, das in keinem der Teile allein vorhanden ist. Viele dynamische Systeme mit emergentem Verhalten können als Netzwerke modelliert werden, in denen einzelne Einheiten entlang bestimmter Verbindungen miteinander interagieren. Ein wichtiges Phänomen, das emergent sein kann, ist die Multistabilität, die Koexistenz vieler stabiler Lösungen - Attraktoren - in einem dynamischen System mit festen Parametern. Multistabilität wird zum Beispiel in Stromnetzen, Gehirnschaltungen und ökologischen Netzwerken beobachtet. Dies hat wichtige Konsequenzen: Ein multistabiles System, das auf einem besonders wünschenswerten Attraktor arbeitet, ist möglicherweise nicht sicher, da eine Störung des Systemzustands dazu führen kann, dass es zu einem anderen koexistierenden Attraktor übergeht. Andererseits kann die Koexistenz von Attraktoren für Systeme, die Berechnungen durchführen, z. B. für den Speicher, nützlich sein. Multistabilität kann durch die Interaktion mehrerer Untereinheiten entstehen, aber die spezifischen Mechanismen, die sie erzeugen, sind nicht vollständig bekannt. Sie kann auch mit einem anderen emergenten Phänomen in vernetzten Systemen koexistieren. Dies ist die Synchronisation, bei der die Interaktionen zwischen den Einheiten dazu führen, dass sie ihre Rhythmen auf eine kollektive Bewegung ausrichten. Frequenzsynchronisation tritt zum Beispiel auf, wenn Einheiten mit unterschiedlichen Eigenfrequenzen ihre Schwingungen auf eine gemeinsame Frequenz abstimmen. Auch die Phasen ihrer Schwingungen können sich aneinander angleichen, was als Phasensynchronisation bezeichnet wird. Synchronisierte Attraktoren können miteinander und mit unsynchronisierten Attraktoren koexistieren. In diesem Fall ist es wichtig, die Robustheit der Attraktoren zu verstehen - beispielsweise ist der Attraktor mit der Frequenzsynchronisation für den ordnungsgemäßen Betrieb von Stromnetzen erforderlich, und ein Wechsel zu einem unerwünschten Attraktor kann zu einem Stromausfall führen.

Nach einer Einführung in die grundlegenden theoretischen Konzepte (Kapitel 2) wenden wir uns zur ersten Arbeit in dieser Dissertation (Kapitel 3), die Netzwerke von Kuramoto-Oszillatoren mit heterogenen Frequenzen untersucht, ein paradigmatisches Modell für Studien über Synchronisation und Dynamik komplexer Netzwerke. Wenn man die Stärke der Kopplung zwischen den Einheiten erhöht und die Topologie der Verbindungen im Netzwerk anpasst, zeigen diese Systeme einen Übergang zur Phasensynchronisation. Darüber hinaus reagieren die Netze in der Nähe dieses Übergangs sehr empfindlich auf Änderungen der Parameter einzelner Komponenten, so dass selbst Änderungen an einzelnen Einheiten die Dynamik des gesamten Netzes verändern können. Wir sagen, dass die Netzwerke eine hohe dynamische Formbarkeit erreichen, und zeigen, dass dieser Anstieg der Formbarkeit auf zwei Effekte zurückzuführen ist: Zunahme der Fluktuationen von Probe zu Probe in der Nähe eines Phasenübergangs und Multistabilität. Diese Arbeit trägt daher zu unserem Verständnis der Robustheit komplexer Netzwerke bei, insbesondere dazu, wie ihre Formbarkeit und Multistabilität von ihrer Topologie abhängen.

In der zweiten Arbeit dieser Dissertation (Kapitel 4) befassen wir uns eingehender mit den Mechanismen der Multistabilität und untersuchen ein Netzwerk aus diffus gekoppelten erregbaren Neuronen. Für sich genommen hat eine Einheit nur einen Attraktor, ein stabiles Gleichgewicht. Bevor sie jedoch diesen Attraktor erreicht, müssen einige Trajektorien im Zustandsraum der Einheit lange Exkursionen (Erregungen) entlang einer

Erregbarkeitsregion durchlaufen. Obwohl die Einheiten für sich genommen keine Oszillationen aufweisen, zeigen wir, dass in den gekoppelten Netzwerken eine Vielzahl stabiler Oszillationen entstehen und koexistieren können. Zwei gekoppelte Einheiten können bereits mehrere koexistierende Attraktoren mit periodischen oder quasiperiodischen Schwingungen aufweisen. Bei zehn gekoppelten Einheiten können noch viel mehr Attraktoren auftreten, einschließlich eines chaotischen Attraktors. Wir decken die Bifurkationen auf, die zu diesen Attraktoren führen, und erklären den qualitativen Mechanismus dahinter. Wir zeigen, dass die Kopplung zwischen den Einheiten mit der Erregbarkeitsregion ihres Zustandsraums interagiert und es schafft, sie immer wieder dorthin zurückzubringen, wo sie effektiv gefangen bleiben. Dies ist ein einfacher, aber wirkungsvoller Mechanismus für die Erzeugung von Multistabilität in Netzwerken und gibt Aufschluss darüber, wie die Topologie von Netzwerken deren Multistabilität beeinflusst.

Interessanterweise entstehen die Attraktoren im vorgenannten Fall durch die Interaktion mit der transienten Dynamik der Einheiten in der Erregbarkeitsregion. Die transiente Dynamik kann auch im weiteren Sinne eine wichtige Rolle spielen. Insbesondere langlebige Transienten sind ein allgegenwärtiges Verhalten bei neuronaler Aktivität. In diesem Zusammenhang liefert die dritte Arbeit in dieser Dissertation (Kapitel 5) einen allgemeinen konzeptionellen Rahmen für langlebige Transienten. Mit Blick auf die neurowissenschaftliche Literatur argumentieren wir, dass langlebige Transienten das Schlüsselkonzept hinter der Metastabilität sind, ein Begriff, der oft ohne klare Definition verwendet wird. Wir verwenden das Konzept der nahezu unveränderlichen Regionen - Mengen im Zustandsraum, in denen sich Trajektorien lange Zeit aufhalten, bevor sie diese verlassen - und argumentieren, dass metastabile Regime in der Zeit Trajektorien entsprechen, die eine nahezu unveränderliche Region besuchen.

Chapter 1

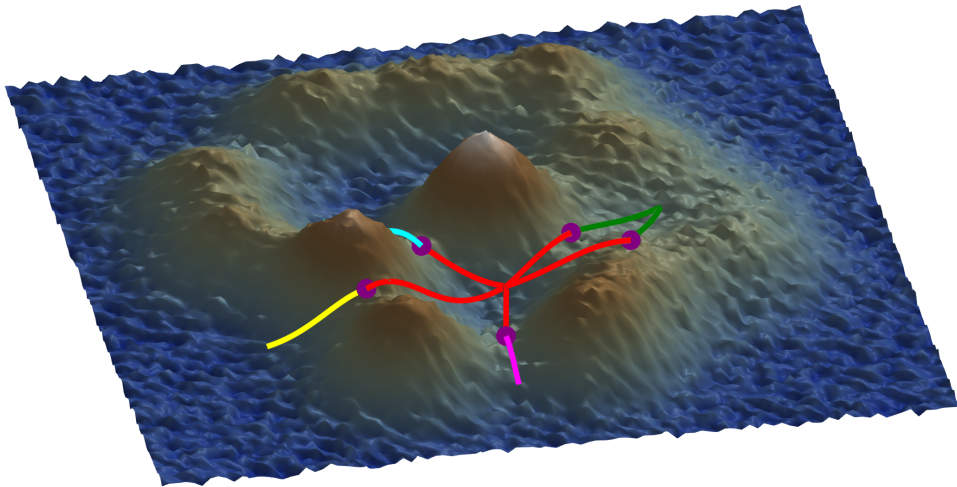
Introduction

Consider the unfortunate situation of falling down a mountain. Subject to the inexorable effect of gravity and friction, the hiker will roll downhill until they reach a certain valley, a spot at which they will finally terminate their unlucky dynamics. This final state is called an attractor, and the preceding rolling period is called a transient. Now, consider a landscape like the one in Fig. 1.1A. The mountain has several valleys, separated by peaks. An example of this separation is shown in Fig. 1.1B. Consider then the even more unfortunate situation of *two* people falling down a mountain. If they start very close together, on the same side of a peak, they will fall down to the same valley. If, however, they were separated by a peak when the fall started, then they will fall into distinct valleys. This is shown by the red trajectories, which converge onto the same attractor, and the other trajectories, that converge to different attractors in Figs. 1.1A-B. Again, each valley is an attractor. Which attractor the person falls into depends on their initial condition. If we consider this particular example to be a mechanical system with inertia, the initial condition corresponds to the person's initial position and velocity. In general, all initial conditions that lead to the same attractor form a set called the basin of attraction of that attractor. All the red trajectories in Fig. 1.1A belong to the same basin. Trajectories are typically separated by peaks in the landscape (green and red of Fig. 1.1B), so the peaks usually form the boundaries between basins of attraction.

The example of the hiking disaster serves as a good introduction to the notion of *multistability* - the simultaneous coexistence of different ending states, different attractors, in a dynamical system with constant parameters (notice that the mountain landscape does not change in time in the example!). This phenomenon is present in a wide variety of notable systems, with important real-world consequences [1, 2, 3]. In biology, multistability can explain how genetically identical cells can exist in multiple metabolically distinct stable states [4, 5]. Similarly, there has been evidence, and models, suggesting that multistability in the gut microbiome can explain microbiome shifts, which are changes in the composition of the microbiome in the gut [6]. On a technological side, power grids - networks of connected generators and consumers of electrical energy - need to operate on an attractor in which all units have their frequencies of oscillation synchronized in the 50-60Hz range [7]. Multistability in the grids can be dangerous, as perturbations can switch the system out of the operating state, potentially leading to blackouts. Modelling studies try to look for conditions that make the desired state as stable as possible [7, 8]. Multistability can also be a powerful mechanism in brain dynamics. Some models for long-term memory consider that each memory corresponds to an attractor in the system [9, 10], and some models of large-scale brain dynamics exhibit multistability [11]. There are many more examples of multistability, such as in artificial neural networks [12], models for ice sheets [13], mechanical systems [14], and in tissue repair [15].

The examples in neural networks and power grids in particular highlight the ubiquitous presence of multistability in networked systems - systems formed by the interactions of smaller subunits, such as neurons or electric generators. Another phenomenon in networks that can coexist with multistability is *synchronization* [16, 17]. Often the interaction between units of a network can cause them to adjust their individual rhythms

A



B

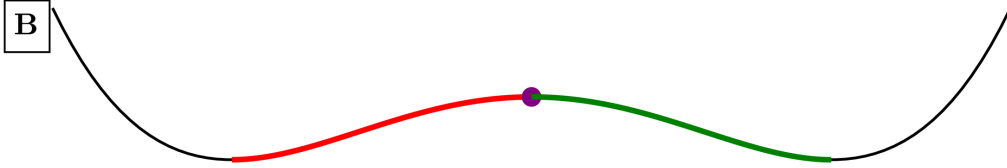


Figure 1.1: **Landscape with valleys and peaks constitutes an example of multistability for an unfortunate falling person.** Panels A and B respectively show a 3D and 2D example of a landscape, with red trajectories converging onto the same attracting region, and trajectories with other colors, which start next to the red trajectories but on the other side of the peak, converging onto other attracting regions.

toward a collective motion, in which their activity becomes similar in some sense [16]. In this case, the network is said to be synchronized. There are many types of synchronization, which can be defined based on what “similar” and “activity” are taken to mean. Three important properties that characterize the state of an oscillation at a certain time are the amplitude, phase, and angular frequency at that time. Roughly, the amplitude describes how high or how low the oscillation itself is; the phase describes the current position of the oscillation along its oscillation cycle; and the angular frequency describes how fast the phase itself is moving [16]. In many applications, the amplitudes of the oscillations turn out to not play a major role [16, 18]. For instance, if the coupling between the units is weak enough, the amplitudes of their oscillations are not particularly altered, but the phases are [16, 19]. When units adjust their individual frequencies to the same value, i.e. when they spontaneously lock onto a common frequency, they become frequency synchronized (also called phase-locked) [16, 19]. One technically relevant example has been mentioned before for power grids, in which all the units must have their

frequencies synchronized at the same value, such as 50 Hz [7]. In some cases, the phases of the oscillations may also converge onto a common value. Then, the units are phase-locked and their phases converge to similar values. This is called *phase synchronization*. It has been proposed as an important mechanism for communication and exchange of information between brain circuits [20, 21, 22]. Interestingly, lack of phase synchrony can also play an important role, e.g. in the flight pattern of fruit flies [23].

The real-world relevance of such systems has stimulated a lot of research into their dynamics [1]. An approach taken by several works has been to study simple models that capture some essential properties of real world systems. A particularly important example, which has become paradigmatic in the synchronization literature, is that of Kuramoto oscillators (see Sec. 2.4). They constitute quite a beautiful example of how units with very simple dynamics can generate complex behavior when interacting together. Each unit in the model is described by a phase (angle) variable that by itself just varies linearly according to its own natural frequency. The interesting dynamics comes from the nonlinear coupling, done via the sine of the phase difference between coupled units, cf. Eq. 2.29. The model is simple enough to allow for analytic treatment but still complex enough to show relevant dynamics [19, 24]. In particular, when the units have heterogeneous natural frequencies, the model exhibits a continuous phase transition from desynchronization to frequency and phase synchronization as the strength of the inter-unit coupling is increased. Roughly, if the natural frequencies are spread too widely compared to the coupling between them, the units oscillate incoherently; if instead the coupling becomes large enough, the units start to oscillate with the same frequency - they become phase-locked. As the coupling increases, the phases also become more clustered together, although complete phase synchronization does not occur.

The Kuramoto model is also generic in the sense that it can be derived as an approximation of general limit cycle oscillators under weak coupling [17]. In this case, one considers units that oscillate on a periodic orbit. If the coupling between the units is weak enough, the amplitude of their oscillation is not significantly affected, only the phase along the limit cycle. Then, the interplay between the differences in frequency and the coupling determines the time evolution of the phases. The Kuramoto model is a somewhat more specific case of this phase reduction, in that one chooses a purely sinusoidal coupling [19]. Still, the combination of simplicity and complexity leading to a synchronization transition, and this argument of genericity, incited a lot of research and inspired new concepts [24, 25, 19].

This also inspired us to translate results we had from spiking neural networks [26]. In those networks we described a phenomenon we called *dynamical malleability*, the sensitivity of a whole network's dynamics to changes in parameters of single components, usually changes in parameters of single units. Similarly to the Kuramoto oscillator networks, the spiking neural networks we studied also present a transition to synchronization, in particular to phase synchronization, when the coupling strength is increased. They also present a transition to synchronization as the topology changes: as the connections in the system are rewired from being restricted only to k -nearest neighbors to being randomly allocated, the neurons also start to synchronize their phases. Types of topologies are described in more detail in Sec. 2.3. In the neighborhood of both of these transitions, we showed that the network's dynamical malleability increases considerably. As we see in Chap. 3, this phenomenology generalizes for Kuramoto networks with heterogeneous frequencies. In fact, it can be quite intense: changing the parameter of a single unit can drastically alter the behavior of the whole network in a very sensitive manner [27],

which was until then not known.

In the literature for Kuramoto oscillators, the phenomenon of dynamical malleability has been studied from the point of view of statistical mechanics [28, 29]. Changing the parameters of a single unit leads to a different network, which is termed to be a different sample. The finite size of the networks leads to an approximate phase transition whose critical parameter varies depending on the sample [28]. Therefore, near this phase transition the *sample-to-sample (STS) fluctuations* increase. The studies on this subject did not, however, look closely at the dynamics of these finite networks. One work that looks at this more closely for all-to-all topologies was Ref. [30], where the authors propose that the kurtosis of the natural frequency distribution correlates with the critical coupling strength of the transition. Therefore, changing the frequency of the units changes the kurtosis and thus changes the critical coupling strength. However, they did not explore how this also interacted with more complex topologies. As we show in our work, their mechanism alone does not explain the malleability we describe: networks with shuffled natural frequencies have the same kurtosis but still can vary significantly. In our work, we therefore complement these studies by looking at the dynamics behind the malleable networks, and show that indeed the sample-to-sample fluctuations are a key effect leading to malleability. But we also show that another important effect comes from multistability, which is another behavior we analyzed.

We looked at *multistability* in the networks as a function of the coupling strength and topology, and showed the emergence of a large number of coexisting attractors at the transition to phase synchronization [27]. This therefore means that the networks we studied are very sensitive to perturbations in the state variables (which can lead the system to switch to other attractors, due to multistability) and in the parameters (which can change the attractor considerably, due to malleability). This was another contribution from our work. Naturally, there have been studies on multistability in Kuramoto networks. In the case of heterogeneous frequencies, Tilles et al. studied multistability arising in nearest-neighbor rings [31]. In a related Kuramoto model, which has an inertial term, some studies have shown the coexistence of multiple attractors in random topologies [32], and in power grid topologies [7, 8]. Ref. [33] looks at how properties of power grid topologies relate to the dynamics of first-order Kuramoto models, but do not report multistability.

Multistability has been studied in detail for units with *homogeneous frequencies* (which are then identical) and which are coupled in k -nearest-neighbor topologies. In this case, the network can be written as a gradient system, meaning its only attractors are equilibria, which are single points in state space (cf., Secs. 2.1.2-2.1.3). This considerably simplifies their study. The networks can have multiple stable equilibria, each being characterized by neighboring units having a fixed and constant phase relationship. These equilibria are called twisted states [34], and their stability depends on the relationship between the number of nearest neighbors k and the size N of the network [34] - see Sec. 2.4.2 for more. For these networks, there have been studies looking at the effect of the topology [35], showing a minimum coupling strength that guarantees complete synchronization globally. Another important contribution has looked at the basins of attraction for these networks: Zhang and Strogatz have shown that the basins behave like octopuses - the head of the octopus contains the attractor, an equilibrium. The head is relatively small compared to the tentacles: most of the volume of the basins is not concentrated around the equilibrium, but spread around in tentacle-like structures in state space [36].

In both the case of heterogeneous and of homogeneous frequencies, we are unaware of any systematic study on the emergence of multistability and effect of changing topology, in particular for first-order Kuramoto models. Our work serves also as a step in this direction, but more research is needed.

In general, the mechanisms that give rise to multistability in networks are still not fully understood. In particular, during my PhD we started to study multistability in a network of bursting neurons coupled diffusively, looking to explain results from previous publications [37]. The neurons, which follow the Hindmarsh-Rose equations [38], have individually a stable periodic orbit as an attractor. By changing parameters of the neurons, one can make a certain region of this periodic orbit very slow, but without going through a bifurcation. Preliminary results showed that multistability only emerges in the coupled networks when the neurons have this slow region. To better understand this, we looked at a simpler conductance-based neuronal model [39] which also has regions of slow flow. We focused on the case when this model has excitable dynamics. The isolated neuron then has only one attractor, a stable equilibrium. And it also has two unstable equilibria, which force some trajectories to go on long excursions before converging to that attractor. These excursions are called excitations, and correspond to the neuron spiking. One of these unstable equilibria also slows down trajectories passing near it. By coupling two such neurons diffusively we show the emergence of different types of oscillating attractors, which can all coexist. We show the bifurcations giving rise to these attractors. Furthermore, we describe a qualitative mechanism for how they occur. The idea is that the diffusive coupling acts to repeatedly reinject the trajectories of each neuron into the region responsible for the excitations, thereby effectively *trapping the trajectories in the previously transient region* - see Chap. 4 for more. The slowness near one the equilibria plays an important role in this mechanism, which might help to explain the behavior of the bursting network we started with. For two units, it can happen that both are trapped in this excitability region, or just one is, generating in total three possible combinations. For more units, the number of possible combinations increases, and therefore so does the number of coexisting attractors. The units oscillate in all emerging attractors, and can do so periodically, quasiperiodically, or chaotically - despite them separately having only equilibria! This mechanism is also a simple example of how coupling can interact with transients to generate attractors, an idea that has been studied in the literature under different circumstances. In particular, Medeiros et al. studied units which have a periodic attractor and a chaotic saddle, an unstable chaotic set, in their state space [40, 41]. They showed that diffusive coupling between them can counteract the divergence tendency near the chaotic saddle, effectively trapping the units in its neighborhood, and creating a chaotic attractor which coexists with the units' periodic attractor [40, 41]. However, the authors did not observe multiple attractors emerging from the trapping in the chaotic saddle. Therefore, the coupled excitable neurons, with their trapping mechanism, constitutes a simple yet powerful mechanism for generating a rich multistability in networks, which had not been described previously in the literature, to our knowledge.

This line of investigation on multistability also contributes to the study of how oscillations arise in non-oscillating units interacting via diffusive coupling. As discussed in Chap. 4, this line of work has a rich history, with an early work by Smale showing that Hopf bifurcations can give rise to oscillations [42] - see Sec. 2.2 for bifurcations. Later works showed the possibility of chaos, and also the emergence of multistability in repulsive coupling. Our contribution in this case has been to show a rich multistability,

with the possible coexistence of periodic, quasiperiodic, and also chaotic solutions - with repulsive or attracting coupling.

These studies on multistability require efficient and reliable algorithms to identify the coexisting attractors of a system. To this end, I have contributed to creating *Attractors.jl*, an open-source package in the Julia programming language that collects such algorithms. In particular, George Datseris and Alexander Wagemakers had already introduced an algorithm to find attractors based on recurrences in state space [43], from an idea by Nusse and Yorke [44]. I then contributed to implementing and refining another algorithm, proposed in Refs. [45, 32], based on finding attractors by grouping trajectories with similar features. These algorithms are described more in Sec. 2.1.7. Together with Datseris and Wagemakers, we built a continuation framework that allows one to use either of these two methods across a parameter range. This idea is similar to linear continuation analysis, but generalizes to any type of attractor, including chaotic attractors. This led to a joint publication [46]. On top of the novelty of the continuation algorithm, and the improvements made to the state-of-the-art algorithms for finding attractors, our contribution here was also to provide a package that is free and easy to use.

Going back now to the excitable neurons, the multistability seen there is remarkable: stable states arise from the interaction with transient behavior (the excitations). Often in the literature we are preoccupied with the final states of the system - usually justifiably so - but anyone who asks the falling hikers in our initial example will probably find out that transients should not be disregarded so easily. In particular for neuroscience, transient dynamics has been the object of a lot of recent work. For instance, transients can be harnessed to perform computations [47], particularly when they are long-lived [48]. Ref. [48] proposes that long-lived transients, particularly in the form of ghosts of saddle-node bifurcations, offer some distinct computational advantages, such as maintaining a dynamical memory of a signal. See Sec. 2.2 for more on ghosts. For instance, Ref. [49] studied a simple model for how cells respond to changing chemical signals and use them to move. Without any signal, the cell operates on a stable equilibrium. A signal causes a saddle-node bifurcation that leads it to another stable equilibrium. As the signal is removed, the inverse bifurcation happens, and the cell eventually converges back to the original equilibrium. But before returning, the cell stays for a while visiting the ghost of the second equilibrium. Biologically, this means that the cell keeps the memory of the signal for a while [49, 48]. Indeed, long-lived transients, such as the ghosts, are a ubiquitous phenomenon observed in neural activity [50, 51], and are often referred to as *metastable*. One interesting example comes from studies measuring how mice encode for tastants fed to them. The study measured the firing rate activity in the gustatory cortex of the mice as a response to different tastants [52]. They identified that the stimulus elicits a sequence of distinct long-lived but transient regimes. By regime here we mean an epoch of the time series with some unique properties - in their case, the configuration of the average firing rate across the ensemble of neurons. Each tastant evoked a specific sequence of such metastable regimes. The duration of these regimes varies across trials, but the sequence itself is consistent [53, 51].

Delving into the metastability literature, we found that a general conceptual framework in neuroscience was lacking. First, the very definition of metastability varied between works, leading to apparent inconsistencies, as explained in more details in Chap. 5. Second, the mechanisms proposed for metastability also varied. Some works propose ghost of saddle-node bifurcations [50] while others propose noise [51], with few works

attempting to compare different proposals [54]. In our work, we drew from tools of dynamical systems theory to provide such a conceptual framework. We provide a simple definition of metastable regimes as long-lived transients, which encompasses the majority of previous works not only in neuroscience, but also dynamical systems and even ecology. Previous inconsistencies between works can be neatly fit into distinct subtypes of metastability - for instance, when transitions between metastable regimes are spontaneously or externally driven. Then we use this definition to study general properties of metastability, making use of the concept of almost-invariant sets [55, 56]. We argue that metastable regimes in time correspond in state space to almost-invariant sets, regions in which trajectories tend to stay for long, but not infinitely long. We also propose several dynamical mechanisms that can generate metastable regimes. Importantly, we connect these dynamical mechanisms to previous literature in neuroscience, complementing the discussions there.

Taking all of this together, my PhD has been a journey into studying the long-term and the transient dynamics of networked systems - how multistability can emerge and how it affects their robustness - and how long transients (metastability) can arise. This thesis describes this journey and will hopefully reflect the excitement of doing all of this research. In Chap. 2 I introduce in greater depth the fundamental concepts needed for the studies performed in this thesis. These will then follow in Chaps. 3, 4 and 5 in the same order introduced here. Finally, in Chap. 6 I will take all of these results together and reflect on what we learned, what our contributions have been to the literature, and the open questions that lie ahead in the future.

Chapter 2

Methodology

2.1 Basics of dynamical systems theory

2.1.1 Dynamical systems and the uniqueness and existence of their solutions

In this thesis we study dynamical systems described by a state variable $x = (x_1, x_2, \dots, x_n)^T \in M$, where $M \subseteq \mathbb{R}^n$ is the state space, and T denotes the transpose operation. The state variable is a point in this n-dimensional state space. In a continuous-time dynamical system, the state evolves according to the equation:

$$\dot{x}(t) = f(x(t)), \quad (2.1)$$

where $f : M \rightarrow M$. Systems obeying Eq. 2.1 are deterministic: there is no randomness, no stochasticity, no noise. This means that, starting from one single state at time t , we can in principle describe the whole past and future evolution of the system. Furthermore, there is a lack of an explicit time dependence in f - i.e., $\partial f_i / \partial t = 0$ for $i = 1, \dots, n$. In this case, the dynamical system is said to be autonomous.

To obtain solutions to system 2.1 we need to provide one state, which we typically call an initial condition $x_0 = x(0) \in M$. The combination of $\dot{x} = f(x)$ with $x(0) = x_0$ defines an initial value problem. A fundamental theorem makes our lives studying this problem much easier. This is the theorem of existence and uniqueness of solutions. For $x \in \mathbb{R}^n$ and $f : \mathbb{R}^n \rightarrow \mathbb{R}^n$, it requires that f is continuous and that all of its partial derivatives $\partial f_i / \partial x_j$, for $i, j = 1 \dots n$ are continuous in some open connected set $D \subset \mathbb{R}^n$. This basically means that it requires our function f to be sufficiently smooth. Then, for initial conditions $x_0 \in D$, the initial value problem has a solution $x(t)$ on some time interval $(-\tau, \tau)$ about $t = 0$, and the solution is unique! [57]

In state space, each solution describes a trajectory, a path, that goes through its initial condition x_0 . The uniqueness of solutions implies that, within this time interval $(-\tau, \tau)$, different trajectories do not intersect in state space. This is a crucial property underlying all systems we study.

A useful notation for the evolution of a continuous dynamical system is through the evolution operator $\Phi^t(x)$, which, informally defined, evolves the point x forward t time units. That is, $\Phi^t(x(0)) = x(t)$.

2.1.2 The fate of linear dynamical systems

Although trajectories do not cross, they can share the same fate, meaning they can converge to the same region in state space. We can introduce this notion with a very simple mathematical example of a linear system. It has the form

$$\dot{x}(t) = Ax(t), \quad (2.2)$$

with A a constant $(n \times n)$ matrix. If the eigenvalues $\lambda_i \in \mathbb{C}$ of A are all unique ($i = 1, \dots, n$), its eigenvectors $v_i \in \mathbb{R}^n$ are linearly independent. Then, the general solution

to this system can be written as Ref. [57]:

$$x(t) = \sum_{i=1}^n C_i e^{\lambda_i t} v_i. \quad (2.3)$$

Each initial condition determines the constant coefficients $C_i \in \mathbb{R}$. From Eq. 2.3 we can already notice that the origin of the system, $o = (0, \dots, 0)^T$, is a solution. In fact, it is an equilibrium: $\dot{x} = f(o) = o$. A trajectory on the origin does not change over time.

As we see from Eq. 2.3, the behavior of trajectories depends on the eigenvalues λ_i of the matrix A . We can classify the equilibrium at the origin based on these eigenvalues, as shown in Fig. 2.1. If the real parts of all the eigenvalues are negative, then all trajectories in state space converge to the origin as $t \rightarrow \infty$. In this case, the origin is said to be a stable equilibrium (Figs. 2.1A-B). If at least one eigenvalue is positive, the trajectories diverge from the origin, which is then an unstable equilibrium (Figs. 2.1C-E). Stability here refers to the behavior of trajectories near the equilibrium. If it is stable, nearby trajectories converge to the equilibrium - or, equivalently, small perturbations that take a trajectory away from the equilibrium will eventually go back to the equilibrium. If it is unstable, then nearby trajectories diverge from it.

Stable equilibria are the only attracting solutions, or attractors, of linear systems. In this case, although different trajectories cannot not intersect, they all converge to the origin as $t \rightarrow \infty$. In summary, the ultimate fate of linear systems is kind of boring: either trajectories end up at the origin or they diverge off to infinity. But the journey, the path that trajectories take before the end, the *transient dynamics*, is more interesting. As shown in Fig. 2.1, this is dictated by the constellation of eigenvalues λ_i . For more details, the reader can refer to standard books on linear/nonlinear dynamics, such as Ref. [57].

2.1.3 The fate of nonlinear dynamical systems I: attractors

As just seen, stable equilibria are the only possible attractors in linear systems. Going beyond Eq. 2.2, nonlinear systems can have more interesting and complicated long-term dynamics (Fig. 2.2). Stable equilibria are still possible, as shown in Figs. 2.2A-B. We use for those figures the conductance-based neuronal model we use in Chap. 4, following equations [39]

$$\begin{aligned} \dot{x} &= (I - g_L(x_i - E_L) - g_{Na}m_\infty(x_i)(x_i - E_{Na}) - g_Ky_i(x_i - E_K))/C, \\ \dot{y} &= (n_\infty(x) - y_i)/\tau, \end{aligned} \quad (2.4)$$

with all parameters and functions defined in detail in Chap. 4. The input current I is chosen to be $I = 2.0$, so that the system has excitable dynamics. Its state space is composed of a stable equilibrium, the only attractor, and two unstable equilibria, which create the excitability in this case. Excitability is a type of transient different from that seen for linear systems. Some trajectories are forced to go on long excursions (excitations) before converging to the stable equilibrium. We study more about this again in Chapter 4.

Besides equilibria, nonlinear systems can also have periodic solutions. These orbits oscillate in time and repeat after a certain period T (Fig. 2.2D) and correspond to closed curves in state space (Fig. 2.2C). In several cases these periodic solutions are isolated, in the sense that there are no other periodic orbits in some neighborhood around them.

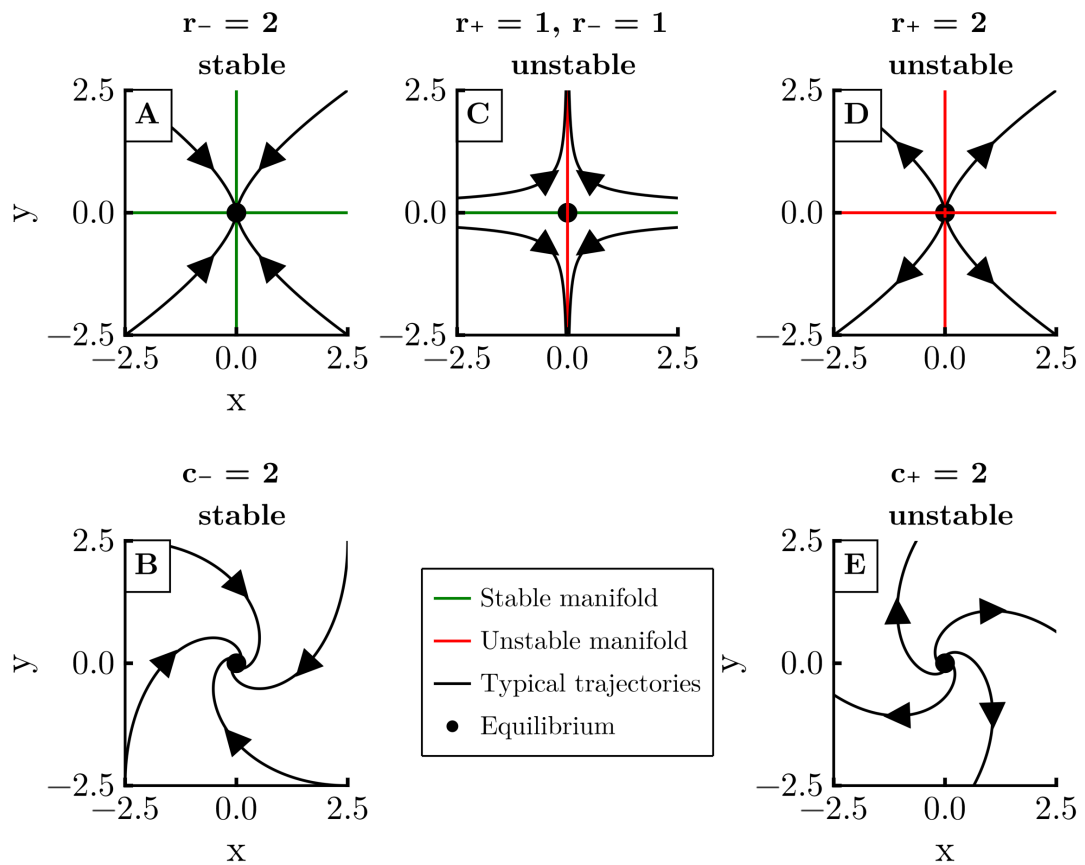


Figure 2.1: **Hyperbolic equilibria in 2D linear systems.** The title specifies the number of eigenvalues that are purely real negative r_- or positive r_+ , or that are complex with real part negative c_- or positive c_+ . The first row shows equilibria whose eigenvalues are purely real, while the second one shows equilibria with complex eigenvalues. In the first column, the equilibria are stable - they are the two possible attractors in linear systems. In the second column, we have a saddle-point for purely real eigenvalues. In the third column, the equilibria are completely unstable, known as repellers.

In that case, they are called limit cycles. The system used in this example is still the neuronal model of Eq. 2.4, but with a different parameter $I = 6.0$, which leads to the system now having a stable limit cycle. We see in this figure again an example of a long transient, with the trajectory initially going on a long excursion before converging to the limit cycle.

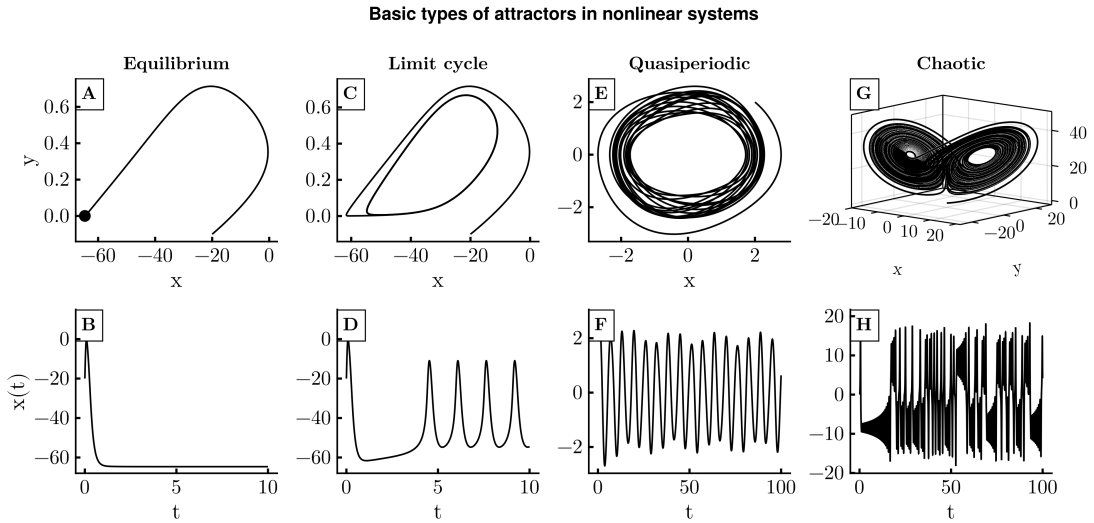


Figure 2.2: **Basic types of attractors in nonlinear dynamical systems.** Each column shows respectively the state space and a time-series of a typical trajectory converging to a type of attractor. The first column corresponds to the neuronal model of Eq. 2.4 with $I = 2.0$, which has excitable dynamics, converging to a stable equilibrium. The second column shows again the neuronal system of Eq. 2.4 but with $I = 6.0$, when the attractor is now a stable limit cycle. The third column shows the system defined in Eqs. 2.5, with a quasiperiodic attractor. Finally, column four has an example of a chaotic trajectory on the Lorenz system (Eq. 2.6).

Not all curves in state space are closed, however. One can have quasiperiodic dynamics, in which trajectories never repeat exactly, although they might almost repeat. This is seen in Figs. 2.2E-F. Simulating the trajectory for longer times would fill up the figure more and more. Further, note the varying amplitude of the time series. The system in this example is the forced Van der Pol oscillator

$$\begin{aligned}\dot{x} &= v \\ \dot{v} &= \mu(1 - x^2)v - \alpha x + g \cos(\omega_f t),\end{aligned}\tag{2.5}$$

with parameters $\mu = 0.1$, $\alpha = 1.0$, $g = 0.5$, $\omega_f = \sqrt{3}$ taken from Ref. [58].

Finally, one can also have chaotic attractors (Figs. 2.2G-H). These solutions have a wild behavior that nearby trajectories tend to diverge at an exponential rate [59]. Despite this local divergence, however, the solutions remain bounded in space. In other words, systems with chaotic attractors are very sensitive to the initial conditions - small changes in initial conditions lead to trajectories that can look very different. The system

used to generate the example is known as the Lorenz system, with equations

$$\begin{aligned}\dot{x} &= \sigma(y - x) \\ \dot{y} &= x(\rho - z) - y \\ \dot{z} &= xy - \beta z,\end{aligned}\tag{2.6}$$

and $\sigma = 10$, $\rho = 28$, $\beta = 8/3$. This chaotic attractor in particular has a shape that resembles a butterfly, with trajectories spending some time on one wing before switching to the other wing [59].

Given now these examples, let us now define the terms we have used a bit more properly.

2.1.4 Formalizing attractors and basins

We have just presented examples of attractors, sets of points in state space to which trajectories eventually converge, and their basins of attraction, the regions containing those converging trajectories. Since in this thesis we will deal a lot with these concepts, we formalize them better. The idea is to have the concepts clear in mind for later. In particular, the definition of an attractor can vary considerably in the literature. Without attempting to claim any superiority, we attempt here to provide a definition that suits our studies.

First, we define an ω -limit set $\omega(x)$ of a point $x_0 \in M$ as [60]:

$$\omega(x_0) = \{x : \forall T \ \forall \epsilon > 0 \text{ there exists } t > T \text{ such that } |\Phi^t(x_0) - x| < \epsilon\}.\tag{2.7}$$

Consider a point $x \in \omega(x_0)$ in the ω -limit set of x_0 . Then, by definition, a trajectory that passes through x_0 comes arbitrarily close to x infinitely often as t increases.

From this, we can define the *basin of attraction* of a set A as $\mathcal{B}(A) = \{x \in M : \omega(x) \subset A\}$. This only looks at the long-term behavior of trajectories; the transient dynamics could be anything, including the case that trajectories go very far from A , as long as they go back to it.

Now to define an attractor, we first define a weaker (or, on the more optimistic side, a more general) version, called the *Milnor attractor*. A set A is a Milnor attractor if:

1. Its basin of attraction $\mathcal{B}(A)$ has strictly positive measure (i.e., if $m(\mathcal{B}(A)) > 0$), where $m(S)$ denotes a measure equivalent to the Lebesgue measure of set S [60]. This condition says that there is some probability that a randomly chosen point will be attracted to A [60].
2. For any closed proper subset $A' \subset A$, the set difference $\mathcal{B}(A) \setminus \mathcal{B}(A')$ also has strictly positive measure. This ensures that every part of A plays an essential role - one cannot decompose A into an attracting part and another part that does not attract [60, 61]. A closed set here means that it contains all its limit points. And proper means its non-empty.

Furthermore, the Milnor attractor does not have to attract all the points in its neighborhood, and there can also be orbits that transiently go very far from the attractor, even if initially close, before eventually getting close to it. Further, it can in principle be composed into the union of two smaller Milnor attractors. To avoid these cases, we call a set A an *attractor* if

1. A is a Milnor attractor.
2. A contains an orbit that is dense in A . Basically, this means that there is an orbit in A that passes arbitrarily close to every point in A . This condition ensures that the attractor is not the union of two smaller attracting sets [61].
3. There are arbitrarily small neighborhoods U of A such that $\forall x \in U$ one has $\Phi^t(x) \subset U \forall t > 0$ and such that $\forall y \in U$ one has $\omega(y) \subset A$. That is, there are arbitrarily small neighborhoods around the attractor in which points inside stay inside and converge to A . This criterion is given in Ref. [62].

2.1.5 Invariant manifolds: structures that organize state space

In Sec. 2.1.2 we only saw how the eigenvalues of the matrix A in the linear system $\dot{x} = Ax$ shape the dynamics of the system. If one eigenvalue λ_k is positive, then trajectories will diverge to infinity following the corresponding eigenvector v_k . When some eigenvalues are positive and some are negative, the origin is a saddle-point. If all eigenvalues are positive, it is called a repeller. Figure 2.1 shows examples of equilibria in 2D linear systems. Note how, in panel C, typical trajectories approach the saddle-point along the x -axis and then diverge along the y -axis. That is, for $t \rightarrow -\infty$, trajectories converge to the x -axis and for $t \rightarrow \infty$ they converge to the y -axis. The x -axis is called the stable manifold $\mathbb{W}^s(o)$ of the origin o and the y -axis is the unstable manifold $\mathbb{W}^u(o)$ of the origin. We can define these manifolds

$$\mathbb{W}^s(o) = \{x \in M : \Phi^t(x) \rightarrow o \text{ as } t \rightarrow \infty\}, \quad \mathbb{W}^u(o) = \{x \in M : \Phi^t(x) \rightarrow o \text{ as } t \rightarrow -\infty\}. \quad (2.8)$$

Let us separate the eigenvectors v_i into two parts: the ones with negative eigenvalues $v_1^-, \dots, v_{n_s}^-$ and the ones with positive eigenvalues $v_1^+, \dots, v_{n_u}^+$. Then we can define the stable and unstable subspaces, respectively, as

$$\mathbb{E}^s = \text{span}(v_1^-, \dots, v_{n_s}^-) \quad \mathbb{E}^u = \text{span}(v_1^+, \dots, v_{n_u}^+). \quad (2.9)$$

For a linear system, the stable manifold of the origin coincides with the stable space \mathbb{E}^s and the unstable manifold coincides with the unstable space. In general, as in the example of the saddle-point, these manifolds act to organize the behavior of trajectories in state space.

These concepts can be extended for nonlinear systems. To do this, the first step is to think about the linearization of the nonlinear system. Suppose our nonlinear system of interest has an equilibrium $x^* \in M$. It turns out that the behavior sufficiently close to this equilibrium is linear, despite the system globally being nonlinear [63, 64]! To see this, we first move the origin of our system to x^* by defining a new variable $y(t) = x(t) - x^*$. Then,

$$\dot{y} = \dot{x} = f(y + x^*) \equiv g(y) \quad (2.10)$$

where we define a convenience function $g(y)$. Expanding $g(y)$ around $y = 0$ (i.e., around the equilibrium $x(t) = x^*$) gives us

$$\dot{y} = g(0) + J_g(0)y + \mathcal{O}(y^2), \quad (2.11)$$

where $J_g(y) = \frac{\partial g_i(y)}{\partial y_j}$ is the Jacobian of g . It is related to the Jacobian of f by $J_g(y) = J_f(x)$, so $J_g(y=0) = J_f(x=x^*)$. Since $g(0) = f(x^*) = 0$, then if we are sufficiently close to the origin we can also ignore the terms $\mathcal{O}(y^2)$ and therefore we get

$$\dot{y} = J_g(0)y. \quad (2.12)$$

That is, the behavior of the nonlinear system sufficiently close to the equilibrium is linear, with the constant matrix function being the Jacobian evaluated at the equilibrium!

But the good news don't stop here! There is the Hartman-Grobman theorem, which states that the state space near a hyperbolic equilibrium in the nonlinear system is topologically equivalent to the state space of the linearized system. An equilibrium is hyperbolic if the eigenvalues of the Jacobian evaluated on it are all nonzero, i.e., if $\lambda_i \neq 0 \forall i = 1, \dots, n$. *Topologically equivalent* means that the linearized state space and the local state space near the equilibrium are distorted versions of each other. They can be bent and warped, but not ripped. In particular, closed orbits have to remain closed, and connections between saddle points have to remain [57]. Mathematically, topologically equivalent means there is a *homeomorphism* (continuous deformation with continuous inverse) from one state space into the other; trajectories can be mapped from one to the other, and the direction of time is the same [57].

Stating the theorem more formally, suppose a hyperbolic equilibrium $x^* \in M$ such that $f(x^*) = 0$ and such that all its eigenvalues are nonzero. Then, there is a neighborhood N of x^* and a homeomorphism $h : N \rightarrow M$ such that [59]

- $h(x^*) = 0$,
- the flow $\dot{x} = f(x)$ in N is topologically conjugate to the flow of the linearization $\dot{y} = Ay$ by the continuous map $y = h(x)$. Topologically conjugate basically meaning a change of coordinates.

This guarantees that the stability of the equilibrium is the same in both cases, so we can use the linearization to gain important insights about the stability of equilibria in the nonlinear system!

What about the stable and unstable manifolds? In analogy to the linear case, we can define local stable and unstable sets near a neighborhood U of an equilibrium x^* for the nonlinear system [59]:

$$\mathbb{W}_{\text{loc}}^s(x^*) = \{x \in M : \Phi^t(x) \rightarrow x^* \text{ as } t \rightarrow +\infty \text{ and } \Phi^t(x) \in U \forall t \geq 0\}, \quad (2.13)$$

$$\mathbb{W}_{\text{loc}}^u(x^*) = \{x \in M : \Phi^t(x) \rightarrow x^* \text{ as } t \rightarrow -\infty \text{ and } \Phi^t(x) \in U \forall t \leq 0\}. \quad (2.14)$$

Herein comes the stable manifold theorem. It states that, for a hyperbolic equilibrium x^* :

- The local stable set $\mathbb{W}_{\text{loc}}^s(x^*)$ is a smooth manifold whose tangent space has the same dimension n_s as the stable space \mathbb{E}^s of the linearization of f at x^* . $\mathbb{W}_{\text{loc}}^s(x^*)$ is also tangent to \mathbb{E}^s at x^* .
- The local unstable set $\mathbb{W}_{\text{loc}}^u(x^*)$ is a smooth manifold whose tangent space has the same dimension n_u as the unstable space \mathbb{E}^u of the linearization of f at x^* . $\mathbb{W}_{\text{loc}}^u(x^*)$ is also tangent to \mathbb{E}^u at x^* .

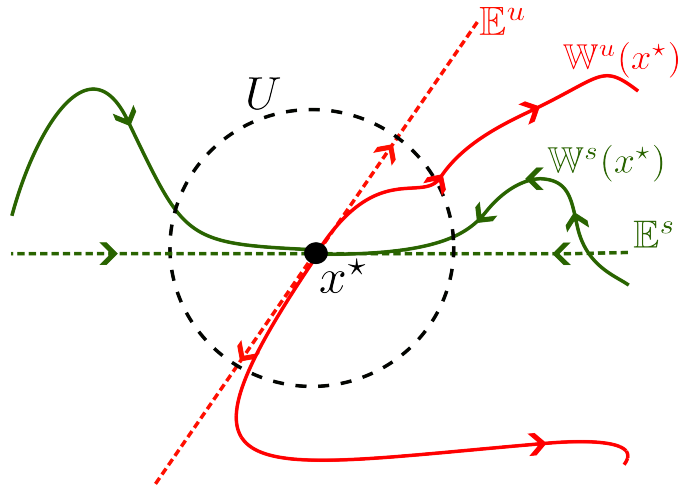


Figure 2.3: **Invariant manifolds of saddle point x^* .** The local stable $\mathbb{W}_{\text{loc}}^s(x^*)$ and unstable $\mathbb{W}_{\text{loc}}^u(x^*)$ manifolds of the saddle point x^* respectively can be associated with the stable \mathbb{E}^s and unstable \mathbb{E}^u subspaces and become tangent to them near the saddle. This follows from the Hartman-Grobman and the stable manifold theorems. The global stable $\mathbb{W}^s(x^*)$ and unstable $\mathbb{W}^u(x^*)$ manifolds extend the definition of the local manifolds beyond the neighborhood U . Figure is inspired by Fig. 6.2.4 from Ref. [59].

The homeomorphism guaranteed by the Hartman-Grobman theorem maps $\mathbb{W}_{\text{loc}}^s(x^*)$ into \mathbb{E}^s and $\mathbb{W}_{\text{loc}}^u(x^*)$ into \mathbb{E}^u one-to-one, as shown in Fig. 2.3. Further, the stable manifold theorem guarantees that \mathbb{E}^s and \mathbb{E}^u actually approximate the local manifolds $\mathbb{W}_{\text{loc}}^s(x^*)$ and $\mathbb{W}_{\text{loc}}^u(x^*)$, respectively [59]. As a consequence, we get the behavior illustrated in Fig. 2.3

The manifolds we just looked at are defined for a local neighborhood U around the equilibrium. We can extend them towards the whole of state space by defining global manifolds as:

$$\mathbb{W}^s(x^*) = \bigcup_{t \leq 0} \Phi^t(\mathbb{W}_{\text{loc}}^s(x^*)) \quad (2.15)$$

$$\mathbb{W}^u(x^*) = \bigcup_{t \geq 0} \Phi^t(\mathbb{W}_{\text{loc}}^u(x^*)). \quad (2.16)$$

That is, the global stable manifold is obtained by integrating the local stable manifold backwards, looking at where the trajectories on it came from. For the unstable manifold, we integrate the local unstable manifold forwards, to see where it goes to.

An important fact about the local and global manifolds that follows from their definitions is that they are invariant: trajectories starting on these manifolds stay on them forever [59]. Furthermore, the uniqueness of solutions prohibits certain crossings of manifolds: stable manifolds of two distinct equilibria cannot cross, unstable manifolds of two distinct equilibria also cannot, and the same manifold cannot cross itself - otherwise, where the crossing points would have to obey two distinct paths! Meanwhile, stable and unstable manifolds, either of the same equilibrium or of two different equilibria can cross.

As mentioned before, these manifolds usually play a big role in organizing state space. As we will see in Chapter 4, they can organize the transient dynamics of systems.

There, we study a dynamical system wherein certain trajectories are forced to go on long excursions before converging to the stable equilibrium, the only attractor in state space (see Figs.2.2A-B). As explained there, this long excursion is generated by the arrangement of the invariant manifolds of the saddle-point that exists in state space. The invariant manifolds can also organize the long-term behavior of systems: the next section briefly shows how stable manifolds of unstable equilibria can act as the boundary separating two basins of attraction.

2.1.6 The fate of nonlinear dynamical systems II: multistability and basins of attraction

In Sec. 2.1.3 we saw that the ultimate fate of nonlinear systems, their attractors, can be much more complicated than that of linear ones. Not only are the attractors themselves complicated, but they can also coexist in state space. If there are two coexisting attractors, this means that the state space will be separated into three regions: the basin of attraction of attractor one, the basin of attractor two, and the boundary between them. Usually, the basin boundary is formed by stable manifolds of saddle-type objects: saddle-points, saddle-limit-cycles, and even chaotic saddles! [2]. Figure 2.4 illustrates this for a relatively simple system with two stable equilibria, where the basin boundary is the stable manifold of the saddle-point in the middle. This system is known as the Duffing oscillator:

$$\dot{x} = v \tag{2.17}$$

$$\dot{v} = -(-kx + cv + lx^3)/m, \tag{2.18}$$

with $k = 1$, $c = 0.5$, $l = 1$, $m = 1$. This system represents a ball of mass m rolling downhill at position x and velocity v on a quartic potential landscape of the form $U(x) = -lx^4/4 - kx^2/2$ with a friction term $-cv$. Following the definition of global manifolds in Eq. 2.16, these global manifolds are essentially obtained by integrating trajectories starting on the local manifolds of the saddle-point.

In this thesis we study two examples of multistability occurring in networked systems. In Chapter 3 we study networks of Kuramoto units, and see there the coexistence of multiple attractors depending on how strongly the units are interacting. We also see how this multistability impacts the sensitivity of the system to small changes in parameters of the units. Later, in Chapter 4 we study how multistability arises when two excitable neurons are coupled together diffusively. Both studies require that we find the attractors in the systems. This is what we deal with in the next section.

2.1.7 How to find attractors

Finding all the attractors of a given dynamical system is not necessarily a trivial task. For equilibria, one can find all the roots of the system function, i.e., $f(x^*) = 0$ and then check their stability through the eigenvalues of the Jacobian evaluated on them. However, the problem becomes more complicated for other types of attractors. To start off, simply proving that a set is an attractor, following the criteria given in Sec. 2.1.4, is usually not possible. Instead, in practice we use the looser definition of an attractor simply as the long-term dynamics of trajectories. Numerically, this means a brute-force approach of simulating several trajectories in state space for long integration times and seeing where they converge to.

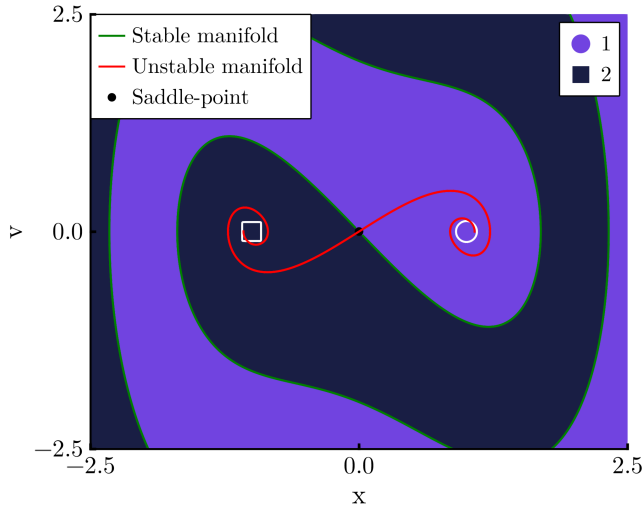


Figure 2.4: **Bistability in Duffing model.** Two stable equilibria (white square and circle) are shown with their respective basins of attraction in two shades of purple. The global stable and unstable manifolds of the saddle-point (black point) in the middle are also shown as green and red lines respectively. The global stable manifold of the saddle coincides with the boundary between the basins, obtained independently.

This comes with two problems. First, it does not rule out the possibility that a certain set is just a very long transient. To remedy this, we usually integrate trajectories on the set for very long and check if there is any escape. Second, some attractors might have very small basins of attraction, such that randomly chosen initial conditions are unlikely to end on them, so it is unlikely that we find those attractors. So far, however, this brute force approach is the best we have for general systems [43, 46]. Within this approach, there are two main methods in the literature for finding attractors. They differ in how they check convergence to attractors.

The first approach was proposed in Ref. [44] and implemented with improvements in Ref. [43]. It parcellates state space into boxes. The idea then is that a typical trajectory, initialized in a certain box in state space, will evolve and visit other boxes until it converges to the attractor. It will then stay on the attractor, repeatedly visiting the same state space boxes. Using this idea, the algorithm integrates trajectories and looks for recurrences. When boxes are visited repeatedly for a certain prescribed amount of time, the algorithm considers that these boxes constitute the attractor. It is also smart in that it keeps track of the state of each box. So it knows that the boxes visited by the trajectory before converging to the attractor - the transient section of the trajectory - belongs to the basin of attraction of that attractor. This algorithm works well for steady-state, periodic, quasiperiodic, and chaotic attractors in low-dimensional systems. For chaotic attractors in high-dimensional systems it does not work well, because the time that trajectories take to recur on a chaotic attractor becomes too long to simulate numerically.

The second method does not rely on discretizing state space, and is designed to work well for high-dimensional systems. In this case, one spreads a number \mathcal{N} of initial conditions in state space and integrates them to obtain \mathcal{N} trajectories. Each trajectory $x(t)$ is then converted to a vector of features $\mathcal{F} \in \mathbb{R}^n$ of n numbers that all collectively

describe the trajectory. This is done by the featurizing function $\phi : M \times \mathbb{R} \rightarrow \mathbb{R}^n$, such that $\mathcal{F} = \phi(x(t), t)$. Each attractor should correspond to a unique \mathcal{F} . Then, the \mathcal{N} vectors of features are grouped together via any of several possible grouping or clustering algorithms, and each grouping corresponds to one attractor. This approach can work very well, but it relies on pre-existing knowledge about the system to find a suitable featurizer function ϕ . To be confident about the results, one also has to verify that the total integration time is long enough, and that the transients of all trajectories were removed. This relies on experimentation. This method has been proposed in Ref. [32] and soon thereafter also in Ref. [45]. Together with colleagues, I implemented efficient and open-source code for this method with improvements in the *Attractors.jl* package Ref. [46].

Both methods can be applied across a parameter range and used in a continuation fashion, as illustrated in Fig. 2.1.7A. For the first parameter, one selects \mathcal{N} initial conditions and identifies from those the attractors of the system using any of the two methods just described. Then, one samples points on these attractors and adds them to the pool of initial conditions for the next parameter value. The originally prescribed initial conditions, together with the original ones, are then used to find attractors in the subsequent parameter value. This process of seeding initial conditions from the previously found attractors is repeated for the whole parameter range. Then, one has all the attractors for each parameter value, and the remaining problem is to link attractors from one parameter to the next.

The matching procedure between attractors is crucial for a continuation procedure. Often in linear continuation analysis one just matches the next point along a continuation curve to the previous point. This works well for infinitesimal perturbations of fixed points but becomes a problem in global stability analysis, where the steps are not necessarily infinitesimal and the attractors may be spatially extended and chaotic [46]. Matching in our algorithm is designed to be very flexible, and can be adapted to the user's needs [46]. There are two main methods for matching attractors. The first is based on distances between the attractors in state space. First, the algorithm computes the distances between attractors at some parameter p_i and some subsequent parameter p_{i+1} . Distance here is any positive semi-definite function. The default used is the Euclidean distance between the centroids of the attractors. Another good option is the Hausdorff distance [46]. With the distances, a new attractor is matched to the previous one with the

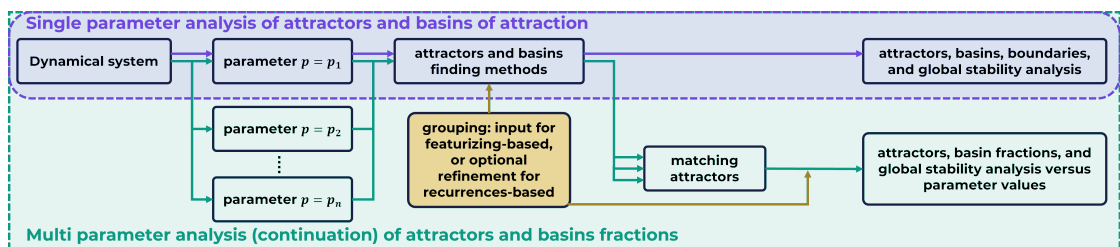


Figure 2.5: **Schematic illustration of the continuation method used to find and match attractors across a parameter range.** The first row illustrates the single-parameter attractor finding algorithms. The second row illustrates how they can be combined across parameters to perform a continuation analysis. Figure taken from Ref. [46].

smallest distance, prioritizing pairs with the smallest distance. This matching respects uniqueness, so that once an attractor from the previous parameter has been matched, it is removed from the matching pool. This method is called matching by state space distance.

The other matching method is based on whether the basin of attraction of a new attractor encloses the basin of attraction of a previous attractor. To be concrete, suppose we find a certain number of attractors at a parameter p_i . Each “previous” attractor occupies a certain region of state space (which can be a single point if it is an equilibrium). Its basin of attraction occupies also a certain region, and encloses the attractor itself. At the subsequent parameter p_{i+1} , “new attractors” are found. Their basins may be different in shape or size. But one can consider that if the basin of a new attractor encloses a previous attractor (i.e., if the previous attractor is inside the basin of the new attractor), then they are the “same attractor” - i.e., they should be matched. It may happen that the basin of a new attractor encloses two or more previous attractors. Then, one can choose the new and previous attractors that are closest in terms of a state space distance. This method works well for systems with several attractors and complicated basin structures. It is called the basin enclosure method, and we use it for results in Chap. 3.

After matching, the continuation is done. The user may also decide to group attractors based on some features of interest. For instance, to group attractors with a certain degree of synchronization [46].

The development and implementation of the attractor-finding algorithms and the continuation procedure in efficient and open-source code led to a joint publication in Ref. [46]. The package is continuously updated with improvements and new features. The latest updates and documentation can be found in the *Attractors.jl* GitHub page.

2.2 Basics of bifurcations

What happens to the attractors - and, in general, to the state space structures - of a dynamical system when we vary its parameters? In terms of the qualitative properties, there are two possibilities: either they stay similar or they change drastically. We can be a bit more rigorous. Two systems are qualitatively similar if they are topologically equivalent. The notion of topological equivalence was already mentioned in Sec. 2.1.5. As a reminder, two systems are topologically equivalent if the state space of one can be obtained by a continuous transformation of the other [65]. Mathematically, this means that they are topologically equivalent if there is a homeomorphism $h : M \rightarrow M$ mapping orbits of the first system onto orbits of the second, preserving the direction of time.

As the parameters of a system are varied, we obtain different dynamical systems that are usually topologically equivalent. The attractors, for instance, may move, but they retain their stability. At some point, however, there may be a drastic change, and the new system may no longer be equivalent. The attractor may have disappeared, or lost its stability. Or a new attractor may have emerged. These drastic qualitative changes in the behavior of a dynamical system are called bifurcations. A bit more rigorously, a bifurcation is a change in the topological type of a system as its parameters pass through a critical (bifurcation) value [65]. There are many types of bifurcations, and one can literally write a whole book about this [65]. For this thesis we focus briefly on just a few bifurcations that will be relevant for later. For simplicity, we focus also on the simplest version of these bifurcations.

2.2.1 Saddle-node bifurcation of equilibria

In a saddle-node bifurcation of equilibria we see the emergence, or destruction, of a stable (node) and an unstable (saddle) equilibrium. Starting from the side of the bifurcation in which the equilibria exist and approaching the bifurcation parameter, we see the equilibria approaching each other, coalescing at the critical parameter, and annihilating each other thereafter (Fig. 2.6A-D). The simplest form of this bifurcation occurs in one dimension in the system

$$\dot{x} = f(x) = \alpha + x^2, \quad (2.19)$$

with the critical value of the bifurcation being $\alpha = 0$. As shown in Figs. 2.6A, for $\alpha < 0$ we see that the parabola $f(x)$ has two roots, so the system has two equilibria, in positions $x^* = \pm\sqrt{-\alpha}$. From the figure directly we can already see that the equilibrium on the left is stable and the equilibrium on right is unstable. We can confirm this with a linearization analysis - the Jacobian here is simply $df/dx = 2x$, so the eigenvalue of the left and right equilibrium are $-2\sqrt{-\alpha}$ and $+2\sqrt{-\alpha}$. As α increases towards 0 the parabola moves up, the equilibria approach each other, their eigenvalues approach zero, and at $\alpha = 0$ they all coalesce into one single equilibrium. At this point, the eigenvalue of the system is zero: this equilibrium is non-hyperbolic! For $\alpha > 0$ there are no more equilibria. Equation 2.19 is called the normal form of the saddle-node bifurcation, because any generic system obeying some conditions will be topologically equivalent to it locally, near the equilibrium.

Just after the bifurcation, the region previously occupied by the two equilibria is still quite slow. Note how \dot{x} is very close to zero near $x = 0$ in Fig. 2.6C. This region of slow flow is called the ghost of the saddle-node [57]. In a way, it retains properties of the two equilibria - particular, trajectories still flow towards the ghost from the side previously occupied by the stable equilibrium, remain in its neighborhood for a while, but then eventually depart through the side previously occupied by the unstable equilibrium [66]. The ghost is not an invariant set, but is an example of a metastable regime, which we study in greater depth in Chapter 5.

Saddle-node bifurcations can also occur analogously for periodic orbits [65] - a stable limit cycle then collides with an unstable limit cycle, and leave behind a ghost of a limit cycle!

2.2.2 Hopf bifurcation

Keeping with the spirit of describing the simplest cases, let us now imagine a system written in polar coordinates (ρ, θ) :

$$\dot{\rho} = f_\rho = \rho(\alpha - \rho^2) \quad (2.20)$$

$$\dot{\phi} = f_\phi = 1. \quad (2.21)$$

Because the two equations are decoupled, we can analyze the ρ equation separately first. First, note that its Jacobian $\partial f_\rho / \partial \rho = \alpha - 3\rho^2$. For all values of α , f_ρ has an equilibrium at $\rho = 0$ - with eigenvalue $\lambda = \alpha$. This is linearly stable for $\alpha < 0$ and linearly stable for $\alpha > 0$. At $\alpha = 0$ it is non-hyperbolic! What happens then? The first equation has another root for $\alpha > 0$ at $\rho = \sqrt{\alpha}$ - so the eigenvalue is $\lambda = -2\alpha$. This equilibrium is then stable. Considered for f_ρ alone, this is an example of a pitchfork bifurcation [65]. Considering the full system, with the rotation induced by $\dot{\phi} = 1$, the

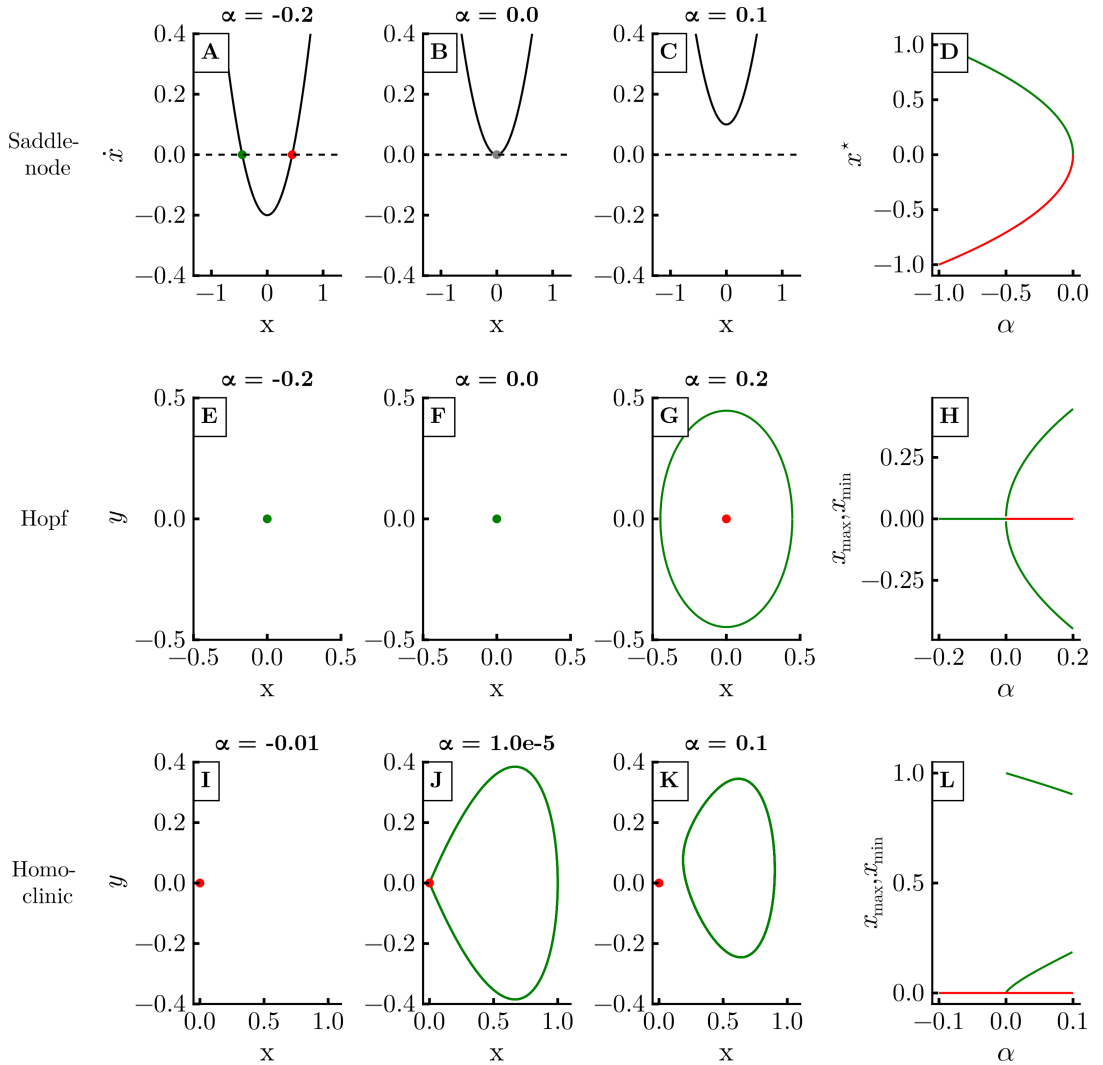


Figure 2.6: Some important bifurcations. The saddle-node bifurcation is shown for the normal form $\dot{x} = x^2 + \alpha$ in panels A-D. A stable and an unstable equilibria, represented respectively by green and red circles (panel A), come together as the bifurcation parameter α is changed. Eventually they coalesce (panel B) and are subsequently destroyed (panel C). The position of these equilibria as a function of α is shown in panel D. The supercritical Hopf bifurcation is shown for Eq. 2.20 in panels E-H. Before and at the bifurcation there is a stable equilibrium in state space (panels E and F respectively), which becomes unstable when a stable limit cycle emerges (panel G). Panel H shows this behavior as a function of α , taking the maximum and minimum values of x to represent the limit cycle. The homoclinic bifurcation to a saddle point is shown in panels I-L. Before the bifurcation there is a saddle point (panel I). At the bifurcation, an orbit homoclinic to this saddle point appears (represented approximately in panel J). After the bifurcation, a stable limit cycle emerges (panel K). This is also summarized in panel L.

equilibrium at the origin remains an equilibrium, but the equilibrium at $\sqrt{\alpha}$ becomes a limit cycle with amplitude $\sqrt{\alpha}$. Putting everything together, we have the behavior in Fig. 2.6G-H. A stable limit cycle becomes unstable at $\alpha = 0$ and from it a stable limit cycle emerges. This is called a supercritical Hopf bifurcation [65]. If we write this system in Cartesian coordinates and compute the eigenvalues of the Jacobian at the origin, we see they are $\lambda_{1,2} = \alpha \pm i$. This gives us another general property of this bifurcation: at the critical point, the eigenvalues at the origin cross the imaginary axis.

Now consider the system

$$\dot{\rho} = f_\rho = \rho(\alpha + \rho^2) \quad (2.22)$$

$$\dot{\phi} = f_\phi = 1. \quad (2.23)$$

Now the Jacobian is $\partial f_\rho / \partial \rho = \alpha + 3\rho^2$. There is still an equilibrium at the origin, in which the eigenvalue is still α - its stability is the same as before. However, the other equilibrium, now $\sqrt{-\alpha}$ has the associated eigenvalue as -2α . It therefore exists for $\alpha < 0$ when it is unstable. This thus corresponds to an unstable limit cycle, which coexists with a stable equilibrium for $\alpha < 0$. For $\alpha > 0$, the limit cycle disappears and the system is left with only an unstable equilibrium. This is called a subcritical Hopf bifurcation [65]. The eigenvalues of the Cartesian Jacobian at the origin behave in the same way as for the supercritical Hopf.

2.2.3 Homoclinic bifurcation

Both the saddle-node and the Hopf bifurcations happen in the neighborhood of equilibria - for this reason, they are called local bifurcations. Now we move to a bifurcation in which this is no longer the case - the state space beyond only the equilibrium is affected, and it is thus called a global bifurcation [65]. The formal description of this bifurcation is consequently more involved, and goes beyond the scope of this thesis. For here it is enough to describe the bifurcation more qualitatively.

In the homoclinic bifurcation we study here, occurring on the plane, we have the emergence of a limit cycle. Before the bifurcation, there is only a saddle point. At the bifurcation, the unstable manifold of the saddle becomes tangential to its own stable manifold - this constitutes a homoclinic orbit. After the bifurcation, the homoclinic orbit becomes a limit cycle whose stability depends on the eigenvalues of the saddle. Defining the saddle quantity $\sigma = \lambda_1 + \lambda_2$, it can be shown that the limit cycle is stable for $\sigma < 0$ and unstable if $\sigma > 0$ [65].

Varying the bifurcation parameter α close to the homoclinic orbit, the limit cycle approaches more and more the saddle point, and touches it at $\alpha = \alpha_c$. The region of the limit cycle close to the saddle-point has a very slow dynamics, such that the period of the limit cycle diverges to infinity as the critical point is approached. In higher dimensional systems, different types of homoclinic bifurcations are possible, with potentially much more complicated dynamics. The homoclinic bifurcations we deal with in this thesis are always related to simple saddle points, and so are analogous to the planar case shown now.

An example of a planar system with this bifurcation is due to Sandstede [67]

$$\dot{x} = -x + 2y + x^2 \quad (2.24)$$

$$\dot{y} = (2 - \alpha)x - y - 3x^2 + (3/2)xy. \quad (2.25)$$

The origin is a saddle which, at $\alpha = 0$, has eigenvalues $\lambda_1 = 1$ and $\lambda_2 = -3$ - its saddle quantity is therefore $\sigma = 2 < 0$, so the limit cycle that emerges here is stable [65].

2.3 Basics of Network Theory

An incredibly powerful abstraction about real-world systems can be achieved through the concept of networks, here used as synonyms for graphs, which are composed of nodes that are connected by edges. Networks can represent friendships - with people being the nodes and their friendships being the edges -, brain circuits - neurons are nodes, synapses are edges [68] -, ecological systems - for instance, ecological regions are nodes, and migrations between them are edges [69]. In this thesis we make use of this abstraction and consider that the nodes are dynamical systems $\dot{x}_i = f(x_i)$, $x_i \in \mathbb{R}^n$ on their own, with certain interactions between them. Together, the whole networked system is a dynamical system of the form:

$$\dot{x}_i = f(x_i) + \sum_{j=1}^N A_{ij}g(x_j, x_i), \quad i = 1, \dots, N, \quad (2.26)$$

with N units, whose interactions are described by the function g . The adjacency matrix A_{ij} describes the strength of interactions between the units. Typically, it is a binary matrix, such that $A_{ij} = 1$ if unit i receives a connection from unit j and $A_{ij} = 0$ otherwise. It can also be weighted, in which case the entry $A_{ij} \in \mathbb{R}$ represents the strength of interactions. Usually for binary matrices, we rewrite Eq. 2.26 as

$$\dot{x}_i = f(x_i) + \sum_{j \in \Omega_i} g(x_j, x_i), \quad i = 1, \dots, N, \quad (2.27)$$

where $\Omega_i = \{j \in [1, N] : A_{ij} = 1\}$ is called the neighborhood of node i . The number of elements in Ω_i , i.e., the number of connections of unit i , is called the unit's degree.

The adjacency matrix A describes the topology of the network, meaning the architecture of the connections. There are many types of topologies, which describe well different types of systems. One type of topology is the regular ring, also called k -nearest-neighbors topology. As the name suggests, one can think of all nodes arranged on a ring, with each node connected to the k nearest nodes on each side. Another type of topology is the random ring, in which connections are chosen at random between the nodes. One consider the regular and random rings as two extremes, and interpolate between them in what is called the Watts-Strogatz algorithm [70]. In this case, one starts with a k -nearest neighbor ring of nodes. Then, choose connections with a probability p . For each chosen connection (i, j) , keep the source node i , randomly choose a new node j' in the network, and switch (i, j) to (i, j') . This effectively switches short-range connections (between nearest nodes) to long range connections (between nodes that are potentially far away). For this rewiring probability p at $p = 0$ one has the regular topology; for $p = 1$ one has the random topology.

Without going into deeper formalizations, a regular network is considerably clustered due to its short-range structures. And the average distance (in terms of numbers of edges) between nodes in the network is considerably high. In a random network, the clustering is very small, and the average distance is also small. One can formalize these concepts and show how this transition occurs as p is changed [70]. Here, we mention that, when p is relatively small but nonzero, only a few short-range connections are

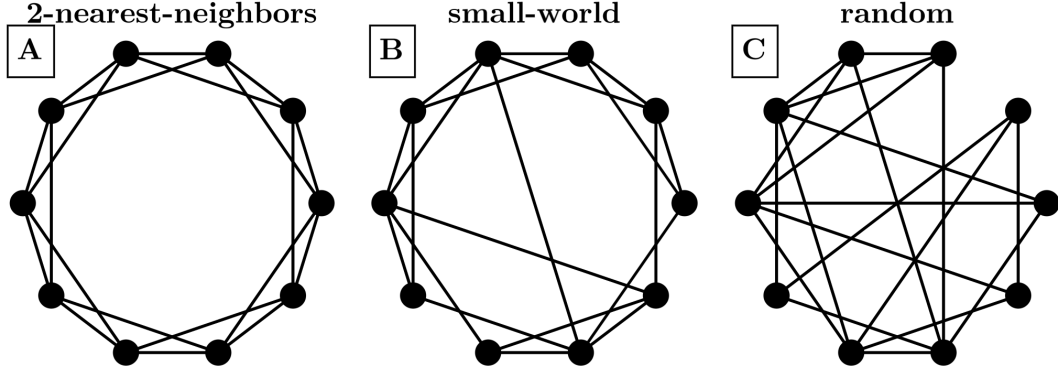


Figure 2.7: **Illustration of networks generated by the Watts-Strogatz procedure.** First, a k -nearest neighbor topology is created (Panel A). Then, some connections are randomly rewired, keeping the source node but changing the target node. With a few rewirings, this creates small-world networks (Panel B). By rewiring all the initial short-range connections, the network becomes randomly connected (Panel C).

rewired as long-range. This does not change the clustering characteristics much, but considerably lowers the average distance between nodes - the few long-range connections act as efficient shortcuts between nodes. Networks in this regime are usually called small-world networks [70].

In Chap. 3 we also study distance-dependent networks. The adjacency matrix is then defined as

$$A_{ij} = \frac{1}{\eta(\alpha)(d_{ij})^\alpha}, \quad (2.28)$$

with $d_{ij} = \min(|i - j|, N - |i - j|)$ is the edge distance along the ring, and $\eta(\alpha) = \sum_{j=1}^{N'} \frac{2}{j^\alpha}$ is a normalization term, with $N' = \frac{N-1}{2}$ denoting half the amount of units to which i is connected to (one half of the ring's length, discounting the unit i itself). All units are thus connected, but the weight of the connections decays with the distance following the α parameter. This parameter can also be called the locality parameter, since $\alpha = 0$ leads to an all-to-all equally connected network and $\alpha \rightarrow \infty$ leads to a first-nearest-neighbor topology ($k = 1$). In between we get distance-dependent weights.

2.4 Basics of Kuramoto oscillators

2.4.1 Derivation of the model and transition to synchronization

The Kuramoto model, written in general as

$$\dot{\theta}_i = \omega_i + \epsilon \sum_{j=1}^N A_{ij} \sin(\theta_j - \theta_i), \quad (2.29)$$

serves as a paradigm for studies on synchronization phenomena [17]. Its usefulness comes from it being simple enough to be mathematically tractable, sufficiently generic, and also complex enough to display interesting dynamics. To reach it, Kuramoto started from generic oscillators near supercritical Hopf bifurcations (also called Stuart-Landau oscillators). Each unit i follows

$$\dot{Q}_i = (\omega + \alpha)Q_i - \beta|Q_i|^2Q_i, \quad (2.30)$$

where ω is the natural frequency of the oscillator, $\alpha > 0$ and $\beta > 0$ are parameters and $Q \in \mathbb{C}$. This is the normal form of the Hopf bifurcation we saw in Sec. 2.2 but written in complex numbers. Kuramoto chose a simple and natural way to couple these oscillators: via a common coupling term, that is proportional to the value Q_i of each oscillator:

$$\dot{Q}_i = (\omega + \alpha)Q_i - \beta|Q_i|^2Q_i + \frac{K}{N} \sum_{j=1}^N Q_j, \quad (2.31)$$

which corresponds to an all-to-all topology, with K being the coupling strength. Here the natural frequencies are assumed to be drawn from a certain distribution $g(\omega)$, usually unimodal.

One can then rewrite Eq. 2.31 in polar coordinates by using $Q_i = e^{i\theta_i} \rho_i$. Substituting it one gets the equations

$$\dot{\rho}_i = (\alpha - \beta\rho_i^2) + \frac{K}{N} \sum_{j=1}^N \rho_j \cos(\theta_j - \theta_i) \quad (2.32)$$

$$\dot{\theta}_i = \omega_i + \frac{K}{N} \sum_{j=1}^N \frac{\rho_j}{\rho_i} \sin(\theta_j - \theta_i). \quad (2.33)$$

Kuramoto studied these equations in the limit of $\alpha \rightarrow \infty$ and $\beta \rightarrow \infty$ with α/β constant. Then, one gets that the radial variables ρ_i approach a stable fixed point arbitrarily fast [17]. The radial variable is therefore just a constant and one just needs to consider the phase variables:

$$\theta_i = \omega_i + \frac{K}{N} \sum_{j=1}^N \sin(\theta_j - \theta_i). \quad (2.34)$$

A very useful way to quantify the spread of the phases θ_i is through the complex order parameter:

$$Z = re^{i\psi} = \frac{1}{N} \sum_{j=1}^N e^{i\theta_j}, \quad (2.35)$$

which corresponds to the centroid of the phases and therefore characterizes well the collective behavior of the system. The radius r measures the phase synchronization of the system: r is close to 0 if the phases are uniformly spread or clustered in anti-phase clusters and r is close to 1 if the phases are aligned together. Here we should clarify that phase synchronization denotes the alignment of phases of oscillations - complete phase synchronization corresponds to $r = 1$, meaning that the phases are the same (up to 2π offsets). On the other hand, frequency synchronization denotes the alignment

of the frequencies of oscillations - complete frequency synchronization corresponds to $\dot{\theta}_i = \Omega$, $\forall i = 1, \dots, N$. Networks that are frequency synchronized are also said to be phase-locked - the phase differences are constant. But it does not imply phase synchronization, as the phase differences may be non-zero. Figures 2.8A-B exemplify the behavior of r for weak and strong phase synchronization.

The angle ψ corresponds to the average phase of the units. Using this order parameter, the Kuramoto model can be rewritten as

$$\dot{\theta}_i = \omega_i + Kr \sin(\psi - \theta_i), \quad i = 1, \dots, N. \quad (2.36)$$

This form highlights the mean-field character of the model [19]. The oscillators now interact through the mean-field quantities r and ψ . The phase θ_i is pulled towards the mean phase ψ . And the effective coupling strength becomes Kr , so it is modulated by the degree of phase synchronization r . This creates a positive feedback loop, wherein as the system phase synchronizes more, the coupling becomes stronger and so the system tends to phase synchronize even more. This is a very clear mechanism for spontaneous synchronization [19].

These equations always have a solution for $\theta_i = 0$, $\forall i$. What about other solutions? Kuramoto considered these equations in the infinite size limit $N \rightarrow \infty$. By seeking steady-state solutions, with r constant, he noted that oscillators will split into two groups: (i) with $|\omega_i| < Kr$, which phase-lock together and (ii) with $|\omega_i| > Kr$ which keep rotating with nonuniform velocity $\dot{\theta}_i$. He then showed that a branch continuously bifurcates from $r = 0$ at $K = K_c$, a critical coupling strength, given by:

$$K_c = \frac{2}{\pi g(0)}. \quad (2.37)$$

Near $K = K_c$, this branch has a square-root behavior: $r \propto \sqrt{K - K_c}$. In particular for $\{\omega_i\}$ following a Lorentzian distribution, one can show that [71, 19]

$$r = \sqrt{1 - \frac{K_c}{K}}, \quad (2.38)$$

as illustrated in Fig. 2.8C. One can verify this behavior numerically: Fig. 2.8D illustrates the results of simulations for a network of $N = 1000$ oscillators under a Gaussian distribution with zero mean and unitary standard deviation. The y -axis denotes the time-averaged behavior of $r(t)$, since $r(t)$ oscillates in time for these finite networks.

Many open questions remain from the treatment just shown, such as the stability of these branches. There have been many extensions made to this model [24, 25]. In the context of multistability, some basic results come from studying an even simpler configuration, where the units are identical and coupled in a k -nearest-neighbor ring.

2.4.2 Multistability in homogeneous case: twisted states

In the case of homogeneous oscillators with $\omega_i = \omega$ coupled in a k -nearest-neighbor topology, the equations become

$$\dot{\theta}_i = \omega + \epsilon \sum_{j=i-k}^{j=i+k} \sin(\theta_j - \theta_i). \quad (2.39)$$

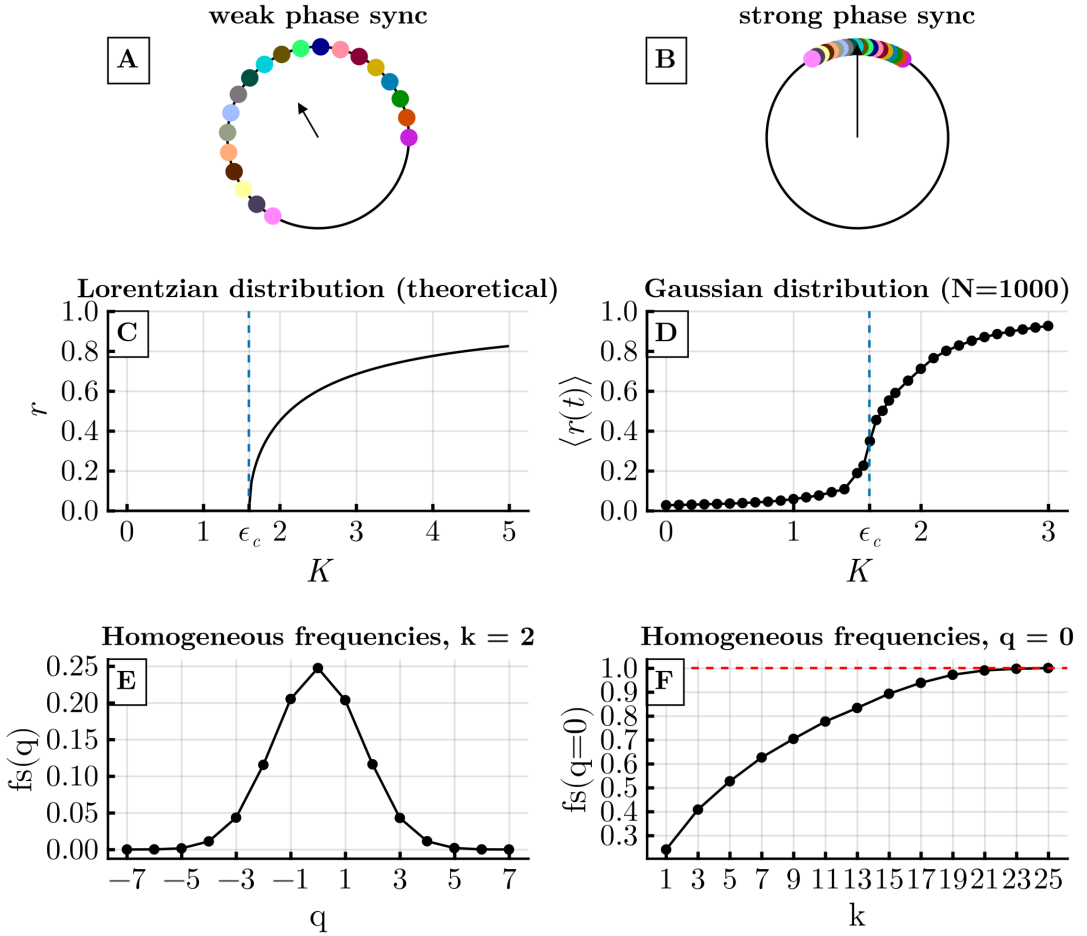


Figure 2.8: Basics of Kuramoto oscillators. Panels A and B respectively illustrate the concept of weak and strong phase synchronization (PS), captured by the complex order parameter Z (Eq. 2.35). The radius r denotes the degree of PS and the angle ψ denotes the centroid of the phases - respectively, they correspond to the magnitude and direction of the arrow in the figure. Panel C illustrates the behavior of the order parameter r as a function of coupling strength K (see Eq. 2.34) for a Lorentzian distribution of the frequencies (Eq. 2.38). The blue line denotes the critical coupling strength for the transition to synchronization. Panel D illustrates a similar behavior obtained from numerical simulations in a network of size $N = 1000$ under a Gaussian distribution of the natural frequencies. Only one attractor is ever observed in the simulations. Going now to homogeneous frequencies, panel E illustrates the fraction fs of randomly chosen initial conditions that converge to each q twisted state, in a network with $k = 2$ nearest neighbors. Panel F looks at this fraction for the completely synchronized state ($q = 0$) only, under different values of k . Panels E and F replicate results from [34].

One can switch to a corotating frame with angular velocity ω to get rid of the ω term and appropriately rescale time to get rid of ϵ and simplify down to

$$\dot{\theta}_i = \sum_{j=i-k}^{j=i+k} \sin(\theta_j - \theta_i). \quad (2.40)$$

Note therefore that changing the coupling strength in this system only rescales time, and does not change the state space significantly! This can be written as a gradient system $\dot{\theta} = -\nabla U(\theta)$, where $U(\theta)$ is a scalar differentiable function of $\theta \in \mathbb{R}^n$ [34, 57]. As a consequence, the only attractors in this system are equilibria [34]. Therefore to find all the attractors in the system one can first find the equilibria and then determine their linear stability. By doing this, one finds that the equilibria obey the relation:

$$\theta_i = \omega t + \frac{2\pi q}{N} i + C, \quad (2.41)$$

where $C \in \mathbb{R}$ is a constant and $q \in \mathbb{Z}$ is the twisting number. If one looks at the phase difference between two adjacent units one sees that it is constant across the ring: $\theta_{i+1} - \theta_i = \frac{2\pi q}{N}$. In particular, the completely synchronized state is included here in the $q = 0$ case. Some important stability results are:

- For small values of k many twisted states can be stable. As k is increased, these twisted states start to lose stability, with higher q values starting earlier. Eventually, the completely synchronized state ($q = 0$) becomes globally stable at $k > k_c \approx 0.34N$ [34].
- If we fix k and look at estimates of the size of the basins of all stable twisted states we find that they can be parametrized by a Gaussian curve [34, 36] (Fig. 2.8E).
- Estimates of the size of the basin of attraction for $q = 0$ increase monotonically with k (Fig. 2.8F): the completely synchronized state starts to dominate the state space for denser networks [34].
- The shape of the basins is still a topic under research, but they appear to form octopus-like structures. The twisted state itself (a point) is on the head of the octopus, which has a small volume around it. The majority of the volume of the basin is concentrated on the tentacles, which are structures that spread around in state space [36].

Studies have also been made for other topologies. Some important results have accumulated to show that networks with homogeneous frequencies are guaranteed to globally synchronize if the nodes are sufficiently well-connected (if the networks are sufficiently dense). Taking the least connected node, with degree k_{\min} , and comparing it with the maximum possible degree of the network, $N - 1$, one can define the network's connectivity μ as the ratio $\mu = k_{\min}/(N - 1)$. Then, in networks with $\mu > \mu_c$, the only attractor is the fully synchronized state. Estimates have that $\mu \in [0.6818, 0.7889]$ [72, 35].

Chapter 3

Small changes at single nodes can shift global network dynamics

Abstract

Understanding the sensitivity of a system's behavior with respect to parameter changes is essential for many applications. This sensitivity may be desired - for instance, in the brain, where a large repertoire of different dynamics, particularly different synchronization patterns, is crucial - or may be undesired - for instance, in power grids, where disruptions to synchronization may lead to blackouts. In this chapter¹, we show that networks of coupled phase oscillators with nonlinear interactions can acquire a very large and complicated sensitivity to changes made in either their units' parameters or in their connections. Even modifications made to a parameter of a single unit can radically alter the global dynamics of the network in an unpredictable manner. This occurs over a wide parameter region, around the network's transitions to phase synchronization. We argue that this is a widespread phenomenon that can be expected in real-world systems, extending even beyond networks of oscillators.

3.1 Introduction

Several systems of practical and theoretical importance are composed of, or can be modeled as, networks of interacting units. Examples from different research areas include power grids (networks of producers and consumers of electrical energy) [73], food webs [74], networks of electronic elements [75], coupled lasers [76], and neurons in the brain [77]. An important question is how the dynamics of single units impact the network's overall dynamics, and what happens if these units are modified. What happens to the dynamics if the units' parameters change? For instance, in ecological systems, what happens if the reproduction rate of a prey increases? In power grids, can a change in the parameters of a single generator cause a large disruption, such as a blackout? Also, what happens if the units' dynamical states are modified, e.g. by shocking the units into a different state? In the brain, how can an epileptic seizure be stopped by employing a current pulse in one particular brain region? These questions highlight the idea that a regime in which single-unit-changes can alter the whole network's behavior can be either dangerous or advantageous, and is an important topic of research which we address in this work.

In both power grids and the brain, an important phenomenon is synchronization, i.e. the coherence of frequencies or even phases of oscillations. For example, it is crucial for power grids to have their elements synchronized in the 50 – 60 Hz regime [78]. Moreover, several functional roles have been ascribed to synchronization in the brain [21, 77, 20].

¹This chapter is a modified form of a published manuscript: Kalel L. Rossi, Roberto C. Budzinski, Bruno R. R. Boareto, Lyle E. Muller, and Ulrike Feudel. *Physical Review Research* **5**, 013220 (2023).

For systems in which synchronization is an essential process for functioning, the question of sensitivity with respect to perturbations becomes particularly important. This has been recognized in the literature, and various types of perturbations have been considered to study the vulnerability either of the synchronized state itself or of the transition to synchronization [16, 18].

In this work, we show that systems become very sensitive to changes in parameters during transitions to synchronization, such that even changes to parameters of single units can radically alter the dynamics of the whole system. We call this phenomenon *dynamical malleability* [26], characterized by the fluctuations in network behavior caused by changes in the units' parameters or connections. Dynamical malleability can cause problems in real-world systems in two major ways: (i) the fluctuations in the dynamics can have a large magnitude, which can lead to drastic changes in the system's spatiotemporal dynamics and (ii) fluctuations are complicated and hard to predict, so that it is unclear which units or new parameter values can keep the networks in a similar synchronization state, and which others can not. Indeed, no method available in the literature to describe phase synchronization worked satisfactorily to predict the fluctuations we observe. This clearly important issue for the design and control of systems motivates our study to analyze the mechanisms that lead to these large fluctuations.

To address it concretely, we study networks of Kuramoto oscillators organized in ring lattices. They constitute a paradigmatic model for synchronization [79, 24, 25] and have been established as a model for real-world systems like the brain [80, 81, 25], Josephson junctions [82, 75], and chemical oscillators [83, 84]. The Kuramoto oscillators are phase oscillators coupled through a sine function of their phase differences. Networks with these units are well-known to have a transition from desynchronization (incoherent phases) to frequency synchronization (i.e. phase-locking, meaning constant phase differences [16]) and to phase synchronization (small phase differences) [85] as the coupling strength between units increases [25, 24].

In this work, we connect the oscillators in either of two classes of network topologies, which are of theoretical and practical importance [86]: Watts-Strogatz [70, 87, 88] and distance-dependent [89, 90]. They have very distinct properties, but in both a change in the topology from short-range to long-range connections leads to a transition to phase synchronization in the networks [91, 89]. During the transitions to phase synchronization, when the systems are only partially phase synchronized, they become dynamically malleable (i.e., sensitive to parameter changes), as illustrated in Fig. 3.1.

Furthermore, we also show that the number of attractors of the Watts-Strogatz networks increases during their transitions to phase synchronization, meaning that these systems also become especially sensitive to perturbations made to their units' states. This goes in line with recent studies for Kuramoto oscillators with identical frequencies [72, 36, 35] and for Kuramoto oscillators with inertia [32]. This increased multistability acts as a dynamical mechanism that can further increase the dynamical malleability.

Therefore, despite the wide literature and importance of synchronization, this phenomenon we describe of increased sensitivity to parameter changes, with complicated, hard-to-predict consequences to the synchronization, and which can be accompanied by multistability, has so been under-explored in the literature. Although reported sporadically in some recent works [30, 92, 93, 94], it has not been the focus, and thus has not been fully explored, until now. This becomes especially relevant when we note that the behavior is widespread, extending well beyond the Kuramoto networks studied here, as supported by our observations in a variety of topologies, by similar observations in

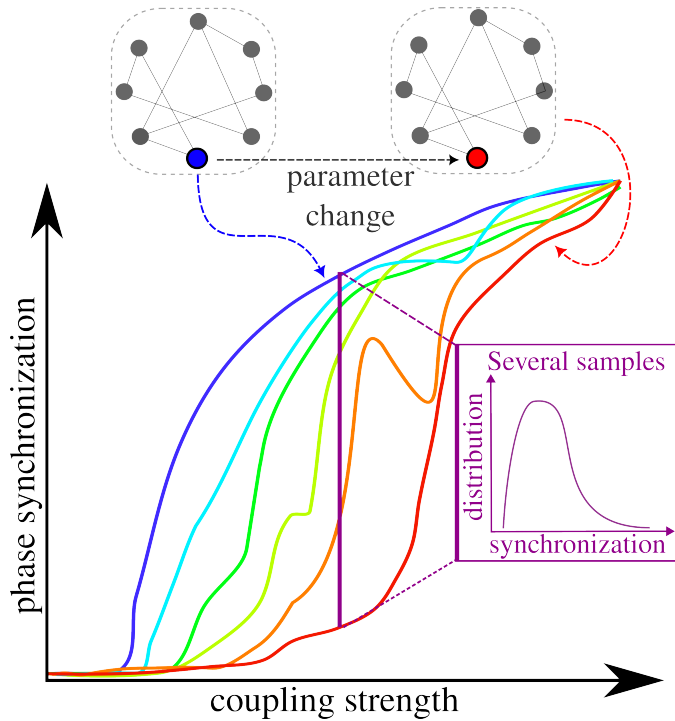


Figure 3.1: Sketch to illustrate the dynamical malleability in a typical transition to phase synchronization. Each realization of the system's parameters leads to a different transition to synchronization, i.e. a different curve in the figure. Realizations may differ from the others, for instance, in the parameter of a single unit. We see that the transitions to synchronization are different, as both the critical value of the coupling strength and the profile of the transitions differ, with the magnitude of malleability peaking during the transitions. Fixing the coupling strength, we can also look at the distribution of the degree of phase synchronization across samples (purple inset).

spiking [26] and bursting [94] neural networks, in cellular automata (which we exemplify in the Supplemental Material), and, importantly, by the statistical physics theory of finite-size effects on phase transitions, which we discuss later in the chapter.

We therefore hope to demonstrate the importance of dynamical malleability, and to encourage further theoretical advancements in this area, which are needed to properly describe the wide range of behaviors and to offer tools for practical applications.

3.2 Methodology

In the Kuramoto model [79, 71], each oscillator is described by a phase which evolves in time according to

$$\dot{\theta}_i = \omega_i + \epsilon \sum_{j=1}^N A_{ij} \sin(\theta_j - \theta_i), \quad (3.1)$$

where $\theta_i(t)$ is the phase of the i -th oscillator at time t , ω_i is its natural frequency, ϵ is the coupling strength, N is the number of oscillators, and A_{ij} is the (i,j) -th element of the adjacency matrix \mathbf{A} . Throughout this work, we initially draw each frequency randomly from a Gaussian distribution with mean $\mu = 0.0$ and standard deviation

$\sigma = 1.0$, generating a sequence $\{\omega_i\}, i = 1, \dots, N$. Then, different realizations can (i) shuffle these frequencies, generating another sequence $\{\omega_i\}_{\text{shuffled}} = \text{shuffle}(\{\omega_i\})$; or (ii) switch the frequency of one selected unit to another value ω_{new} .

The networks in this work are coupled in a ring lattice of $N = 501$ units with periodic boundary conditions, and follow one of two classes of topology. The first class is the Watts-Strogatz (WS) [70], which interpolates between regular and random topologies with a parameter p , the rewiring probability: at one extreme ($p = 0$), the topology is a k -nearest-neighbor lattice. From it, connections are randomly chosen according to the probability p and rewired to another randomly chosen connection. In doing this, the networks have a significant decrease in the mean distance between nodes, but remain very clustered, generating small-world topologies. The other extreme ($p = 1$) is then a random topology. These networks are unweighted, so their adjacency matrix's elements are $A_{ij} = 1$ if i and j are connected, and 0 otherwise.

The second class of networks follows a distance-dependent (DD) powerlaw scheme, in which any given node receives connections with weights decaying based on the distance to it. Each element of the adjacency matrix is $A_{ij} = \frac{1}{\eta(\alpha)(d_{ij})^\alpha}$, where d_{ij} is the edge distance between oscillators i and j , defined as $d_{ij} = \min(|i - j|, N - |i - j|)$, and $\eta(\alpha)$ is a normalization term given by: $\eta(\alpha) = \sum_{j=1}^{N'} \frac{2}{j^\alpha}$, such that the temporal evolution of the phases can be written as:

$$\dot{\theta}_i = \omega_i + \frac{\epsilon}{\eta(\alpha)} \sum_{j=1}^{N'} \frac{1}{j^\alpha} [\sin(\theta_{i+j} - \theta_i) + \sin(\theta_{i-j} - \theta_i)], \quad (3.2)$$

where $N' = \frac{N-1}{2}$ denotes half the amount of units to which i is connected to (one half of the ring's length, discounting the unit i itself). The equation explores the symmetry in the network to switch the summation across the network to a summation across only half, multiplied by 2. The powerlaw decay is thus controlled by α , the locality parameter. For $\alpha = 0$, the network is globally coupled with equal weights between every node. As α increases, the weights are redistributed, so that closer units (in terms of edge-distance) have bigger weights. At the extreme of $\alpha \rightarrow \infty$, only first-neighbors are connected.

The two classes have similarities: they have topologies dominated by short-range connections at one extreme and by long-range connections at another [95, 96]. They also have differences: the first class is sparsely connected, the other densely; the first has link-disorder (different rewirings lead to different networks), the second does not.

Integration was performed using the Tsitouras 5/4 Runge-Kutta (Tsit5) method for Watts-Strogatz networks, and an adaptive order adaptive time Adams Moulton (VCABM) method for distance-dependent networks. The integrator method was chosen for distance-dependent networks for increased simulation speed, and results were robust to different integration schemes. All methods used the DifferentialEquations.jl package [97], written in the Julia language [98]. Additional computational packages used were PyPlot [99] for plotting and DrWatson.jl [100] for code management. The code used for simulations is accessible in the repository [101], with the parameters used in the simulations. In particular, the control parameters we used (α , p and ϵ) were generated from a uniform distribution in the range of parameters showing interesting behaviors (e.g. the transitions to synchronization), then rounded to five decimal places and used in the simulations (in the case of p , the distribution was uniform in the log scale). These values are reported in all figures and text, and we emphasize that no value was chosen

specifically by hand: the behaviors we show in the figures are typical of the systems and can be obtained by randomly generating other values for the parameters.

We quantify the degree of phase synchronization of the network through the standard Kuramoto order parameter [79, 71, 24], which is the circular average of the units' phases

$$r(t) = \frac{1}{N} \left| \sum_{j=1}^N \exp(i\theta_j(t)) \right|, \quad (3.3)$$

with $i = \sqrt{-1}$. The quantifier ranges from 0 to 1: if $r(t) = 1$, all the phases are the same, and the system is completely globally phase-synchronized; if $r(t) = 0$, each oscillator has a pair that is completely out-of-phase, and the system can be completely globally phase-desynchronized or in a twisted state with units having distinct but linearly spaced phases. We typically describe networks by the temporal average $R := \frac{1}{T} \sum_t r(t)$ of their phase synchronization, with T being the total simulation time excluding transients.

3.3 Results

3.3.1 Introduction to dynamical malleability

The networks we study here, described in Eq. (3.1), follow the basic phenomenology of transitions to synchronization in Kuramoto networks [79, 24]. For very small coupling strengths ϵ , the oscillators are effectively uncoupled, and the phases oscillate without any significant correlation. As this ϵ increases, the instantaneous frequencies $\dot{\theta}_i$ align first, and the units' phases become locked, but not aligned: the system becomes frequency but not phase synchronized [16].

Then, whether the phases can align or not depends on the topology [102, 91]. In a two-nearest neighbor lattice, where only four nearby units are connected (two on each side), there is a topological limitation in the spread of interactions across the network that makes the oscillators arrange themselves in shorter-range patterns (Fig. 3.2(a)) (an exception might occur if the coupling strength is extremely high, much bigger than the relevant values studied here). If the short-range connections are randomly rewired to long-range connections, following for instance the Watts-Strogatz (WS) algorithm, the shorter-range patterns give way to longer-range patterns, and the oscillators start to phase synchronize ((b) and (c)), until eventually a strong (though not complete) phase synchronization (PS) is reached (d). This occurs at different stages for each realization: for instance, panels (c) and (k) reach a high degree of PS, with the longer-range patterns, but panel (g) does not.

In Fig. 3.2, the natural frequencies $\{\omega_i\}(i = 1, \dots, N)$ were kept constant across panels (a)-(d). Changing the frequencies, keeping the initial conditions $\{\theta_i(0)\}(i = 1, \dots, N)$ fixed, leads to a different realization (also called sample), with possibly different dynamics. If the frequency of a single unit ω_i is changed to an arbitrary new value, for instance $\omega_{\text{new}} = 3$, the network's behavior can be significantly altered (panels (e)-(h)). This is especially the case for networks with intermediate rewiring probabilities p , in which this single unit frequency change can bring the network from high to very low phase synchronization (panels (c) to (g)). The instantaneous frequencies typically remain synchronized, though their values might change. For random networks, phase synchronization is always maintained, though the instantaneous frequency values may also change.

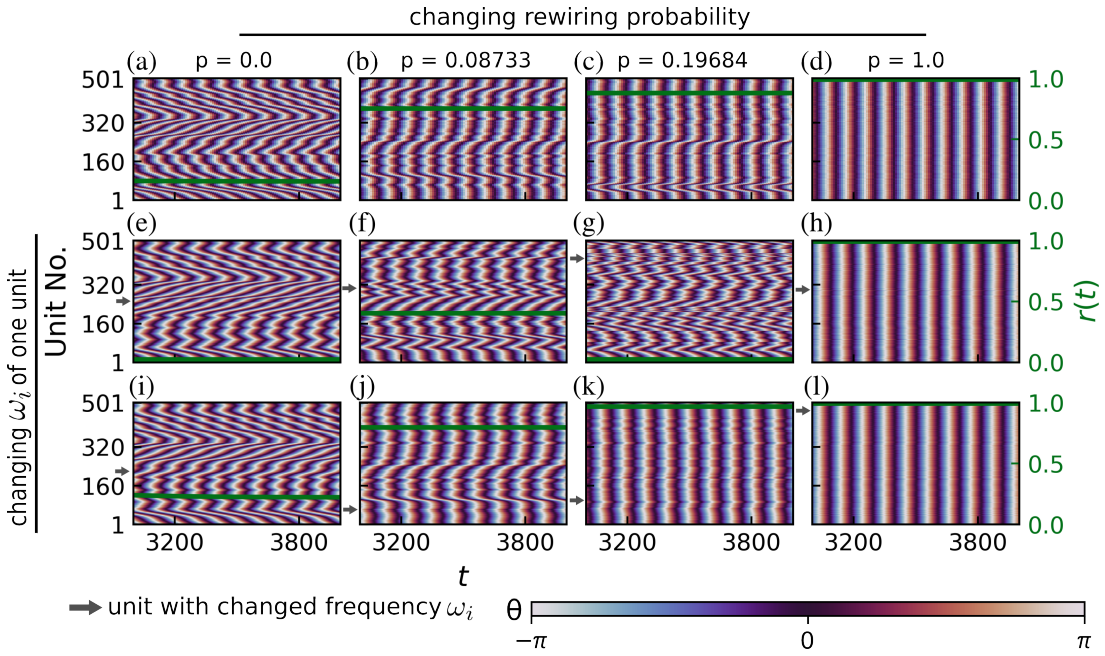


Figure 3.2: Transition to phase synchronization and the effect of a single-unit change. The figure shows the color-coded phases θ of all oscillators in the network and the degree of phase synchronization $r(t)$ (green line) across time for Watts-Strogatz networks. The coupling strength ϵ is fixed at $\epsilon = 4.51282$ and the natural frequencies ω_i in the first row are the same, generated by randomly drawing from a Gaussian distribution with zero mean and unitary standard deviation. Networks in the left column are two-nearest-neighbor lattices (rewiring probability $p = 0$); the short-range connections in these networks are then rewired in the following columns, with probability $p = 0.08733$ in the second column, $p = 0.19684$ in the third, and $p = 1.0$ in the fourth (leading to random networks). Increasing the proportion of long-range connections thus leads generally to more phase-synchronized networks. In the second and third rows, the natural frequency ω_i of a single unit i (indicated by the gray arrows) is changed to a new value $\omega_i \rightarrow \omega_{\text{new}} = 3.0$, with all other parameters being kept fixed. The units shown in the figure were those which led to the smallest (second row) or highest (third row) degree of phase synchronization R out of all $N = 501$ units in the network for each value of p . Initial conditions were the same for all simulations, and were randomly drawn between 0 and 2π .

Figure 3.2 thus illustrates that the long-term dynamics and phase synchronization differ in each realization. The realizations, created by changing the natural frequency of one unit, are distinct dynamical systems, so it is not surprising to observe distinct long-term dynamics. It is, however, interesting to observe how large these changes in dynamics can be, and how they depend on the topology. For instance, in networks of intermediate p (second and third columns of Fig. 3.2), the phase synchronization changes drastically. In random networks ($p = 1$, fourth column), they preserve the phase synchronization but alter the instantaneous frequencies of the oscillators (seen in the figure by the number of vertical lines). We also note that the behavior we describe is typical of the systems, and the values of p and ϵ used here were generated as described in Section 3.2. Since the fluctuations in the phase patterns (reflected in the phase synchronization) are clearer

and more pronounced than the instantaneous frequency patterns, we now focus on the phase synchronization of the networks.

3.3.2 Comprehensive view of dynamical malleability

To obtain a comprehensive picture we now study an ensemble of samples obtained by shuffling the frequencies ($\{\omega_i\}_{\text{original}} \rightarrow \{\omega_i\}_{\text{shuffled}} = \text{shuffle}(\{\omega_i\}_{\text{original}})$) or by changing the frequency of only a single unit to a new value ($\omega_{i,\text{original}} \rightarrow \omega_{\text{new}}$). We show in Fig. 3.3 the transitions to phase synchronization with increasing coupling strength or with switching from short-range to long-range connections. As expected from Fig. 3.2 we also find a large dynamical malleability (sometimes simply called malleability) during the transitions.

We study two classes of topology, Watts-Strogatz (WS, small-world) and distance-dependent (DD), described in Sec. 3.2. We consider ensembles as collections of networks with fixed coupling strength ϵ and topology (fixed rewiring probability p or locality parameter α) but distinct realizations of the natural frequencies $\{\omega_i\}$ [103]. Each ensemble in the figure contains 501 samples (realizations). We present the results using the mean degree of phase synchronization R for each realization, and the gap $\Delta := R_{\max} - R_{\min}$ between the most and least phase synchronized realizations in each ensemble. The gap Δ is chosen simply to illustrate the wide range of R values clearly, and we remark that very similar curves are observed by using the standard deviation over samples.

In Fig. 3.3, thicker lines represent an “original” sequence of frequencies $\{\omega\}_{\text{original}}$, from which other realizations (light lines) are created by shuffling all frequencies or changing the frequency of one unit to a new value $\omega_{\text{new}} = 3.0$. Each sample is a different dynamical system, and has a different transition to phase synchronization, which occurs at different values of ϵ , p , or α , and with a different profile (some have a small region of desynchronization while others do not, for instance).

This means that changing samples can lead to large changes in the behavior of the system, as we see throughout Fig. 3.3. First, we study the transitions induced by increasing the coupling strength ϵ for four representative types of networks (panels (a)-(d)), characterized by four specific values of rewiring probability p and locality parameter α .

In the red curves, networks are dominated by long-range connections, with $p = 1$ (random) and $\alpha = 0$ (all-to-all) and have a complete transition to phase synchronization (reaching $R \sim 1$), with the dynamical malleability (measured by Δ) increasing during the transition and returning to zero after. The all-to-all case is the finite-size version of the system originally studied by Kuramoto [71], and the critical ϵ values, when the transition occurs in each sample, are close to the $\epsilon_c = \frac{2}{g(0)\pi} = \frac{2\sqrt{2}}{\sqrt{\pi}} \approx 1.596$ predicted in the thermodynamic (infinite network size) limit. Its finite-size scaling properties and behavior have also been studied in [28, 30]. It is worth mentioning that this parallel between random networks and all-to-all networks, which have similar phenomenology, has been described in other works. Both have the same scaling exponents, belonging to the mean-field type [95, 96].

In the green curves ($p = 0.19684$ and $\alpha = 1.538463$) some connections have been rewired in the Watts-Strogatz networks, and weights redistributed for distance-dependent networks, from long-range to effectively short-range connections. On average, phase synchronization R decreases, though still remaining high. Some samples of WS networks also start to display regions of desynchronization: after the initial transition to high R , a

further increase in ϵ can desynchronize them (visible in panels (a) and (c), for ϵ roughly in [6, 7]). Therefore, the huge changes in R ($\Delta \sim 0.99$) due to changing samples can be attributed to two effects: the difference in their critical coupling strength (when the transition begins) [104], and also in their different post-transition behaviors (such as the desynchronization gaps that occur at different intervals of ϵ .)

In the purple curves ($p = 0.08733$ and $\alpha = 1.76923$), even more short-range connections become present. Phase synchronization R on average decreases, while the fluctuations Δ remain high and occur more evenly spread across samples.

Finally, for cyan curves ($p = 0$, two-nearest-neighbor chains and $\alpha = 3$, close to nearest-neighbor chains), the connections are short-range. Their phase synchronization is much smaller, and they do not reach a high degree of phase synchronization for any value ϵ we tested. These networks with short-range connections still have some degree of malleability, but not as high as the previous two cases.

Returning to frequency synchronization, we mention that for weak coupling strengths (roughly below $\epsilon \approx 3$), most of the samples in any ensemble are not frequency synchronized (see Fig. 3.13). Above this value, frequency synchronization becomes more common, especially for networks with more long-range connections, such that for sufficiently high coupling all samples become frequency synchronized. This is not the case for networks with mostly short-range connections ($p \lesssim 0.01$), in which some samples do not reach frequency synchronization even despite strong coupling. The presence of frequency synchronization in the short-range networks is consistent with the literature [105, 24] showing that frequency synchronization in first-nearest-neighbor chains is possible for sufficiently high ϵ in strictly finite systems. There are therefore also sample-to-sample fluctuations in the frequency synchronization of Kuramoto networks. They occur similarly to the fluctuations in phase synchronization, but are somewhat harder to visualize and have a less interesting dependence on parameters, justifying our focus on phase synchronization in this chapter.

We now move to the topology induced transitions, which occur by switching from short-range to long-range connections (varying p and α) while keeping the coupling strength ϵ fixed (Figs. (e-h)). A similar scenario occurs with a transition to phase synchronization, induced by changing either p or α . The dynamical malleability increases during the transitions, reaching significant values for both shuffled realizations and single-unit changes. The nearest-neighbor networks show some malleability, while the long-range dominated ones (random or all-to-all) show no malleability. We note here that the transition for WS occurs at $p \sim 0.1$, so we plot the figures on logarithmic scale to show the full transition to synchronization. This transition was already reported for WS networks in [91], but the authors used a linear scale for p and missed the full details of the transition that we see here, especially the sample-to-sample fluctuations; for distance-dependent powerlaw networks, a transition in phase and frequency was reported in [89]. However, none of these references studied the sample-to-sample fluctuations.

We conclude that either shuffling or changing a single unit can significantly alter the behavior of these systems, leading to a large dynamical malleability, in some cases over a very large range of parameters. This is particularly strong for WS networks, reaching $\Delta \sim 0.99$, close to the maximum possible value of $\Delta = 1.0$. The distance-dependent networks have weaker fluctuations, though still significant, reaching up to $\Delta \sim 0.7$.

Furthermore, we note that the networks with intermediate p or α and the short-range networks have dynamical malleability even for high ϵ . This is consistent with the known increase in the fluctuations near a phase transition [28, 106, 107] because the

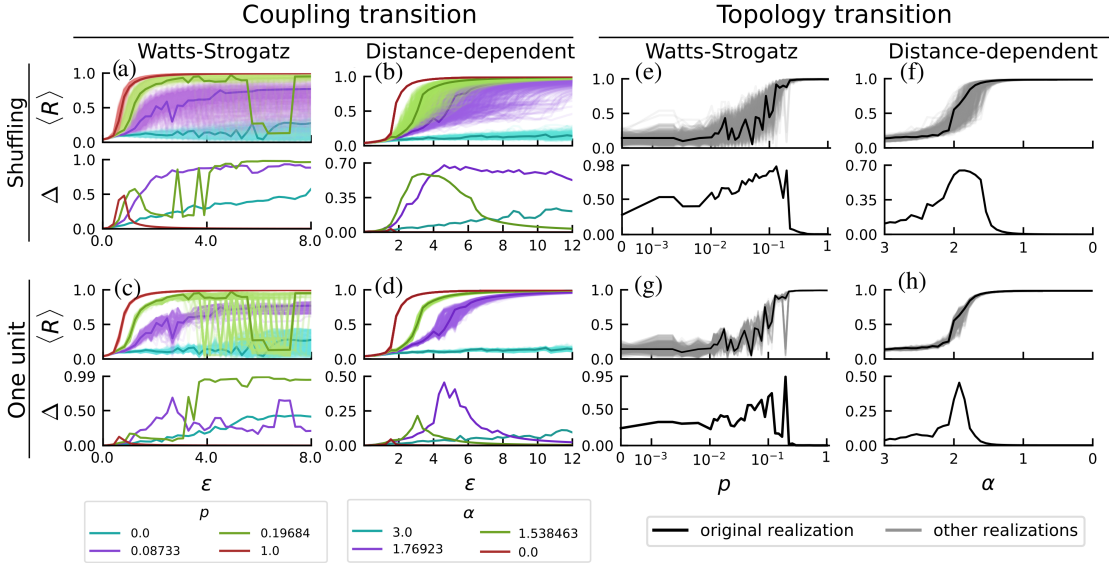


Figure 3.3: Transitions to phase synchronization and dynamical malleability. Networks under Watts-Strogatz (WS) and distance-dependent (DD) topologies reach phase synchronization through either an increase in coupling strength ϵ (given the topology has a sufficient amount of long-range connections) or by switching short-range connections to long-range. Fluctuations in the degree of phase synchronization R between samples increase during the transitions, as can be seen by the differences in the same-colored curves and by $\Delta := R_{\max} - R_{\min}$. Starting from a natural frequency sequence originally drawn from a Gaussian distribution (thicker lines), the other samples (thinner lines) can be generated by shuffling the natural frequencies or by switching the natural frequency of one unit to $\omega_{\text{new}} = 3$. For intermediate networks (purple and green curves), the increase in the fluctuations (i.e. in dynamical malleability) extends for a wide range of parameters and becomes considerably large. Each panel contains $501 = N$ realizations, with rewiring probabilities fixed for the coupling transition, with values shown in the legend, and coupling strength fixed in the topology transition at $\epsilon = 4.51282$ for WS and $\epsilon = 6.46154$ for DD. The initial conditions are the same across all realizations, and are randomly distributed from 0 to 2π . The curves of Δ are qualitatively similar with other dispersion measures, such as standard deviation, a possible difference being that the curves may be slightly shifted, as the measures can peak at slightly different values of the control parameter. We remark that the parameter values used in the simulations were generated as described in Section 3.2 and correspond to the typical behaviors in the system.

networks with these parameters remain close to the topology-induced transition. This is illustrated for WS networks in Fig. 3.4. It shows, in the $p-\epsilon$ parameter space, the average phase synchronization across samples \bar{R} on the first panel and the dynamical malleability measured by Δ on the second panel. Figure 3.4 provides a comprehensive view on both the coupling strength and the topology-induced transitions. The samples are realized here as shuffles, though a similar figure would be obtained by changing one unit. There is a single region of phase synchronization for sufficiently high coupling strength ϵ and rewiring probability p (panel (a)). Around the borders of this region, where the system is transitioning, the dynamical malleability is much higher (panel

(b)). It then becomes clear that the intermediate networks (green and purple lines), are near the topology-induced transition (for instance, black line) for all $\epsilon \gtrsim 1$. As ϵ increases, the networks remain near this p -transition, and so their dynamical malleability does not decrease. For the regular networks, we first note that the p -axis is shown on a logarithmic scale, such that these networks, with $p = 0$, are still relatively close to the transition at $p_c \approx 0.1$, and thus they also present significant malleability.

Figure 3.4 also illustrates the existence of two qualitatively different types of transitions: one induced by increasing coupling strength (for sufficiently high p), and another induced by increasing p (for sufficiently high ϵ). The difference between both is in their starting points. Both are globally phase desynchronized, but in the former (red, green, and purple lines), the weak coupling strength regimes have mostly uncorrelated oscillators, with no discernible structures in the phases or even synchronization in the frequencies. In the latter (black line), there are shorter-range structures with frequency synchronization for most samples.

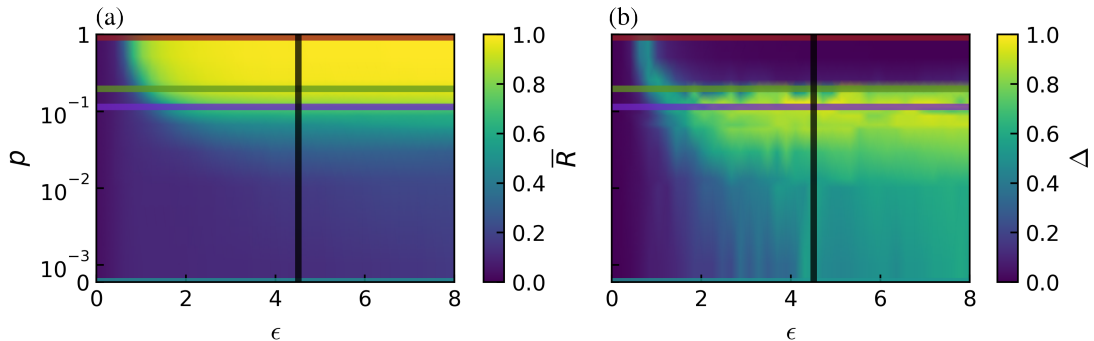


Figure 3.4: Dynamical malleability increases around the regions of transition to phase synchronization. The surface on the left shows the average degree of phase synchronization \bar{R} across the ensemble (1000 realizations of shuffled natural frequencies). The region of high phase synchronization is clearly seen for sufficiently high coupling strength ϵ and rewiring probability p . The colored lines correspond to the parameter values shown in Fig. 3.3. The right panel displays Δ , the difference between the most and least synchronized realizations for each pair (p, ϵ) , and we see that the fluctuations from sample to sample increase during the transitions to phase synchronization. The green and purple curves remain close to the region of transition for all $\epsilon \gtrsim 1$, such that their fluctuations do not decrease with an increase in ϵ . The figure uses Gouraud interpolation to ease visualization by smoothing the curves with a linear interpolation.

3.3.3 Unpredictability of dynamical malleability

For Watts-Strogatz networks, samples can be generated by resampling the topology instead of changing the natural frequencies. Since they are generated by a random rewiring process, different realizations generate different networks (there is link-disorder [96]). Therefore, different samples can also be generated by resampling the network while keeping the natural frequencies fixed. This generates a profile of dynamical malleability similar to that shown in Fig. 3.3(e), where the network was fixed and the natural frequencies were changed (see Fig. 3.11 for details).

Now, we wish to illustrate that no network, or natural frequency sequence, is alone responsible for leading to more, of less, synchronized states. Instead, the samples depend

sensitively on both, especially in the region of large STS fluctuations. Figure 3.5(a) shows the degree of phase synchronization for different realizations of the networks and different shuffles of the natural frequencies, all for $\epsilon = 4.51282$ and $p = 0.08733$ with fixed initial conditions. To aid the visualization, red rectangles indicate the network with the largest R for each shuffle. No network synchronizes more (or less) for any sequence of natural frequencies; and no sequence of natural frequencies synchronizes more for any network. Furthermore, if the ϵ , p , or initial condition are changed, the whole profile of the figure also changes. Another way to illustrate the complicated sensitivity in the

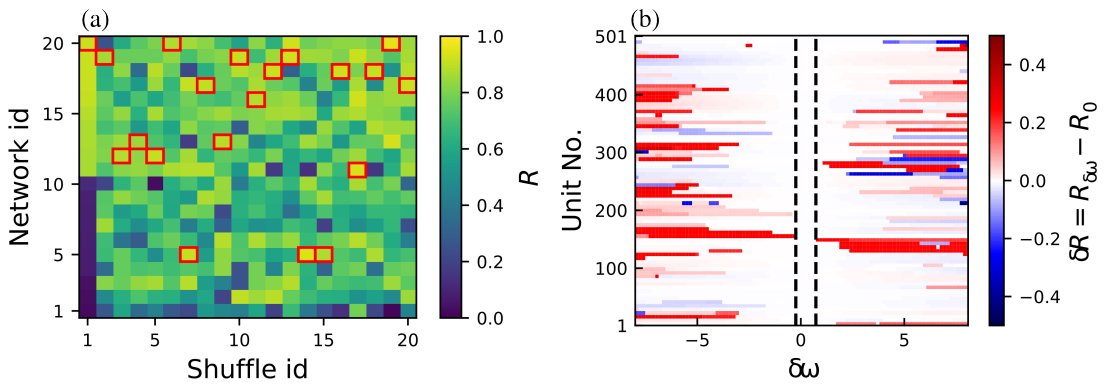


Figure 3.5: Fluctuations in dynamically malleable systems are unpredictable. Panel (a) shows the average phase synchronization R for fixed coupling strength $\epsilon = 4.51282$ and rewiring probability $p = 0.08733$ for different 20 shuffles of the natural frequencies $\{\omega_i\}$ and samples of networks generated by the Watts-Strogatz algorithm. For ease of visualization, the networks are ordered such that the highest network ids correspond to higher synchronization for Shuffle id = 1. For each shuffle, the network with the highest R is marked with a red rectangle. We thus see that no network synchronizes more for all shuffles: R is a function of both the specific frequency and topology samples. Panel (b) shows the changes δR in the phase synchronization R when the natural frequency of each unit is changed by an amount $\delta\omega$, such that $\omega_i \rightarrow \omega_i + \delta\omega$. Other parameters are fixed, in particular $p = 0.1145$ and $\epsilon = 4.51282$. There is a rough threshold (indicated by the black dashed lines), below which changing ω_i does not significantly alter R ($\delta R < 0.1$ for the figure). Furthermore, changing the frequency does not have a monotonic impact on the change in R : small alterations in ω_i , above the threshold, can have the same impact on R as bigger alterations.

region of high sample-to-sample fluctuations is by now fixing the network, and changing the frequency of a single unit by an amount $\delta\omega$. Fig. 3.5(b) illustrates the change δR in the phase synchronization, compared to the synchronization of the "original" ($\delta\omega = 0$) frequency realization. There is a rough threshold, at $|\delta\omega| \gtrsim 0.1$, below which perturbations in one unit do not significantly affect the network's phase synchronization. Above this threshold, however, large changes occur. They are asymmetric on $\delta\omega$ and occur non-monotonically (increasing $|\delta\omega|$ does not necessarily lead to bigger changes). This complicated pattern we observe could make the design and control of these systems quite difficult in practice.

3.3.4 Ratio of short to long-range connections

As we have seen, the rewiring of connections in WS networks, or the redistribution of weights in DD networks, from short-range to long-range connections leads to a transition towards globally phase-synchronized regimes. During these transitions, the dynamical malleability peaks for some ratio of short-range to long-range connections. To quantify this ratio, we first define the short-range connections to/from a node i as all existing connections to/from other nodes j within an edge distance d (with index $j \in [i-d, i+d]$), with d being the range of short connections ($d = 2$ here). For WS networks, we calculate the average degree (number of connections) for short-range (K_s) and long-range connections (K_l). For DD networks, we define an analogous measure of topological influence, which is:

$$K_s := \frac{2}{\eta(\alpha)} \sum_{j=1}^d \frac{1}{j^\alpha} \quad (3.4)$$

$$K_l := \frac{2}{\eta(\alpha)} \sum_{j=d+1}^{N'} \frac{1}{j^\alpha}. \quad (3.5)$$

Note that due to the symmetry of the DD networks, nodes share the same value of K_s and of K_l . The ratio κ of short-range to long-range connections is then defined as:

$$\kappa := \frac{K_s - K_l}{K_s + K_l}, \quad (3.6)$$

so that $\kappa = 1$ if only short-range connections exist, and $\kappa = -1$ if only long-range connections exist, with intermediate cases in between. In WS networks, the number of connections is $K = kN$ (k being the amount of neighbors of each node), with the number of long connections approximately $K_l = pK$ and short-range approximately $K_s = (1-p)K$. Therefore, the ratio κ can be easily calculated to be approximately $\kappa = 1 - 2p$. For DD networks, the ratio κ is given as

$$\kappa = \frac{\sum_{i=1}^d i^{-\alpha} - \sum_{i=d+1}^{N'} i^{-\alpha}}{\sum_{i=1}^{N'} i^{-\alpha}}. \quad (3.7)$$

Figure 3.6 shows this ratio κ calculated for the same setup of Fig. 3.3(e) and (f), shuffling natural frequencies with fixed coupling strength and changing p or α . The dynamical malleability is measured here by standard deviation χ across the samples, instead of Δ . The former makes the figure clearer, but the same analysis also works using Δ . A remark when comparing with Fig. 3.3 is that the two measures may peak at slightly different values of p or α . For both types of networks, the malleability peaks when there is a relatively small number of long-range connections present in a short-range-dominated network. It is more extreme for WS, as the ratios are closer to 1 than in the DD networks. This discrepancy in the ratios leading to higher malleability shows that κ is not an universal feature for any topology, but can still be important to understand their behavior.

3.3.5 Multistability

So far, we have changed natural frequencies while keeping initial conditions fixed. Now we invert this, and shuffle initial conditions to study the system's multistability. We

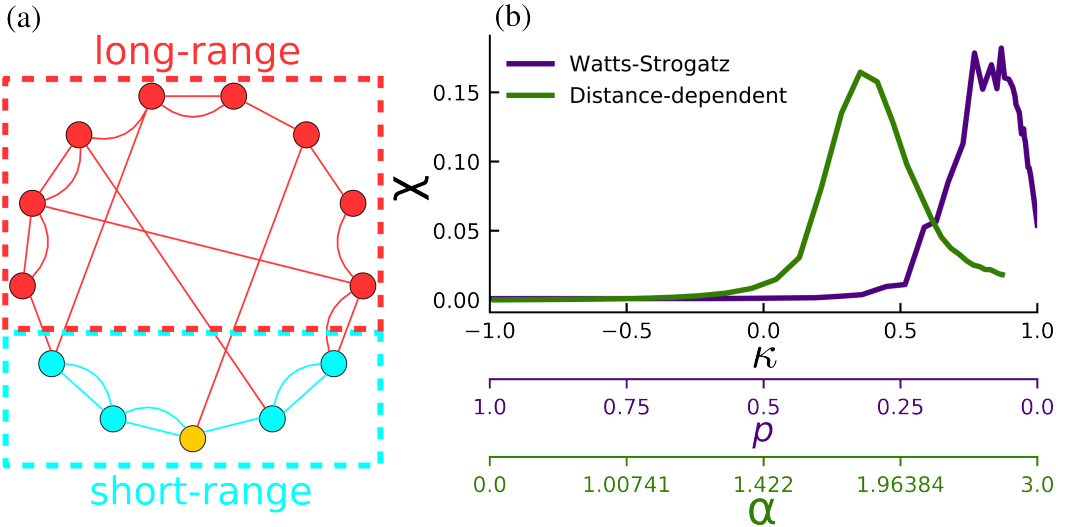


Figure 3.6: Dynamical malleability peaks within a narrow interval in the relation of short-range to long-range connections. Panel (a) illustrates the short-range (blue) and long-range (red) connections from the yellow unit for $d = 2$. Panel (b) shows the sample-to-sample fluctuations in the phase synchronization measured as the standard deviation χ of the distribution function of R against the ratio κ of short-range to long-range connections calculated for several distinct topologies p and α . The green curve corresponds to the distance-dependent networks, with $\epsilon = 6.46154$ and 501 realizations per α ; purple corresponds to Watts-Strogatz networks, $\epsilon = 4.51282$ and 1501 realizations per p . The bottom axis show the values of p and α for the respective ticks in κ (note that values of α are not equally spaced).

continue examining phase synchronization (PS) R , although we know that R is only a rough measure of multistability. Being a mean value, the same R could represent different attractors. Therefore, the number of attractors estimated based on R can only be considered as a lower bound. To remedy this, we also verified the findings by comparing several other features of the dynamics. These included the standard deviation of PS in time, the PS between each unit and its neighbors, the PS between sections of 100 units, the time-averaged instantaneous frequencies $\dot{\theta}_i$ of units, and the standard deviation, inter-quartile interval and gap between the unit's instantaneous frequencies. Realizations with unique values of all these features were considered as a distinct attractor. The number of such attractors agrees qualitatively with the dispersion we see in R , increasing during the transition.

The phase synchronization is thus shown in Fig. 3.7. Random networks ($p = 1$, red) seem to be monostable, with the small peak during their transition to phase synchronization being a numerical difficulty due to long transients. We confirm this in Fig. 3.8. Intermediate networks ($p = 0.19684$, green; $p = 0.08733$, purple) have a high degree of multistability, meaning coexistence of several attractors, with very distinct degrees of phase synchronization. No shuffle of the initial conditions leads here to the same attractor, so the system has at least 501 attractors, the number of different realizations tested. The 2-nearest-neighbor lattice has significant multistability for $\epsilon \gtrsim 4$. This is consistent with the literature for 1-nearest-neighbors, in which multistability occurs after the transition to phase-locking [31].

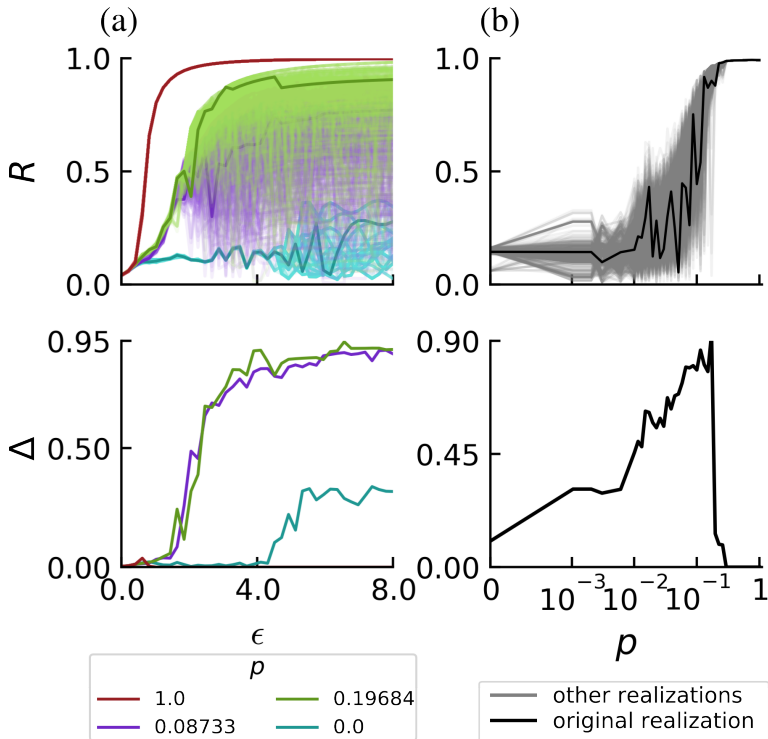


Figure 3.7: Multistability in WS networks. Phase synchronization and its dispersion for 501 different shuffles (thinner lines) of the initial conditions, taken from the original initial conditions (thicker lines) used throughout the rest of this work. All other parameters are fixed, including the natural frequencies as the original frequency distribution. The coupling strength ϵ (left panel) and rewiring probabilities p (right panel) are the same ones used for WS networks in Fig. 3.3. The multistable behavior is thus very similar to what we observed before by changing the frequencies (Fig. 3.3(a) and (e)), and so shuffling the initial conditions for this network also leads to large fluctuations in the phase synchronization.

To investigate further the multistability, we switch briefly to a smaller network with $N = 100$ nodes to facilitate the multistability analysis. We use the featurizing method introduced in Sec. 2.1.7. We have used the phase differences between the units as features for identifying the attractors, and performed extensive testing to ensure this works correctly. In particular, we compared these features with other well-known features, previously described, such as the network's global degree of phase synchronization and local degree of phase synchronization. The results were identical, and no attractor seemed to be missed. Further, we verified that the number of initial conditions used was enough, and that increasing the simulation or transient time did not alter the results. The attractors are identified in a continuation scenario, where previously found attractors are sampled and added to the pool of initial conditions used for the subsequent parameter. To match the attractors across parameters, the basin enclosure matching method proved to work best after extensive testing. This was also described Sec. 2.1.7.

We start analyzing a network with $p = 1.0$. For sufficiently long transient times, the algorithm finds only one attractor in state space for each coupling strength ϵ . In Fig. 3.8 we show three distinct networks, each with a different shuffle of the natural frequencies.

We see that the attractor of all networks has a transition to phase synchronization as ϵ increases. The very beginning of the transition is similar, and the very end is also similar. However, in the middle, during the transitions, the differences between the networks become large, since each network starts their transition at different ϵ . In this region where each network is different, switching from one network to the other (e.g., by shuffling the natural frequencies) brings the trajectories from one attractor that is highly synchronized to another that is still desynchronized, for instance. This corresponds to the increase in sample-to-sample fluctuations near phase transitions in finite networks.

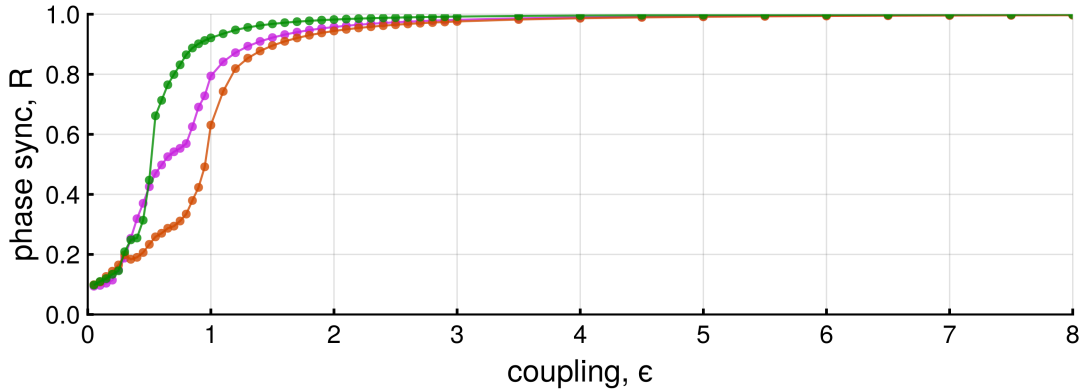


Figure 3.8: **Multistability in random networks with $N = 100$.** Each color in this figure corresponds to the single attractor existing across ϵ for different shuffles of the natural frequencies, with the topology fixed at $N = 100$ and $p = 1.0$. Only one attractor is found for each value of ϵ . These random networks therefore seem to be monostable. However, they are still malleable, as the different shuffles transition to phase synchronization at different coupling strengths ϵ , leading to sample-to-sample fluctuations.

The random networks therefore do not seem to be multistable. If we now switch to small-world networks we see the emergence of many attractors. Figure 3.9 shows the identified attractors for one realization of the natural frequencies - meaning only the coupling strength is changed across simulations. The top panel again shows the degree of phase synchronization of the identified attractors. We see that the initial attractor, in purple, present for small ϵ remains as ϵ is increased. And more attractors eventually appear in the system. One such attractor, in gray, eventually becomes the most synchronized attractor (MSA). The basin of attraction of the MSA also seems to dominate the state space, as shown in the bottom panel, where the fraction of initial conditions converging to each attractor is shown. The MSA already emerges with a large basin of attraction. Interestingly, the size of the basins varies considerably across attractors, suggesting a rich organization of the basins in state space. This analysis uncovers the rich multistability in these systems, and confirms the results we obtained previously for the $N = 501$ networks. It does not immediately reveal the bifurcations giving rise to the attractors, and does not provide information about the structures of their basins of attraction. Further work is needed in the future to better understand this.

The multistability can enhance the sensitivity of the networks to parameter changes,

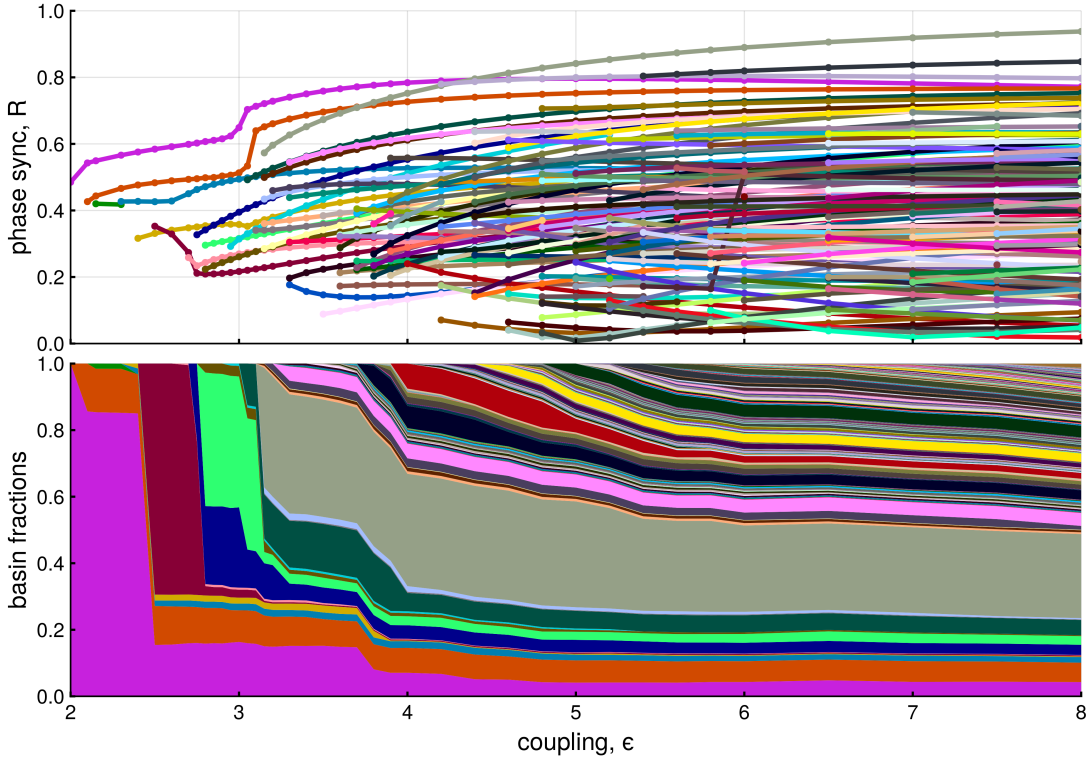


Figure 3.9: **Multistability in a small-world network with $N = 100$.** The network is fixed, including the natural frequencies and topology with $N = 100$ and $p = 0.08$. Each color in this figure corresponds to an attractor, matched across different ϵ . The top panel shows the time-averaged degree of phase synchronization R while the bottom panel shows the fraction initial conditions converging to each attractor for each ϵ . A rich multistability is therefore observed, with attractors having differently sized basins of attraction, as ϵ becomes sufficiently large. The gray attractor exhibits a typical transition to phase synchronization, but other attractors do not necessarily. The analysis was done using the featurizing and continuation algorithms described in Sec. 2.1.7.

and helps to explain the large fluctuations we observe. In this case, a parameter change needs only to change the boundaries of the basins of attraction for the same initial condition to land on a completely different attractor. Attractors do not have to be necessarily drastically changed for the large dynamical malleability to be observed. However, multistability is not in principle required for STS fluctuations; in fact, the random and the distance-dependent networks appear to be monostable (not shown), though they are malleable.

3.3.6 Distributions of samples

As we have seen, shuffling initial conditions can also generate realizations with widely different dynamics, similarly to shuffling natural frequencies. But the two methods to create an ensemble of samples have different effects, and can generate samples with distinct distributions. As shown in Fig. 3.10 for Watts-Strogatz networks, shuffling frequencies usually leads to a broader, and smoother, distribution of R . This increased

broadness shows that new attractors are indeed created by shuffling the frequencies, so that multistability itself cannot account for the dynamical malleability we discussed previously. Furthermore, the transitions to phase synchronization occur through an increase in the distribution's average. The accompanying increase in the width of the distribution shows an increase in dynamical malleability, which goes to zero only for long-range networks ($p = 1$).

Specifically, the distributions for the two-nearest-neighbor lattice ($p = 0$, panels (a)-(e)) are quite different: shuffling frequencies leads to a smooth distribution, whose average shifts to the right as ϵ is increased; for shuffling initial conditions there is also a slight increase in the distribution's average as ϵ is increased, but the distribution itself is dominated by several peaks. For intermediate networks ($p = 0.08733$ and $p = 0.19684$, panels (f)-(o)), the skewness of the distribution becomes negative, and shuffling initial conditions has a smoother behavior, more similar to shuffling frequencies. Interestingly, the distribution can be bi-modal, with the two modes being separated on either extreme of R (panels (n) and (o)). For $p = 1$ (random network), the two first coupling strengths (panels (p)-(q)) occur during the narrow interval of significant malleability, during the transition to phase synchronization. Soon after $\epsilon > \epsilon_c \approx 1.6$, the distribution becomes extremely narrow.

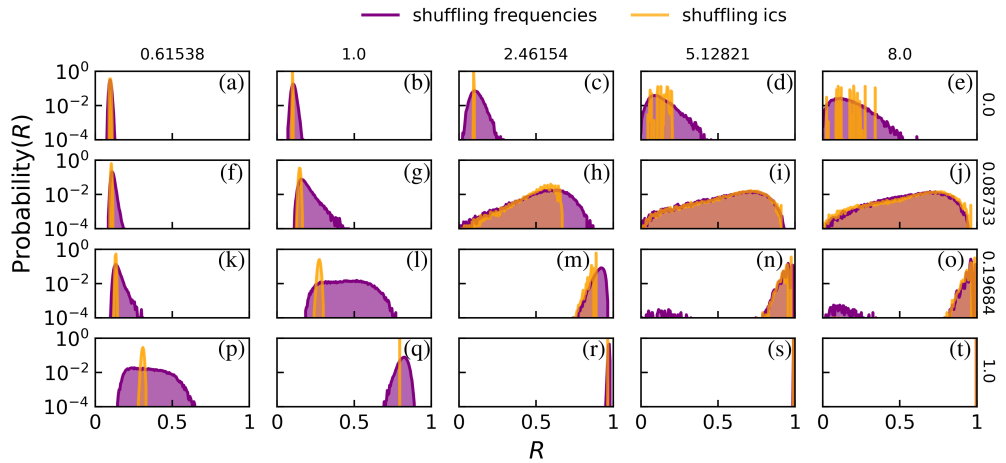


Figure 3.10: Distributions of R due to shuffling frequencies or initial conditions. Each panel contains the distribution of the mean degree of phase synchronization R across 20000 shuffles of natural frequencies (in purple) or initial conditions (orange) for Watts-Strogatz networks. The rewiring probabilities p are indicated on the right of each row, and are the same as used in Fig. 3.3(a); the coupling strengths ϵ are indicated on the top of each column. Bin size is 0.005, and the probability for each bin is calculated as the occupation of the bin divided by the total occupation across all bins, and is shown in logarithmic scale.

It is worth mentioning that very similar distributions are obtained if, instead of shuffling the frequencies or initial conditions, we re-sample them from the distribution (i.e. change the seed in the random number generator). Interestingly, the distributions are not Gaussian, which is inconsistent with the assumptions made in other works [28, 96]. In these works, the authors argue that the fluctuations must be normally distributed for sufficiently large networks and many samples due to the central limit theorem. This

inconsistency is likely generated by the finite size of the networks studied here. Even in all-to-all networks, in which there is no topological disorder, the distributions are not Gaussian for $N = 501$. Results (not shown) indicate that the distributions approach Gaussian distributions as N is increased to 5000.

3.4 Discussions and conclusions

Summary

In this work, we have studied the sensitivity of networks to changes in their units' parameters or connections, which we call their dynamical malleability, and showed that, near transitions to phase synchronization, this behavior acquires (i) a large magnitude, as changes to single units can radically alter the spatiotemporal dynamics, and (ii) a complicated sensitivity, as no analytical method we have tried was able to satisfactorily describe the changes to the dynamics. Parts of this behavior have been observed in isolation previously [26, 92, 91, 30, 93, 94] but this is, to the best of our knowledge, the first work to focus specifically on it and show its full phenomenology.

To study this concretely, we have chosen ring networks of Kuramoto phase oscillators and connected the units in two distinct classes of topology, Watts-Strogatz (WS) and distance-dependent (DD). We have either changed the frequency of a single unit or changed the frequencies of all units by shuffling (i.e., redistributing) the values of the frequencies across units. The first has allowed us to verify the impact of relatively small changes, which are still not small enough to be described in the linear regime; the latter allowed us to verify the impact of redistributing the values in the network while keeping the distribution of parameters exactly the same, which is helpful for identifying mechanisms for the fluctuations.

Mechanisms for dynamical malleability

The two classes of topology we used have different characteristics (see Sec. 3.2) but are similar in that they lead to networks that have two distinct types of transition to phase synchronization: one induced by increasing the coupling strength and another by increasing the dominance of long-range connections. They also have differences, mostly notably that (i) the WS networks acquire a large number of attractors during their transitions to phase synchronization (i.e. become highly multistable), while the DD networks remain with one main attractor (and possibly other attractors that would have very small basins of attraction), and that (ii) the WS networks have a larger magnitude of dynamical malleability. We believe that this larger magnitude is caused by two effects: the increased number of attractors and the topology's link-disorder.

Firstly, we remark that the dynamical malleability is manifested in the networks' transitions to phase synchronization in two distinct ways. The first is through diverse onsets of the transition, as different realizations start their transitions at different values of the control parameter. This is the well-known blurriness of phase transitions described in studies of finite-size effects [106, 108]. This effect is clearly present in both networks (see, e.g., Fig. 3.3(a) and (b)). The second manifestation of malleability is in the post-transition fluctuations, i.e., in the sudden changes of synchronization that occur after the network has seemingly transitioned to synchronization (see, e.g. Figs. 3.3(a) and (c)). This effect is present here mostly in the WS networks, but is also known in other

systems of finite size (see, e.g. Figs. 3.15(b) and (d) for the case of cellular automata). It is caused at least partly by the system's multistability, as increasing the parameter can change the shape of the attractors' basins of attraction, making the same initial condition suddenly go to another attractor. So the WS networks, which have a much larger number of attractors, exhibit this additional effect that increases their malleability, while the DD networks do not.

We further remark that multistability could have an even more pronounced impact on malleability if the basins of attraction were complexly interwoven. Then, even very small changes could lead to significant fluctuations. But this does not appear to be the case in any of the networks we studied, all of which seem to have smooth basin boundaries (Fig. 3.14) - it is thus noteworthy that the already high dynamical malleability we have described can occur even with smooth basin boundaries. It can even occur in the absence of multistability, as seen in the DD networks.

The second mechanism for the increased malleability in WS networks is their link-disorder [96]: different realizations lead to different topologies for a same parameter, and we observe a very similar phenomenology by comparing different realizations of these topologies (Fig. 3.11). This is a source of disorder, and thus, of fluctuations, that is not present in the DD networks.

Mechanisms for the fluctuations

As we have mentioned, the fluctuations in the malleable networks are also hard to predict. The behavior of the systems is clearly a complicated function that involves the coupling strength, topology, natural frequencies, and initial conditions all together. For instance, we have not found a sequence of frequencies, or a specific network realization, that always leads to more (or less) synchronized networks (Fig. 3.5(a)). Even for fixed frequencies and topology, the most phase synchronized realization changes depend on the initial condition or the coupling strength. Changes in the natural frequency of single units also lead to non-monotonic changes in the network's phase synchronization: the change in frequency can either increase or decrease the synchronization level, depending on the chosen unit, coupling strength, and topology (Fig. 3.5(b)).

As a consequence, we are unable to identify a specific unit, or magnitude of perturbation, that is always responsible for the greatest disruption. That is, no available theory in the literature that we have tried revealed a mechanism for the fluctuations capable of predicting them. This is a surprising result, considering the quality of the available theories, the amount of research and important advancements in the description of networks similar to the ones studied here [30, 109, 110, 111]. We believe that this is mainly caused by the networks' multistability, which cannot be handled by some theories, and by the wide range of synchronization patterns.

The first theory we tried is the synchrony alignment function, which depends on the topology and natural frequencies and was shown analytically to be related to the degree of phase synchronization in the limit of strong synchrony [109]. It does not work satisfactorily for any dynamically malleable network that we tested. One reason for this is the weak phase synchronization in some realizations, which breaks the assumption of the method. Another, even stronger, reason is that our networks are multistable, such that the relation between the synchrony alignment function and the degree of phase synchronization given by the method cannot be satisfied for all attractors of the system. Indeed, it only worked perfectly in the strongly phase synchronized regime, which is also

monostable.

The second theory we tried is due to Peter and Pikovsky [30], who showed in all-to-all networks that different realizations of the natural frequencies synchronize differently depending on the kurtosis of the distribution. This mechanism cannot even be expected to work for the shuffling scenarios we study since they conserve the frequency distributions and thus the kurtosis as well, but we have verified that it also does not work when the units' frequencies are changed. An additional reason why this does not seem to apply in our systems may be in the topologies, which are not all-to-all.

Thirdly, we have tested other measures that have been observed in the literature to correlate to phase synchronization, and they do not work in the malleable networks. These are: (i) the proportion p_- of links connecting nodes with natural frequencies of different signs [110]; (ii) the correlation c_ω between the oscillators' natural frequencies, taking into account the connectivity of the network [110, 111]; (iii) the correlation between natural frequencies and the node's number of connections [109]; and (iv) the correlation between the average frequency between neighbors of a node and the node's own frequency [112, 109]. These results also cannot be expected to work in multistable networks, and indeed did not work in our networks.

Relation to statistical physics and scaling

As noted previously, there is a relation between our dynamical study here and studies on the statistical physics of networks. The transitions to phase synchronization that we see correspond to non-equilibrium phase transitions [71, 30], such that we can connect the dynamical malleability we analyze with the well-known sample-to-sample (STS) fluctuations in statistical physics. These are usually described in finite systems, in which different samples have different statistical properties that lead to distinct phase transitions - the transitions are usually said to be shifted between samples [113, 29, 28], which is one of the mechanisms we described for the malleability. As seen in these studies, the size N of the system (i.e. the number of nodes) influences the magnitude of the dynamical malleability as well as the interval of parameters in which it occurs. The networks we have presented in the results have $N = 501$ oscillators, and scaling analysis (Fig. 3.12) reveals that the intervals of high malleability decrease with the size N , as expected from other studies. For instance, authors in [28] describe the range of ϵ for high malleability as scaling with $N^{-2/5}$ for all-to-all networks.

For the WS networks, malleability is still significant for even up $N = 5000$ oscillators. Moreover, the maximum magnitude of the fluctuations does not decrease significantly, and networks with $N = 5000$ can still reach $\Delta = 0.9$. This suggests that the malleability gets restricted to a smaller region in parameter space, but might not decrease significantly in magnitude for bigger networks. In the limit of infinite-size networks, it would get restricted to a single line, defining the two types of transitions to phase synchronization, and remain non-zero there. This is consistent with a study in all-to-all networks of Kuramoto oscillators, where this behavior was observed [104]. In fact, this behavior is well-known for phase transitions with quenched disorder (heterogeneous parameters), when systems are said to be non-self-averaging [114]. In any case, networks of $N = 5000$ units can be regarded as rather large in several real-world applications [30], so the STS fluctuations we describe here occur for a significant range of system sizes.

Generality of the behavior

Additionally, we show that the increase in dynamical malleability is widespread in the parameter space of the systems. Looking at this space, spanned by coupling strength and the parameter controlling the topology, the dynamical malleability remains high over a wide parameter range around the two types of transitions to phase synchronization. In particular, networks with an intermediate amount of long-range connections are highly malleable for any coupling strength ϵ we tested (e.g. green and purple lines in Fig. 3.3). This is because the topology is fixed, so the networks remain close to the topology-induced-transition even though they are far from the coupling-strength-induced-transition.

We also remark that the phenomenology we describe also occurs for wide ranges of topology and coupling strength values, for distinct frequency distributions, such as Cauchy-Lorenz (not shown), and for other dynamical models. For instance, previous works on spiking [26] and bursting [94] neural networks have revealed a very similar phenomenology. We also show similar behavior for cellular automata (see Fig. 3.15). We have observed (not shown) similar behavior in small-world networks generated by adding long-range connections and keeping the short-range ones [115]. Other works have also observed dynamical malleability in Kuramoto oscillators coupled under both human-connectome structural networks and hierarchical-modular networks [116, 117]. Additionally, of course, the theory of phase transitions and, consequently, of sample-to-sample fluctuations is known to apply for a variety of distinct systems.

Practical importance of malleability

The discussions lead to an interesting question: is dynamical malleability good or bad? On the one hand, large fluctuations can be undesired. For instance, a large fluctuation could take power grids from a phase synchronized regime to a desynchronized one, and lead to blackouts. On the other hand, fluctuations can be desired due to the increased flexibility in the systems. They could be a useful mechanism for adaptation, learning or memory formation in neural circuits. More specifically, an important property of the brain is that it can separately process information from different types of input in segregated areas, and then integrate them all into a unified representation [118, 119, 120]. For this reason, Tononi and colleagues conjectured that the brain needs to have an optimal balance between segregation and integration of areas [118]. In this optimal balance, the synchronization between different brain regions needs to fluctuate from low synchronization to high synchronization [121]. Therefore, having a large dynamical malleability can be an advantageous feature, allowing for this high variability to be achieved through small changes in the neurons, e.g. their firing rate, or their connections. There is also interesting evidence for this in [122], which reported that high-frequency firing of neurons can drive changes in the global brain state.

Future research and conclusions

An interesting line of research opened here is to understand ways to quench or to explore the fluctuations between realizations, using the framework we establish here, for practical applications. Another interesting line of research is to consider the effects of noise or time-dependent forcing on malleable systems: since they have a wider range of dynamical states available by changing parameters, a time-dependent change in the parameters,

induced by the noise or forcing, can lead to transitions between several different states. The complicated and sensitive dependence on the parameters would mean that even small amplitude changes could lead to drastic fluctuations. For the Watts-Strogatz networks, multistability can complicate the dependence on external inputs, and make the effects dependent on the timing of perturbations, as different states, all of which coexist, can react differently to the parameter changes. Understanding these behaviors is important, for instance, in the context of neural systems, where external influences are common and where temporal fluctuations are essential.

Future research is also needed to fully describe the mechanism for the fluctuations between realizations. An interesting possibility could be to extend the synchrony alignment function [109] to weakly synchronized regimes or to multistable systems. Another promising approach would also be to apply the formalism introduced in [123, 124]. A third possibility would also be to use the model reduction method by [125]. These would be important theoretical contributions for the understanding of phase synchronization in oscillator networks and for the role of each unit in a network.

To summarize, the increased magnitude and complexity of dynamical malleability shown here is a general phenomenon in finite-size systems that can be expected to occur in real-world systems.

Acknowledgments

We would like to thank Jan Freund and Arkady Pikovsky for helpful discussions. K.L.R. was supported by the German Academic Exchange Service (DAAD). R.C.B. and L.E.M. acknowledge the support by BrainsCAN at Western University through the Canada First Research Excellence Fund (CFREF), the NSF through a NeuroNex award (#2015276), SPIRITS 2020 of Kyoto University, Compute Ontario (computeontario.ca), Compute Canada (computecanada.ca), and the Western Academy for Advanced Research. R.C.B gratefully acknowledges the Western Institute for Neuroscience Clinical Research Postdoctoral Fellowship. B. R. R. B. acknowledges the financial support of the São Paulo Research Foundation (FAPESP, Brazil) Grants Nos. 2018/03211-6 and 2021/09839-0. The simulations were performed at the HPC Cluster CARL, located at the University of Oldenburg (Germany) and funded by the DFG through its Major Research Instrumentation Program (INST 184/157-1 FUGG) and the Ministry of Science and Culture (MWK) of the Lower Saxony State, Germany.

Additional information

Malleability due to changes on the topology

In the main text of this chapter, we focus on the dynamical changes arising from changing natural frequencies of the oscillators. However, similar changes occur if the natural frequencies are kept fixed and the topology is changed instead. To show this, we study the dynamical malleability during the topology-induced transition in Watts-Strogatz networks. Since the Watts-Strogatz networks are generated by a random rewiring of connections with probability p , different realizations of the rewiring (i.e. of the link-disorder) lead to different networks. In Fig. 3.11, we show the result for 500 distinct realizations for each value of p , and we see an increase in the dynamical malleability during the transition to phase synchronization, very similarly to the results for shuffling

natural frequencies. These results corroborate the generality of the increased dynamical malleability near synchronization transitions - networks are similarly sensitive to disorder in both parameter types, frequency and topology.

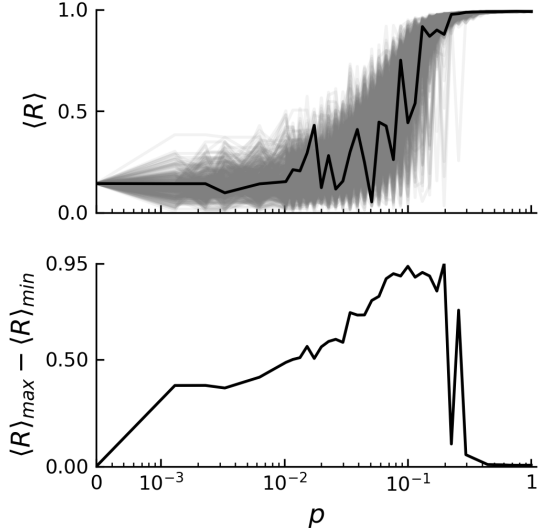


Figure 3.11: Resampling topology has very similar effects to shuffling frequencies. Analogous to Fig. 3.3e, keeping the original frequencies and initial conditions, but simulating networks generated via the Watts-Strogatz algorithm with a different seed for the random rewiring. Resampling topology has a similar effect to resampling the natural frequencies by shuffling, for instance.

Scaling of malleability

How does the amplitude of dynamical malleability (i.e. the sample-to-sample fluctuations) depend on the size of the networks? To study this, we repeat the parameter space shown in Fig. 3.4 of the main text for smaller and bigger networks. Smaller networks have significant dynamical malleability spread over a wider region of the parameter space, which is consistent with the fact that phase transitions become more blurred in smaller networks, meaning the transitions occur over wider regions. As the network size increases, the region with dynamical malleability decreases, as the transition curves move closer to the transition in the thermodynamic limit. This is qualitatively consistent with calculations made in (Hong et al., *Physical Review Letters* 99, 184101, 2007) for all-to-all networks. The amplitude of the malleability is extremely large for smaller networks, and the difference Δ between the most and least synchronized samples for $N = 25$ can reach $\Delta = 0.99$. Interestingly, this amplitude does not decrease rapidly with network size, and remains high for even $N = 5000$. In this case, $\Delta = 0.88$ was reached in the most malleable cases. This suggests that the dynamical malleability remains non-zero in the vicinity of the transition (the critical line) for networks with size $N \rightarrow \infty$, a phenomenon called non-self-averaging. Indeed, all-to-all networks were suggested to be non-self-averaging in (Hong et al., *Journal of the Korean Physical Society*, 49 5, 2006). The results point out qualitative consistency in the scaling for Watts-Strogatz and all-to-all networks already reported in the literature, and show that the behavior we observe here can occur for a wide range of network sizes.

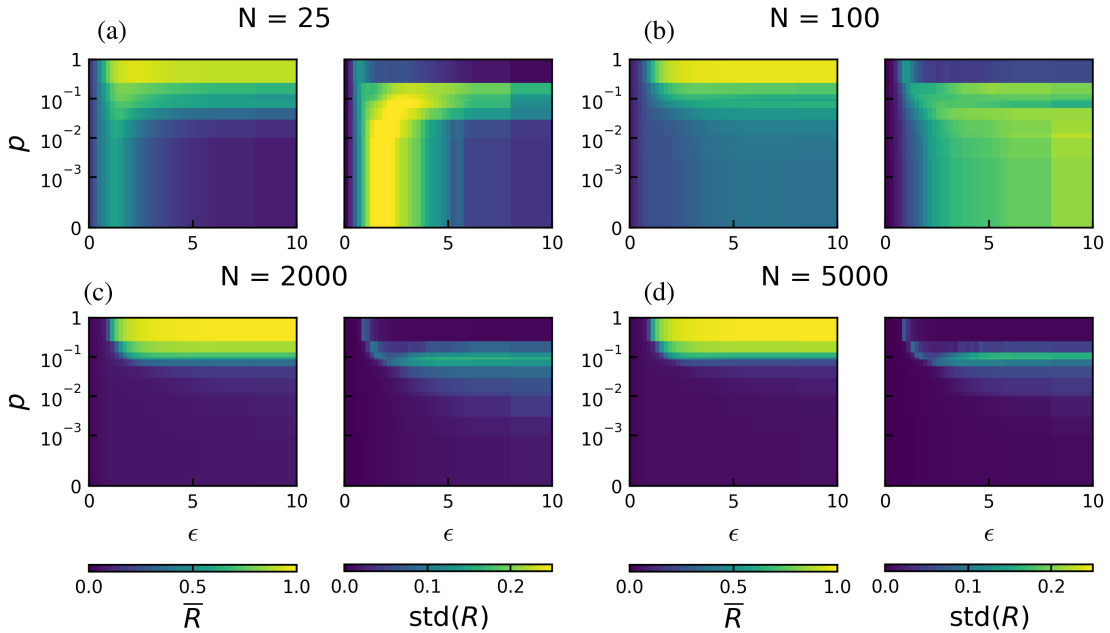


Figure 3.12: **Scaling of malleability with system size.** For each network size N , the left panel shows the time-averaged degree of phase synchronization averaged over 501 samples of the natural frequencies and over 5 samples of topology; while the right panel shows the standard deviation over the samples, averaged over the topologies. The region of significant sample-to-sample (STS) fluctuations decreases with the network size N , but the peak of fluctuations (measured through either standard deviation of gap Δ) decreases only slightly up to $N = 5000$, reaching $\Delta = 0.9$ there. The decrease in the size of the STS fluctuations region is described by (Hong et al., *Physical Review Letters* 99, 184101, 2007) for all-to-all networks as scaling with $N^{-2/5}$. The scaling in the magnitude of the STS fluctuations seems to suggest the networks are non-self-averaging.

Frequency synchronization and temporal fluctuations

We have focused in this work mainly on the synchronization of the phases θ , and not on the instantaneous frequencies $\dot{\theta}$. As stated in the main text, this is because the arrangement of the phases, measured by the degree of phase synchronization, is the quantity that changes most and more clearly. To understand this, we can look at measures of the degree of frequency synchronization in the same parameter space as in Fig. 3.4. Commonly, the instantaneous frequencies $\dot{\theta}$ are distributed across different orders of magnitude, with several units having $\dot{\theta}$ close to the average, at 0, and a few outliers with $|\dot{\theta}| \sim 10$. Because of this, we use three different dispersion quantifiers, measuring different aspects of the distribution : (i) the interquartile interval IQI measures the difference between the 75th and 25th percentile of the distribution, and so is a measure of dispersion of the bulk frequencies, excluding outliers; (ii) the standard deviation, calculated as usual, which thus considers the bulk and the outliers; (iii) the gap of the distribution, meaning the difference between the maximum and minimum values, which thus only considers the outliers. Each of these quantifiers is applied at each time step of the time-series and then averaged over time so that we obtain $FS_k := \langle k(\{\dot{\theta}(t)\}) \rangle$, in which $k = \{IQI, std, gap\}$. This value, averaged over 1000 samples, is shown on the left

part of panels of Fig. 3.13. On the right part, we see the standard deviation of these values across samples. We thus see, as expected, that for very small coupling strengths ϵ (roughly, $\epsilon \lesssim 0.8$), there is no frequency synchronization, as all dispersion measures are high, and there are none or very little sample-to-sample fluctuations. As the coupling gets stronger, the instantaneous frequencies get more synchronized. But the quantifiers start to decrease (towards zero, meaning frequency synchronized) at different values of ϵ . We see that $\overline{FS_I}$ decreases first, meaning the bulk frequencies start to synchronize first; then $\overline{FS_s}$ decreases and later $\overline{FS_g}$ decreases, meaning the outlier units are the last to synchronize their frequencies. For these averages across samples, there is a weak dependence on the topology, as networks with more shorter-range connections tend to reach frequency synchronization later.

The sample-to-sample fluctuations of the frequency synchronization also increase during the transition from frequency desynchronization to frequency synchronization, and peak right before the samples reach frequency synchronization, similarly to the behavior for phase synchronization (see Fig. 3.3e, for instance). Therefore, the frequency synchronization has a similar phenomenology as the phase synchronization, but the latter has a stronger dependence on the topology, which is more interesting. The sample-to-sample fluctuations for phase synchronization are also clearer, motivating our choice to focus on it.

Boundaries of basins of attraction are smooth

As we demonstrate in Fig. 3.7 of the main text, the Watts-Strogatz networks possess a large number of coexisting attractors (multistability) during the transition to phase synchronization. A possible behavior would be that the boundaries separating the basins of attraction are fractal. This would mean that arbitrarily small changes in the basin boundaries, for fixed parameter changes, or even arbitrarily small noise, could have a large consequence for the network. We chose initial conditions inspired by findings in (Halekotte, *Journal of Physics: Complexity*, 3 2, 2021) which suggested that fractal boundaries are obtained when the initial conditions of units whose degree differ most are changed. Even with this procedure, we obtained a few distinct attractors, each with very distinct degrees of phase synchronization and distinct instantaneous frequencies, and plotted the cross-section of the basins of attraction. We obtain complicated patterns, but still with seemingly smooth basin boundaries. This is also consistent with our results in Fig. 3.5b, which show that there is a rough minimum threshold for changes in parameters to lead to significant changes in the network's dynamics.

Malleability in simple excitable units

As an example of the generality of the phenomenon we describe in the main text, we show here a very similar phenomenology in a very different type of unit: excitable units (cellular automata). Networks with these units have analytically-proven phase transitions from a quiet to an active network state. During these transitions, we observe malleability, very similarly to the Kuramoto networks.

The results we show are inspired by (Hesse and Gross, 2014, *Frontiers in Systems Neuroscience*, 8 166, 2014), in which the analytical argument for the phase transition is also shown. The excitable units are inspired by neuronal dynamics, but very simplified: the units' states and time are discretized. The units have two states: excited or not, and time evolves only in integer numbers. An excited unit at a time step t becomes silent at

time $t + 1$. To become excited, a unit has to be excited by others. This occurs in the following way: an excited unit has a probability p of exciting the units it is connected to. The units are connected in a network with randomly chosen connections - for our simulations, an Erdos-Renyi network - of size N and average connectivity z an undirected connections.

An initial activation state (initial condition) can evolve towards a silent state (a fixed point) or towards an active state. This evolution depends on the parameters - the higher the average probability of exciting other units, the higher the chance that activation persists in the network. The system can be analytically shown to have a phase transition from the silent to the active states as the average connectivity z increases - a phase transition of onset of activity. The order parameter for measuring the transition is, naturally, the average activation A : it is the time average of the network average activation. The transition occurs at a critical z value of $z_c = 1/p$. For finite systems, the transition is blurred (different realizations transition at different z values) and shifted towards the right (for higher z values).

These behaviors can clearly be seen in the simulations, as illustrated in Fig. 3.15. In (a) and (b), the transition is clearly shifted towards the right of $z_c = 1/p = 10$. Increasing N to $N = 500$ shifts the transition towards the left, closer to z_c (panels (c) and (d)). For panels (a) and (c) we see the malleability: from the topology there is already disorder on the connections, so we can expect malleability by changing the topology realization, which is what we indeed see. Note the large fluctuations, very similar to what is seen in the Kuramoto networks. Besides malleability, we also see a similar profile for multistability by keeping the topology fixed and changing initial conditions (panels (b) and (d)).

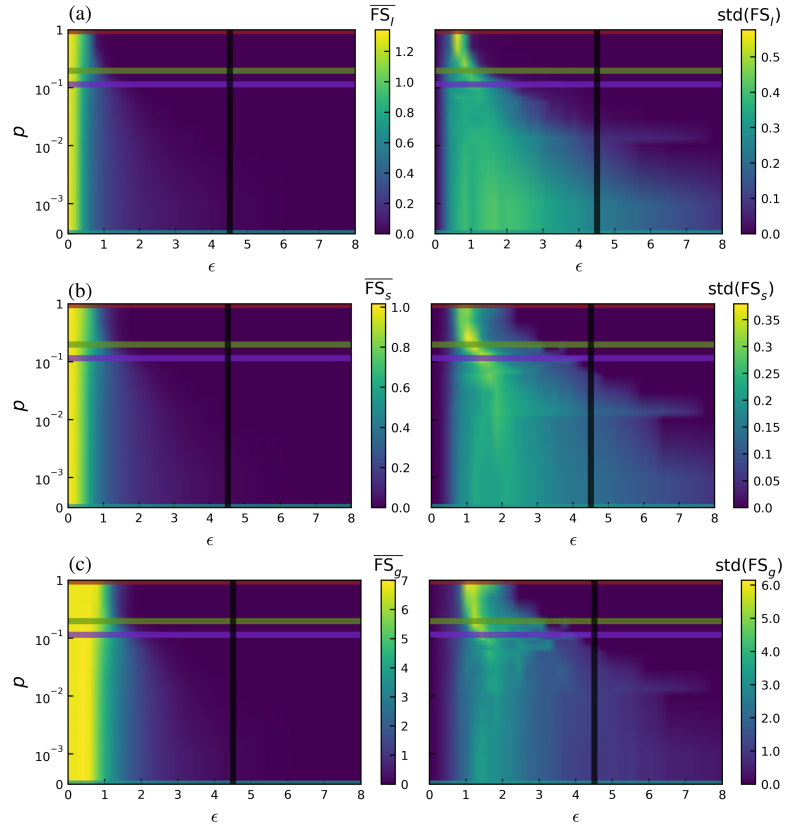


Figure 3.13: Frequency synchronization in parameter surface. The panels show additional quantifiers for the same setup as Fig. 3.4: they are color-coded over the same parameter space $p-\epsilon$ and analyzed over the same 1000 simulations. Within each panel, the left part shows the average over the simulations, while the right shows the standard deviation. Panel (a) shows quantifier $FS_I := \langle IQI(\{\dot{\theta}(t)\}) \rangle$, the temporal average over the interquartile interval of the instantaneous frequencies $\dot{\theta}_i$, a measure of dispersion of the bulk frequencies (difference between 75th and 25th percentile); panel (b) shows $FS_s := \langle \text{std}(\{\dot{\theta}(t)\}) \rangle$, the standard deviation over the instantaneous frequencies; panel (c) shows $FS_g := \langle \text{gap}(\{\dot{\theta}(t)\}) \rangle$, the gap (difference between extremes) of the instantaneous frequencies. All are thus measures of the synchronization of instantaneous frequencies, with the latter two more sensitive to the behavior of outliers.

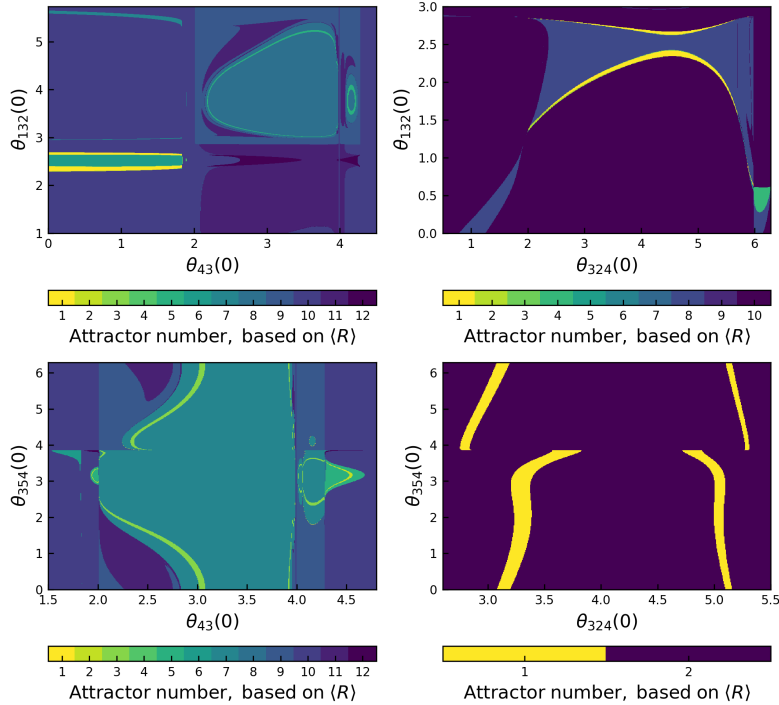


Figure 3.14: **Cross sections of basins of attraction for WS networks.** Varied initial condition of two units, keeping all others fixed. These are surfaces of section of the full basins. Attractors here are considered different if their R and other features of the dynamics are different, and the same if all are equal, up to several decimal places, (see discussion in Section 3D for the features). This criterion could be extended to include other comparison features, and results would be the same. Units on the y -axis have the highest degree in the network (10) and on the x axis have the lowest degree (3). They were chosen following findings in (Halekotte, *Journal of Physics: Complexity*, 3 2, 2021) which suggested that the cross sections taken from units with more distinct degrees tended to be fractal. Even with these choices, basins boundaries seem to be smooth. Parameters are for high malleability, $\epsilon = 4.51282$, $p = 0.13111$.

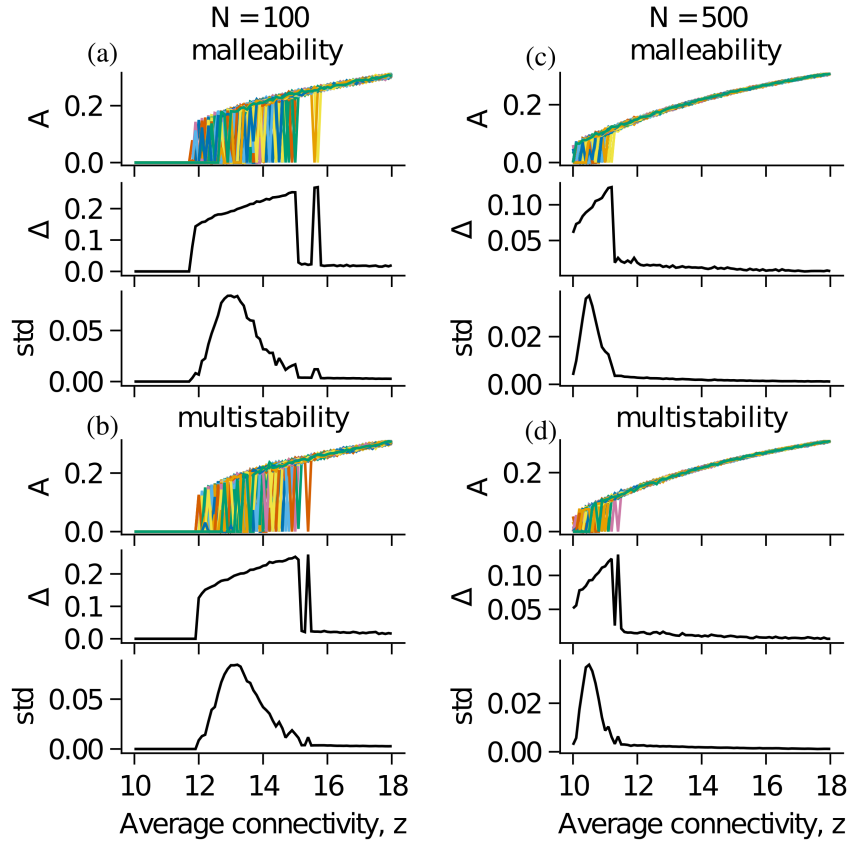


Figure 3.15: **Phase transition and malleability in excitable units** (a) and (c) show malleability in the mean activitation of networks of size $N = 100$ and $N = 500$ respectively. There, 500 topology samples were simulated with the same initial conditions. As in the main text, malleability is measured via either Δ , the gap between the maximum and minimum values of A , and with std , the standard deviation over all values of A . In panels (b) and (d) we see multistability: keeping the topology fixed and changing 500 initial conditions. We see that increasing the system size towards the thermodynamic limit reduces both the system's malleability and multistability.

Chapter 4

Transients versus network interactions give rise to multistability through trapping mechanism

Abstract

In networked systems, the interplay between the dynamics of individual subsystems and their network interactions has been found to generate multistability in various contexts. Despite its ubiquity, the specific mechanisms and ingredients that give rise to multistability from such interplay remain poorly understood. In this chapter ¹, for a network of coupled excitable units, we show that this interplay generating multistability occurs through a *competition* between the units' transient dynamics and their coupling. Specifically, the diffusive coupling between the units manages to *reinject* them in the excitability region of their individual state space and effectively trap them there. We show that this trapping mechanism leads to the *coexistence* of multiple types of oscillations: periodic, quasiperiodic, and even chaotic, although the units separately do not oscillate. Interestingly, we show that the attractors emerge through different types of bifurcations - in particular, the periodic attractors emerge through either saddle-node of limit cycles bifurcations or homoclinic bifurcations - but in all cases the reinjection mechanism is present.

4.1 Introduction

The long-term behavior of dynamical systems is determined by their attractors, which are stable states that attract certain sets of initial conditions. Dynamical systems can possess several attractors coexisting for the same parameters, such that different initial conditions can lead to different long-term behaviors - a phenomenon called *multistability* [3, 126]. In power grids, this can mean the difference between the proper functioning of the grid and a blackout [73]; in ecological systems, it can mean the difference between extinction of a certain species and their survival [127]. In neuronal circuits, multistability has been shown to be important for computations [128], and may, for instance, implement memory storage if the attractors correspond to different memories [10, 9].

Many systems display multistability, particularly networked systems, in which individual units are coupled together according to some type of interaction [3]. An important type of interaction in networked system is diffusion. One example is found in interacting ecological patches, in which each patch has its own dynamics but also interacts with other patches by migration, or diffusion, of species [129]. Another example is found in

¹This chapter is a modified form of a manuscript under preparation: Kalel L. Rossi, Everton S. Medeiros, Peter Ashwin and Ulrike Feudel. Transients versus network interactions give rise to multistability through trapping mechanism.

neuronal networks, in which neurons interact with each other through the transport of ions across their cell membrane [130, 131]. In these two examples, the interaction between units can be modeled by a linear diffusion term dependent on the difference $x_j - x_i$ between the state variables x_i and x_j of units i and j [132, 133, 134, 135, 136, 137, 138]. Understanding the emergence of multistability in networked systems with this kind of interaction therefore finds applications in many fields, and is still an area of active research.

For networked systems with diffusive coupling, multistability is known for cases in which the units oscillate individually. The emergence of different types of attractors has been shown [139], often with these attractors coexisting [140, 141, 27, 142, 143, 144, 145, 146, 147, 148]. For instance, Ref. [141] studied two coupled repressilators, 7-dimensional units that have stable oscillations when uncoupled, and find the emergence of different types of attractors. Some attractors have two units oscillating with a large amplitude and some have one unit at a large amplitude and another with a very small amplitude, called inhomogeneous limit cycles. When more units are coupled in a big network with $N = 100$ units, the authors showed in Ref. [140] that a large number of such attractors can coexist. In coupled mechanical oscillators, two coupled rotors have also been shown to exhibit large multistability (more than 3000 attractors) [14].

Less is known about multistability when the units individually do not oscillate, although it is known that oscillations can still arise due to the coupling. This originates from work by Smale in 1976 based on an idea by Turing in 1952 [132]. Smale proposed the emergence of oscillations from non-oscillating units which have only one equilibrium that is stable and globally attracting in a region of their state space. It was shown that the oscillations come from a Hopf bifurcation, in which the equilibrium becomes unstable and a stable oscillation emerges [42, 149]. Chaotic oscillations can also emerge from diffusive coupling applied to units with a single stable equilibrium in a region of state space. An example was given in Ref. [150] for two coupled Chua circuits. Recently, researchers provided rigorous conditions for the emergence of chaos due to diffusive coupling [151]. However, these works generally do not look at multistability. Furthermore, they deal with a single equilibrium in a region of state space, and have not yet looked at a scenario in which more invariant sets, such as unstable equilibria, may also play a role.

The presence of unstable equilibria can alter the transient dynamics of non-oscillating systems. In some classes of models, which we study here, the unstable equilibria lead to a type of excitability [39]. In this case, the unstable equilibria force part of the trajectories to go through a long excursion in state space, called an *excitation*, before reaching the stable equilibrium. These excitations are common in neuronal models, where they correspond to a neuronal spike [39]. Reference [142] has described multistability emerging in two excitable FitzHugh-Nagumo neurons that were coupled repulsively, but over a relatively small parameter range. For attractive coupling, the authors did not observe multistability.

In this work, we present two findings. First, we show that an attractive diffusive coupling can indeed create new attractors in coupled excitable systems. In fact, a wide variety of them: periodic, quasiperiodic and even chaotic oscillations arise by coupling excitable units, with $N = 2$ units already being sufficient for periodic and quasiperiodic attractors. For larger networks of $N = 10$ units, we show that these attractors, periodic, quasiperiodic and chaotic attractors can *coexist* in the same system, for a range of coupling strengths, in line with results of strong multistability in networks with many

units [27, 140, 32].

The second finding contributes to an understanding of one mechanism through which these attractors emerge. We study their geometry, looking at the interaction between the units' local dynamics, which creates the excitability, and the diffusive coupling term, which pulls the units toward each other. We show that the competition between these two terms manages to trap the units in a particular region of their state space where excitability occurs. Based on this mechanism, the previously transient excitable dynamics is now repeatedly activated, generating permanent oscillations. This occurs for all the attractors observed, which emerge under different bifurcation scenarios. It also extends to networks with more than two interacting units, suggesting a powerful mechanism for the coexistence of a multitude of attractors in networked systems.

A similar idea of attractors emerging when units are trapped in transient regions of state space has been previously reported in the literature [40, 41, 152, 153, 154]. The mechanisms underlying this trapping were different, and multistability had not been reported. In Refs. [40, 41, 152] the authors study units with chaotic saddles (unstable chaotic sets) in their uncoupled state space. They show that the diffusive coupling manages to trap the units in that region, generating a seemingly stable chaotic motion. Meanwhile, authors in Ref. [153] have shown the emergence of solutions in the vicinity of canard transitions. Because the local dynamics we study here is relatively simple, and yet can create rich multistable dynamics, our study serves as a simple yet powerful example of the more widespread phenomenon of multistability through trapping.

The chapter is organized as follows. We describe the model and algorithms in Sec. 4.2. Then, Sec. 4.3 introduces the rich multistability seen in a network of $N = 10$ units, from which we reduce to $N = 2$ units to better understand the mechanism giving rise to this multistability. In Sec. 4.4 we then discuss these findings in relation to each other and to preexisting literature.

4.2 Methods

4.2.1 Model

In this work we study networks formed by coupling two-dimensional units with state variables x and y whose evolution we write as:

$$\dot{x}_i = f_1(x_i, y_i) + \epsilon_1 g_i(\mathbf{x}) \quad (4.1)$$

$$\dot{y}_i = f_2(x_i, y_i) + \epsilon_2 g_i(\mathbf{y}) \quad (4.2)$$

with $\mathbf{x} = (x_1, \dots, x_N) \in \mathbb{R}^N$ and $\mathbf{y} = (y_1, \dots, y_N) \in \mathbb{R}^N$ are the state variables of the system. We refer to $\mathbf{f}_i = \mathbf{f}(x_i, y_i) = (f_1(x_i, y_i), f_2(x_i, y_i))$ as the local dynamics of unit i and to $\mathbf{g}_i = (g_i(\mathbf{x}), g_i(\mathbf{y}))$ as the coupling term of unit i , which allows it to receive influence from other units. The parameters ϵ_1 and ϵ_2 control the strength of the interactions, with $\epsilon_1 = \epsilon_2 = \epsilon$ unless stated otherwise. The interaction is specified by a diffusive coupling of the form:

$$g_i(\mathbf{z}) = \sum_{j \in \Omega_i} (z_j - z_i), \quad (4.3)$$

where \mathbf{z} is either \mathbf{x} or \mathbf{y} , and Ω_i is the set containing the indices j of units connected to unit i , also called the neighborhood of i .

For the local dynamics, we choose a simple two-dimensional model for a spiking neuron following the Hodgkin-Huxley formalism, as written by Ref. [39]. The dynamics of this model is described by the following functions:

$$\begin{aligned} f_1(x_i, y_i) &= (I - g_L(x_i - E_L) \\ &\quad - g_{Na}m_\infty(x_i)(x_i - E_{Na}) \\ &\quad - g_Ky_i(x_i - E_K))/C, \end{aligned} \tag{4.4}$$

$$f_2(x_i, y_i) = (n_\infty(x) - y_i)/\tau, \tag{4.5}$$

where the neuron membrane potential and conductance variable are represented by x and y , respectively. The activation functions $m_\infty(x_i)$ and $n_\infty(x_i)$ are given by:

$$m_\infty(x_i) = \frac{1}{1 + \exp((x_{1/2,m} - x_i)/k_m)}, \tag{4.6}$$

$$n_\infty(x_i) = \frac{1}{1 + \exp((x_{1/2,n} - x_i)/k_n)}. \tag{4.7}$$

The parameters used are $\tau = 0.16$ ms, $C = 1$ μ F/cm², $E_L = -80$ mV, $g_L = 8$ mS/cm², $E_{Na} = 60$ mV, $g_{Na} = 20$ mS/cm², $E_K = -90$ mV, $g_K = 10$ mS/cm², $x_{1/2,m} = -20$ mV, $k_m = 15$ mV, $x_{1/2,n} = -25$ mV, $k_n = 5$ mV and $I = 2.0$ μ A/cm². The dynamics of this system is very similar to that of the Morris-Lecar model [155, 39]. A slight increase in the membrane voltage x leads to a quick increase in the Sodium current, which is negative ($(x - E_{Na}) < 0$) and acts to increase the voltage even further in a positive feedback that rapidly increases x , initiating the excitation (spike). At sufficiently high voltage, the Potassium current increases, being activated by the conductance variable y . This current is positive ($(x - E_K) > 0$) and becomes sufficiently large that it overcomes the Sodium current and decreases the voltage back to baseline, terminating the excitation and returning to the stable equilibrium. For a more in-depth explanation of the model and a complete explanation of the parameters, we refer the reader to Ref. [39]. For simplicity, from now on we refer to the parameters without their corresponding units.

For fixed $I = 2.0$, the neuronal dynamics of the uncoupled units ($\epsilon_1 = \epsilon_2 = 0$) is excitable. The state space of the unit, shown in Fig. 4.1, is composed of a stable node (green circle), a saddle-point $\mathbf{x}_s^{\text{unc}}$ (red circle close to the node), and an unstable focus (red circle). The stable manifold $\mathbb{W}^s(\mathbf{x}_s^{\text{unc}})$ and the unstable manifold $\mathbb{W}^u(\mathbf{x}_s^{\text{unc}})$ of the saddle are depicted in green and red lines, respectively. Additionally, the x -nullcline, defined as $\dot{x} = 0$, and the y -nullcline, defined as $\dot{y} = 0$, are shown in gray and white, respectively. As indicated by the vector field, the stable manifold $\mathbb{W}^s(\mathbf{x}_s^{\text{unc}})$ roughly separates the state space into two regions: one that directly converges to the stable equilibrium, and another wherein trajectories go through long excursions before converging to the equilibrium. The long excursions are called excitations, and the region is called the *excitability region*.

In the main text of the chapter, we focus on the phenomenology underlying the excitable case prescribed by $I = 2.0$. In the Supplemental Material, we show that increasing I leads to a homoclinic bifurcation, creating a stable limit cycle, followed by a saddle-node bifurcation that destroys the node and saddle of the units. We then discuss the effects of these bifurcations on the results presented in the chapter.

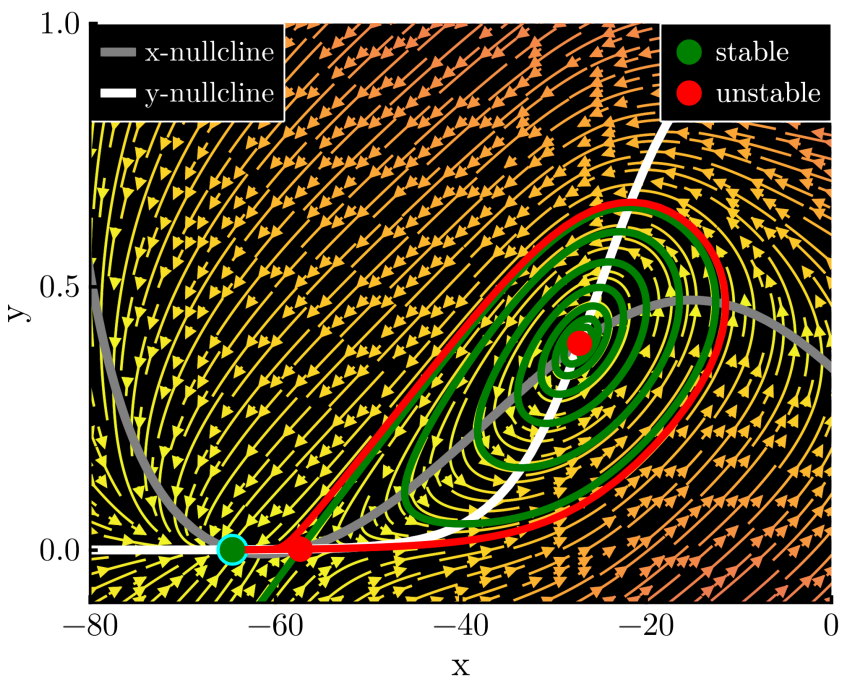


Figure 4.1: Phase portrait of the excitable uncoupled units. The green dot represents the stable node of the system, the red dots represent the unstable focus and the saddle point, with its stable and unstable manifold branches in the green and red lines. The phase portrait is represented by the arrows, indicating the directions of the flow. As the flow indicates, there is a wide region in which trajectories must go around the stable manifold to reach the node. They correspond to a neuronal spike, since this is a sharp increase and then decrease in the membrane potential. This region is called the excitability region. Attractors emerging from the coupling live in this region of long transients.

4.2.2 Numerical algorithms

To find the attractors in our networked systems, we followed the method developed in Refs. [46, 32, 45], which distinguishes between attractors based on user-defined features that uniquely characterize the attractors. To achieve this, it first integrates randomly chosen initial conditions in a specified region of the state space. The corresponding trajectories are then labeled based on their features, such as the mean value of their amplitude. These features must be chosen so that trajectories on different attractors exhibit distinct feature values. Subsequently, the features are separated using a grouping algorithm, which may involve clustering or simply distinguishing features that are more distant than a predefined threshold. This method works well for both low- and high-dimensional systems. We performed extensive numerical studies to ensure no attractors were missed, but this cannot be guaranteed. An attractor with a sufficiently small basin may, by chance, not be found. To reduce the risk of missing attractors, we used 5000 initial conditions for the $N = 10$ results and 1000 for $N = 2$. Test runs with more initial conditions did not find any further attractors. Each trajectory was integrated for a very long time, with a total transient time of 7000 and total integration time of 40000. The features used were the average pairwise Euclidean distance between the states of the units, their frequencies, amplitudes, and average position in state space. For equilibria, only the average position is considered, as the frequencies and amplitudes are zero. The algorithms, with a complete documentation, are implemented in the Julia [98] package `Attractors.jl` [43, 46]. We also verified the accuracy of results shown through continuation analysis using the XPPAUT 8.0 software [156], finding the bifurcations giving rise to the attractors.

Integration was done with the package `DifferentialEquations.jl` [97], with the aid of packages `DynamicalSystems.jl` [157] and `DrWatson.jl` [100]. Plots were made with `Makie.jl` [158]. The Tsitouras 5/4 Runge-Kutta method was used for the integrations, with absolute and relative tolerances of 10^{-9} . The code for the analysis is publicly available in a GitHub repository [159].

4.3 Results

4.3.1 Rich multistability of oscillations with 10 units

The diffusive coupling between the excitable units can generate rich oscillatory dynamics, in which equilibria coexist with periodic, quasiperiodic, and even chaotic oscillations. As we see later, these oscillations arise from the interplay between the diffusive coupling and the local flow field of the units. An example of these attractors is shown in Fig. 4.2A-I, in a network of $N = 10$ excitable units randomly connected with each other, following the topology shown in Fig. 4.2J. In this figure, we project the network state space into subspaces $x_i - y_i$ corresponding to each unit i , and overlay them all on top of each other. In addition, the coupling strength is chosen as $\epsilon_1 = \epsilon_2 = \epsilon = 0.15$.

The first type of attractor is shown in Fig. 4.2A. It corresponds to all units on the stable equilibrium, which is already present in the uncoupled units. This is the simplest solution, which must exist because, when the units are completely synchronized, the coupling term becomes zero and they follow their uncoupled dynamics, converging to the equilibrium.

The second type of attractor corresponds to one unit oscillating periodically with a large amplitude while the $N - 1$ other units oscillate with a very small amplitude at a

position between the stable equilibrium and the saddle of the uncoupled dynamics. The dynamics in this type of attractor resembles the so-called solitary states, since one unit behaves differently from the rest of the network. Such symmetry-broken solutions have been observed in regular [160, 161, 162, 7], adaptive [163], and complex networks [164]. For the chosen parameters, we have identified four stable solitary states, shown in Figs. 4.2B-E. The unit displaying a high-amplitude oscillation is said to be solitary. Interestingly, the amplitude of its oscillation is inversely proportional to the number of neighbors it has. With more neighbors, the coupling terms $\mathbf{g}_i(\mathbf{x})$ and $\mathbf{g}_i(\mathbf{y})$ of the solitary unit i increase, and the amplitude of its oscillation decreases. The reason for this will become clearer in Section 4.3.2, where we study in depth the case $N = 2$. Bifurcation analysis (not shown) reveals that these periodic attractors emerge in homoclinic bifurcations and disappear in saddle-node of limit cycle bifurcations (SNLC).

The third type of attractor corresponds again to periodic oscillations, but with two high-amplitude units, shown in Figs. 4.2F-G. In Fig. 4.2F, the units exhibiting high-amplitude oscillations are 2 and 9. Note that unit 2 has one more neighbor than unit 9, and its amplitude is smaller. In Fig. 4.2G, the units are 4 and 5. They have the same number of neighbors, so their amplitudes are identical. This type of attractor is thus a two-unit cluster periodic state. Bifurcation analysis reveals that these attractors emerge and disappear through SNLC bifurcations.

A fourth type of attractor also involves two units (1 and 10) oscillating with large amplitude, but now quasi-periodically, as shown in Fig. 4.2H. Similarly to the previous cases, the amplitude of their oscillations is proportional to the number of neighbors they have. As shown in the topology in Fig. 4.2J, the oscillating units (1 and 10) are connected, so they also pull each other in directions perpendicular to their oscillations as they oscillate. Intuitively speaking, we can imagine that this interaction enlarges the width of the torus. Indeed, if one introduces a coupling parameter directly between units 1 and 10, i.e., setting $g_i(\mathbf{z}) = \sum_{\Omega_i} \epsilon_{i,j} (z_j - z_i)$, and specifically increasing $\epsilon_{1,10} = \epsilon_{10,1}$ from 0 to ϵ , the width of the torus in the $x_i - y_i$ projection increases. Thus, when oscillating together with different amplitudes, the coupling between the units causes their quasi-periodic curves to become broader. We see the emergence of tori in greater depth when we study the $N = 2$ case in Section 4.3.2.

Finally, the fifth type of attractor involves all units oscillating together chaotically. All neuronal units are thus spiking chaotically in this attractor in a desynchronized fashion. The chaotic behavior, along with the periodic and quasiperiodic examples from earlier, has been verified by calculating the Lyapunov exponents of these attractors.

The results conveyed in Fig. 4.2 occur for an intermediate range of coupling strength values, at and around $\epsilon = 0.15$. Bigger coupling strengths tend to generate fewer attractors, and ultimately for strong coupling only the stable equilibrium exists. For weaker coupling, even more attractors can appear. In fact, for a range roughly between $\epsilon = 0.05$ and $\epsilon = 0.1$, more than 50 attractors can be found. These correspond to the various combinations of units having a very small amplitude oscillation, and units having a large amplitude oscillation.

Furthermore, in the network we analyzed so far the units are coupled in both x and y directions (i.e., $\epsilon_1 = \epsilon_2 = \epsilon$). If only the x -direction is coupled ($\epsilon_1 = \epsilon$, $\epsilon_2 = 0$), there still is multistability, but with fewer attractors. The x -coupling tends to stabilize attractors with more units oscillating at a higher amplitude, such that one can have 5 units oscillating periodically at a large amplitude and 5 with small amplitude, for instance.

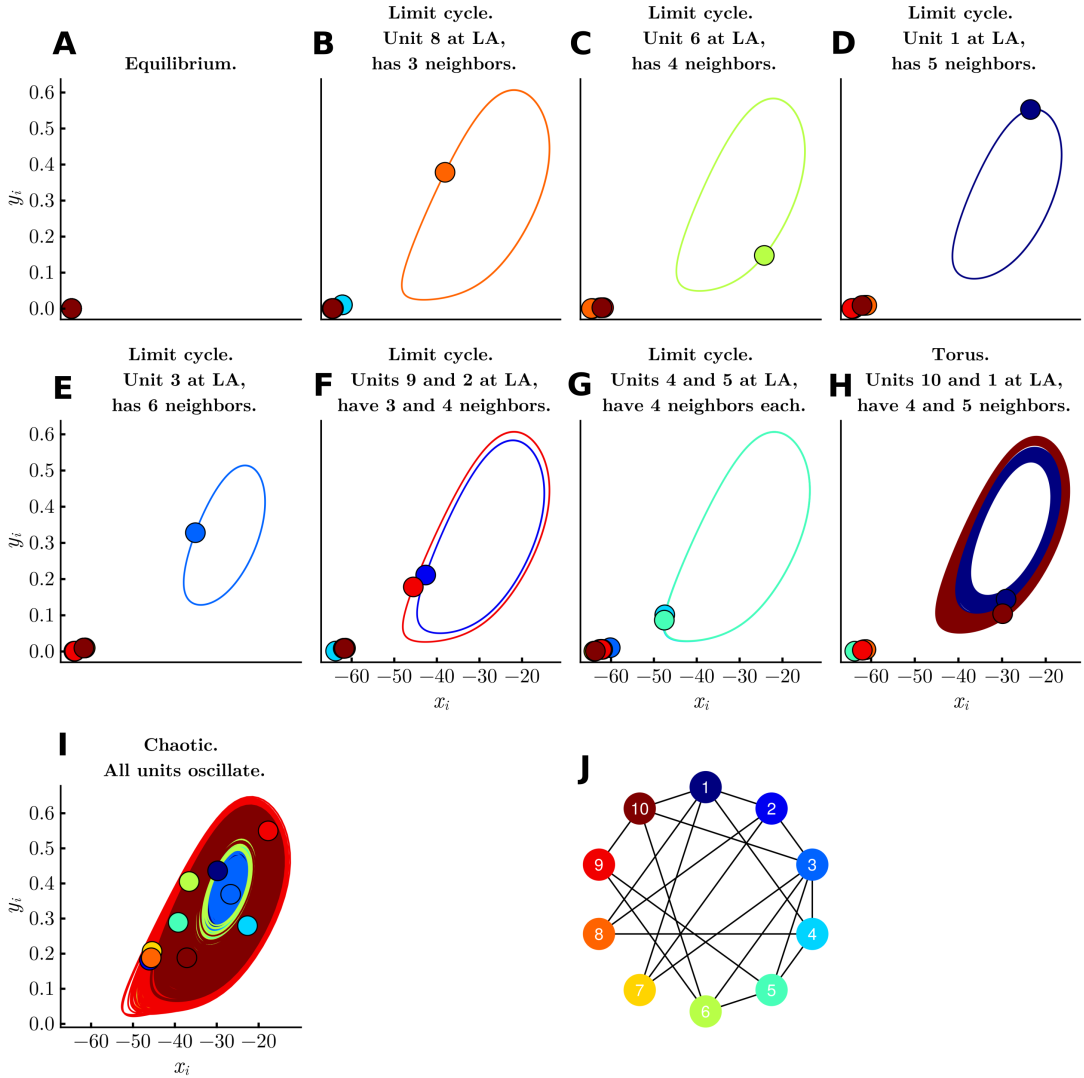


Figure 4.2: Rich multistability arising from diffusive coupling. Panels I-H show the stable equilibrium, periodic, quasi-periodic and chaotic attractors that coexist in the same network with $N = 10$ randomly coupled units (shown in Panel J) with $\epsilon = 0.15$. Each panel shows a trajectory on one of the attractors, projected onto the $x_i - y_i$ subspaces of each unit, all overlaid on top of each other. Circles correspond to the positions of the units at some arbitrarily chosen time point. The units are colored from blue to red according to their index, as shown in the topology of panel J, such that unit 1 is a deep blue and unit 10 is a deep red.

To summarize, the addition of a simple linear interaction through the attractive diffusive coupling creates a plethora of oscillations from non-oscillating units in an excitable regime. The coupling is clearly able to counteract the units' tendency to converge onto the stable equilibrium. Our goal in the following sections is to elucidate this mechanism in more detail. To achieve this, we simplify our system and reduce the problem to $N = 2$ interacting units.

4.3.2 Emergence of attractors in a two-unit network

To illustrate the effect of the diffusive coupling on the excitable neurons, we show the attractors of the system for different coupling strengths for $N = 2$ coupled units. Similarly to Fig. 4.2, each panel in Fig. 4.3 shows the variables $x_i - y_i$, now for $i = 1, 2$. An important difference now is that the colors refer to the attractors. The units are distinguished by markers: circles for unit 1 and diamonds for unit 2. These markers correspond to the positions of the units at some arbitrarily chosen time point.

To begin this analysis, we recall that each uncoupled unit has three equilibria. Consequently, a system of two coupled units, under sufficiently weak coupling, has $3^2 = 9$ equilibria, corresponding to all combinations of the individual equilibria. Naturally, the symmetric combinations node-node, saddle-saddle, and focus-focus correspond to the two units being together in the same equilibrium. Since the coupling term becomes zero when the units are completely synchronized, these symmetric equilibria occupy the same positions as their uncoupled counterparts when projected into the units' subspace $x_i - y_i$. The other equilibria are asymmetric and have non-zero coupling terms, which shift their positions as a function of the coupling strength ϵ . However, for simplicity, we still label the equilibria as combinations of the uncoupled equilibria, e.g. node-saddle denoting an equilibrium with 3 negative eigenvalues and 1 positive eigenvalue.

For $\epsilon = 0.05$, the node-node is the only attractor in the system (Fig. 4.3A). In this solution, both units are in a steady state (SS), so we label the attractor as SS-SS (also called homogeneous steady state HSS [141]).

Next, at $\epsilon \approx 0.065$, a stable oscillation emerges, in which both units oscillate with a large amplitude (Fig. 4.3B). Therefore, we label this attractor LA-LA. It initially forms near the saddle point $\mathbf{x}_s^{\text{unc}}$, located near the lower left corner. This proximity to the saddle point causes trajectories in that region to slow down significantly. As the coupling increases, the limit cycle moves farther away from the saddle point, resulting in a decreasing amplitude. This progression can be observed by comparing the attractors in subsequent panels.

At $\epsilon \approx 0.117485$ a pair of asymmetric attractors emerges, in which one unit has a large amplitude oscillation (LA) and the other unit has a small amplitude oscillation (SA), and vice-versa (Fig. 4.3C). Because the units are identical, the system has a permutation symmetry, so both attractors, LA-SA (large amplitude in unit 1 and small amplitude in unit 2), and SA-LA (reciprocal case) are simply permuted versions of each other. Consequently, these attractors overlap each other in Figs. 4.3C-D. They can be distinguished by the position of the units, indicated by the markers. Please note that the small amplitude oscillation has such a small amplitude that it is barely visible in the figures. In the literature, the LA-SA attractors have also been called inhomogeneous limit cycles [141, 165] (IHLC).

At this coupling strength $\epsilon \approx 0.117485$, the system has four coexisting attractors, three of them being oscillations, even though the uncoupled dynamics only has equilibria! Eventually, for stronger coupling the pair LA-SA and SA-LA disappears around $\epsilon \approx 0.22$, and the system becomes bistable again. The result is shown in Fig. 4.3E. At $\epsilon \approx 0.27$, the periodic LA-LA attractor is replaced by a quasi-periodic LA-LA attractor, which again has both units oscillating with a large amplitude. In the quasi-periodic attractor, the units have different frequencies, and are desynchronized in both frequency and phase (cf. Fig. 4.3F). Eventually it disappears and only the stable equilibrium remains for sufficiently strong coupling.

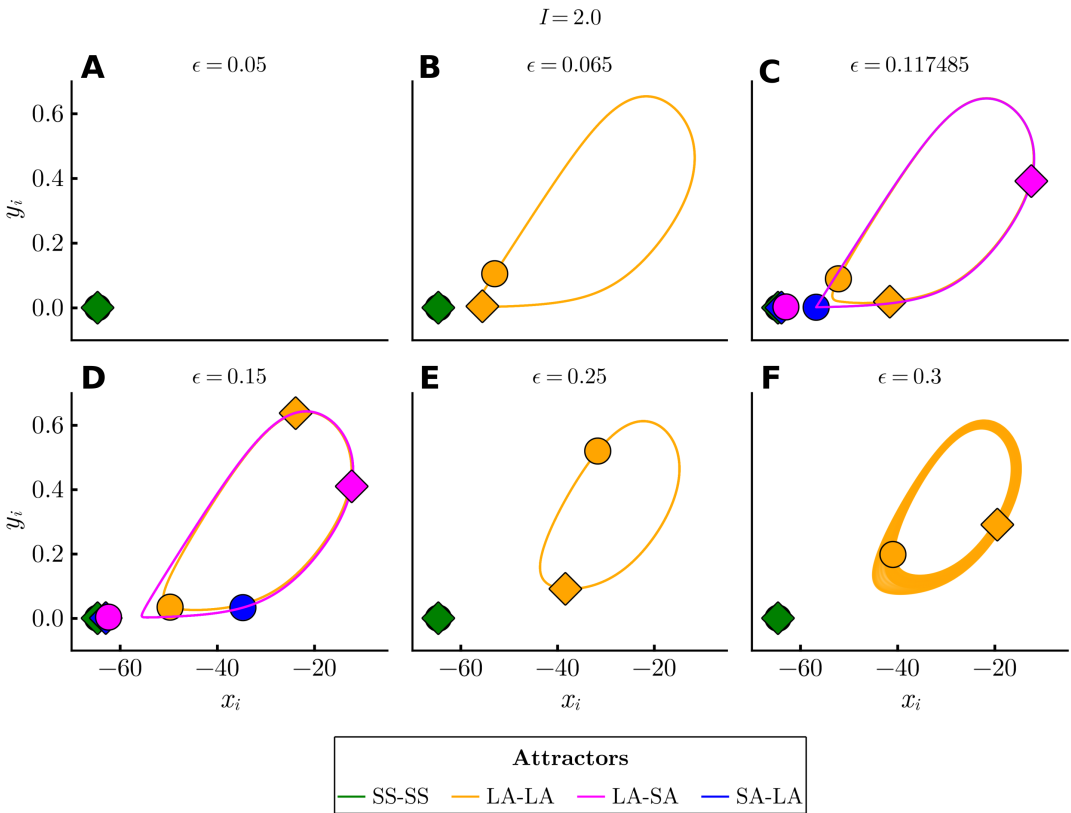


Figure 4.3: **Attractors created by the diffusive coupling for $N = 2$.** Each panel is a projection onto 2D space of $x_i - y_i$ for different coupling strengths. The markers denote the positions of the units for an arbitrarily chosen time point, with unit 1 shown as a circle and unit 2 as a diamond. The stable equilibrium is the only attractor existing for weak coupling strengths, as shown for $\epsilon = 0.05$. Another attractor emerges at $\epsilon \sim 0.065$ corresponding to two units oscillating with large amplitude - it is thus labelled as LA-LA. A pair of asymmetric attractors emerges at $\epsilon \sim 0.117485$ corresponding to one unit oscillating with large amplitude and the other oscillating with small amplitude; they are labeled respectively as LA-SA and SA-LA. The pair eventually disappears and the system becomes bistable again at $\epsilon = 0.25$. At $\epsilon = 0.3$, the LA-LA attractor is quasi-periodic. For stronger coupling ϵ , only the stable equilibrium is left.

4.3.3 Bifurcations giving rise to the attractors

To understand the emergence and disappearance of the attractors in the $N = 2$ case, we start by studying their associated bifurcations. We perform a continuation analysis using the XPPAUT 8.0 software [156]. This analysis is shown in Fig. 4.4, where the period T of oscillation is estimated as a function of the coupling strength ϵ . In this figure, the green and red colors indicate stable and unstable solutions, respectively. First, in Fig. 4.4A, we present the continuation analysis for the LA-LA attractor, where both units oscillate with a large amplitude. We observe that this attractor arises from a saddle-node bifurcation of limit cycles (SNLC) at $\epsilon \approx 0.06432$. Subsequently, the stable limit cycle undergoes a Neimark-Sacker (torus) bifurcation (TR) at $\epsilon \approx 0.2701$, becoming unstable and being

replaced by a stable torus. Next, this unstable limit cycle disappears in a supercritical Hopf bifurcation (HB) at $\epsilon \approx 0.4088$. Meanwhile, the saddle limit cycle that emerges at the SNLC bifurcation disappears in a homoclinic bifurcation (HOM) involving a saddle-saddle equilibrium at $\epsilon \approx 0.07285$. While it exists, the saddle limit cycle forms the basin boundary between the stable equilibrium and the stable limit cycle. When it disappears in the homoclinic bifurcation, it is immediately replaced by a pair of asymmetric saddle limit cycles that also emerges in a homoclinic bifurcation to the same equilibrium at the same parameter value, as shown in Fig. 4.4B. These saddle limit cycles then compose the basin boundary between the attractors. They correspond to the unstable version of the LA-SA and SA-LA attractors, which are later born also in a homoclinic bifurcation at $\epsilon \approx 0.1175$, but involving a saddle-node equilibrium. Eventually, both the stable and the unstable limit cycles collide and disappear in a SNLC bifurcation at $\epsilon \approx 0.2179$. The files used to perform the analysis are freely available at [159].

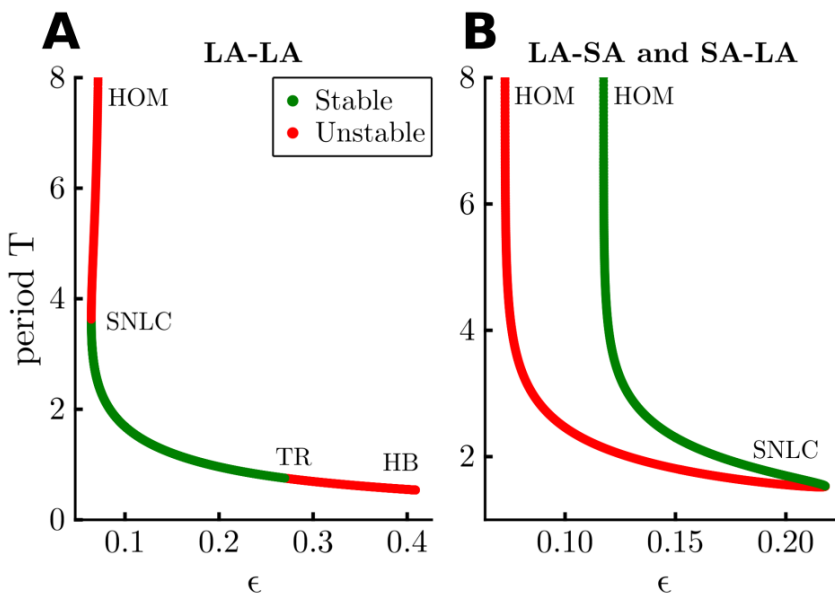


Figure 4.4: Continuation analysis for oscillations in two-unit case. Each panel shows a continuation of the limit cycles, plotting their period T as a function of the coupling strength ϵ for fixed $I = 2.0$. The left panel shows the analysis for the LA-LA attractor, which emerges in a saddle-node bifurcation of limit cycles (SNLC) together with an saddle limit cycle (red curve) at $\epsilon \approx 0.06432$. The unstable LC goes through a homoclinic bifurcation (HOM) where it collides with a saddle-saddle equilibrium at $\epsilon \approx 0.07285$ and disappears. The LA-LA attractor (in green) remains stable until it loses stability due to a Neimark-Sacker bifurcation (TR) and then disappears due to a supercritical Hopf bifurcation (HB). In panel B, the LA-SA, shown in the green curve, emerges due to a homoclinic bifurcation involving a saddle-node equilibrium at $\epsilon \approx 0.1175$ and then disappears due to a SNLC, when it collides with its unstable counterpart, in red, that is also born in a homoclinic bifurcation to a saddle-saddle equilibrium at $\epsilon \approx 0.07285$. The bifurcation diagram is identical for the SA-LA attractor, due to their symmetry.

4.3.4 Emergence of oscillations through reinjection mechanism

To gain insights into how the coupling between the units supports the emergence of oscillations in a system whose uncoupled units exhibit only steady states, we now examine the geometry of the emerging attractors. As we see in Eqs. 4.1, the dynamics of unit i can be decomposed into two terms: the local dynamics, governed by $\mathbf{f}_i(x_i, y_i)$, and the coupling, governed by $\epsilon \mathbf{g}_i(\mathbf{x})$. The local dynamics $\mathbf{f}_i(x_i, y_i)$ generates a vector field dictating the trajectories of the uncoupled units. As described in Sec. 4.2.1, \mathbf{f}_i creates an excitability region, on which trajectories go through long excursions in state space before converging to the stable equilibrium. They follow the stable manifold $\mathbb{W}^s(\mathbf{x}_s^{\text{unc}})$ of the saddle point $\mathbf{x}_s^{\text{unc}}$ in the uncoupled system on their way to the equilibrium. The coupling dynamics $\mathbf{g}_i(\mathbf{x}) = (x_j - x_i, y_j - y_i)$ generates a vector field that points from unit i to unit j , with an amplitude proportional to their distance. For $\epsilon > 0$, the coupling $\epsilon \mathbf{g}_i$ is attractive, as it pulls unit i towards unit j . In the following examples, we see how interaction between these two terms leads to the emergence of the stable oscillations.

Figure 4.5A1 illustrates this scenario for the LA-LA attractor at $\epsilon = 0.065$, already introduced in Fig. 4.3B. In Fig. 4.5A1, the structures in the complete 4D space are projected onto the $x_i - y_i$ subspace of each unit. For reference, we overlay on top of this plot the structures of the uncoupled unit, as seen already in Fig. 4.1. The stable equilibrium is represented as a green cross, while the saddle point $\mathbf{x}_s^{\text{unc}}$ and the focus are shown as red crosses. The stable manifold $\mathbb{W}^s(\mathbf{x}_s^{\text{unc}})$ of the saddle is a green line, while its unstable manifold $\mathbb{W}^u(\mathbf{x}_s^{\text{unc}})$ is a red line. A trajectory converging to the LA-LA attractor is shown as a solid black line. Starting from an initial condition near the focus, at the center of the figure, the trajectory spirals outwards. This spiralling can be understood as the coupling being weak enough that the local dynamics \mathbf{f}_i dominates the trajectory here, such that it roughly follows $\mathbb{W}^s(\mathbf{x}_s^{\text{unc}})$.

Looking at an amplification of the region near $\mathbf{x}_s^{\text{unc}}$ in Fig. 4.5A2, we see that the trajectory follows $\mathbb{W}^s(\mathbf{x}_s^{\text{unc}})$ almost until the saddle $\mathbf{x}_s^{\text{unc}}$ (red cross). Then, we see the crucial effect of the coupling. Without it, the trajectory would have followed along the left branch of $\mathbb{W}^u(\mathbf{x}_s^{\text{unc}})$ and converged to the stable equilibrium. This is shown in the black dashed line, which shows a trajectory of the uncoupled system starting at the same initial condition (in (x_1, y_1)) as the black solid line. However, the coupled trajectory does not do that. Instead, it goes rightward, influenced by the coupling $\epsilon \mathbf{g}_i$. This effect can be seen by the rightward pointing arrows attached to the circles. The arrows correspond to the coupling vector $\epsilon \mathbf{g}_i$ on unit i , depicted as the circles whose colors vary along the trajectory, from dark blue to light blue. Under this coupling, the trajectory crosses $\mathbb{W}^s(\mathbf{x}_s^{\text{unc}})$ in this projection, and is effectively reinjected into the excitability region. For clarity, the trajectory of the coupled 4D system, when projected into the $x_i - y_i$ plane, crosses the stable manifold $\mathbb{W}^s(\mathbf{x}_s^{\text{unc}})$ of the saddle of the uncoupled 2D system. Naturally, it does not cross any invariant manifolds of the coupled system.

As this attractor is symmetric, the behavior described for unit 1 occurs identically for unit 2. The reinjection into the excitability region thus happens for both units, causing them to repeatedly pull on each other and reinject each other into the previously transient region. In this sense, we say that *the coupling traps the units in the excitability region*, preventing them from following their local dynamics' tendency toward the stable equilibrium.

Why does this crossing happen so close to $\mathbf{x}_s^{\text{unc}}$? As we have seen in Sec. 4.3.3, the LA-LA attractor emerges in a saddle-node bifurcation of limit cycles (SNLC), and is not directly related to $\mathbf{x}_s^{\text{unc}}$. However, the local dynamics has a magnitude $|\mathbf{f}_i|$ that is small

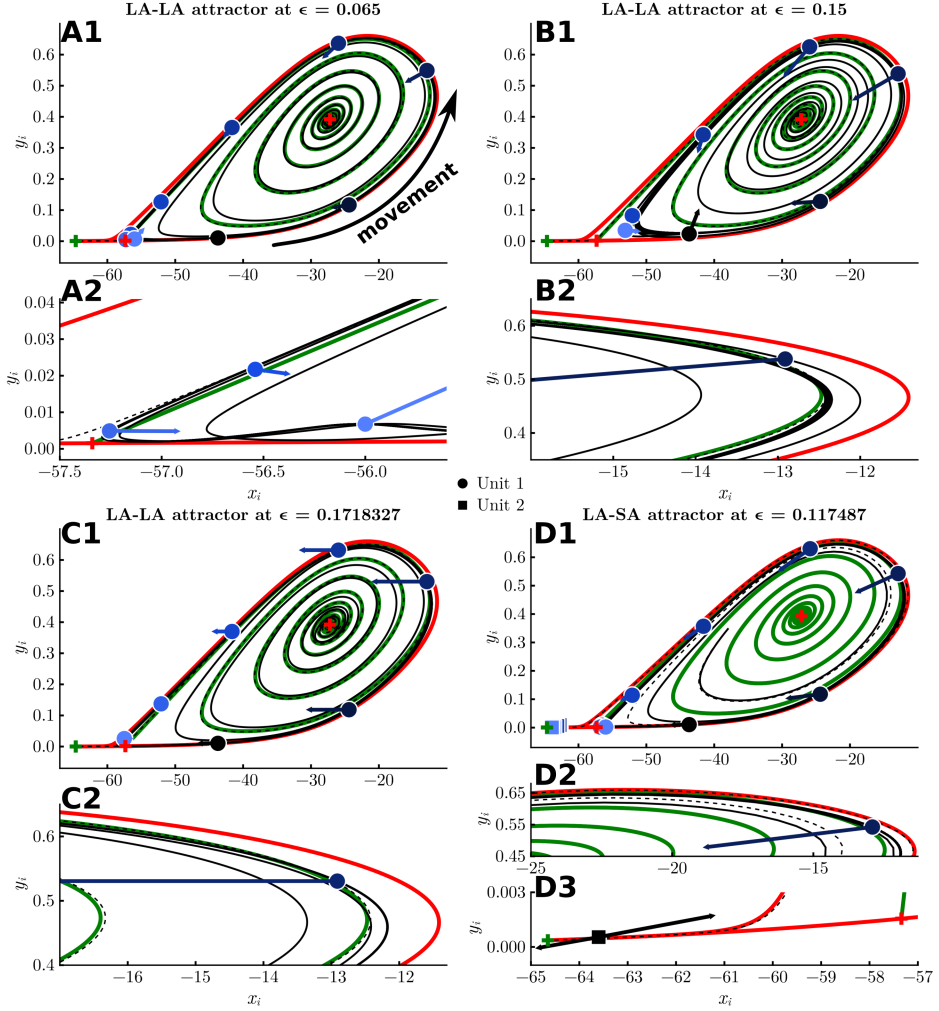


Figure 4.5: Illustration of the trapping phenomenon. Each panel shows a projection of the full 4D state space into the subspace $x_i - y_i$ of unit i. The three symmetric equilibria in the coupled system are shown: the stable equilibrium as a green cross, the unstable focus and the saddle point $\mathbf{x}_s^{\text{unc}}$ as red crosses. The stable $\mathbb{W}^s(\mathbf{x}_s^{\text{unc}})$ and unstable $\mathbb{W}^u(\mathbf{x}_s^{\text{unc}})$ manifolds of the saddle $\mathbf{x}_s^{\text{unc}}$ in the uncoupled system are also shown as green and red lines, respectively. The black solid lines represent an illustrative trajectory converging to one of the emerging attractors. A trajectory starting with the same initial condition but with $\epsilon = 0$ is shown in black dashed lines. The position and coupling vector $\epsilon \mathbf{g}_1$ of unit 1 at specific time points are plotted respectively as circles and arrows. The unit's colors vary from black to light blue to indicate the passage of time. The emerging attractor in panels A1-A2 is the LA-LA attractor for $\epsilon = 0.065$. The attractor is the same in B1-B2 but at a stronger coupling $\epsilon_1 = 0.15$. Panels C1-C2 show that this attractor still emerges if $\epsilon_2 = 0$, at the cost of requiring a larger value of ϵ_1 . Panels D1-D3 show the geometry of the LA-SA attractor, with the position of unit 2 (projected into $x_2 - y_2$) also shown as squares. Panel D3 is added specifically to indicate the behavior of unit 2, with two arrows: the upward and rightward pointing arrow is the coupling $\epsilon \mathbf{g}_2$, and the leftward and downward arrow is the unit's uncoupled dynamics \mathbf{f}_2 .

in the vicinity of $\mathbf{x}_s^{\text{unc}}$. So in this region the relative effect of the coupling $\epsilon \mathbf{g}_i$ increases. Near $\mathbf{x}_s^{\text{unc}}$ the unit tends to move very slowly due to its local dynamics, but at the same time the coupling intensity is relatively strong. As a result, the coupling overcomes the local dynamics and manages to pull the unit rightwards. In summary, the slowness near $\mathbf{x}_s^{\text{unc}}$ helps the coupling $\epsilon \mathbf{g}_i$ to overcome the local dynamics.

The slowness near $\mathbf{x}_s^{\text{unc}}$ also allows us to understand the bulge that occurs right after the trajectory crosses $\mathbb{W}^s(\mathbf{x}_s^{\text{unc}})$, on the right-hand side of Fig. 4.5A2. The trajectory in this region is quite slow. In fact, unit i spends most of its time on it while unit j traverses the rest of the oscillation. As j moves around the oscillation, the distance between the units increases significantly, and therefore so does \mathbf{g}_i (note the longer blue arrow for unit 1 in the bulge). The combination of the slowness of \mathbf{f}_i and the high value of \mathbf{g}_i means that the coupling dominates the sum, significantly impacting the trajectory, pulling it towards unit j , creating the upwards movement of the bulge for unit i (and vice-versa for unit j , because of the symmetry).

For bigger values of ϵ , the coupling becomes stronger and the slowness near $\mathbf{x}_s^{\text{unc}}$ becomes less relevant. In Fig. 4.5B1, note how the coupling is larger (longer arrows) for $\epsilon = 0.15$. Consequently, the coupling manages to pull unit i , in this $x_1 - y_1$ projection, across $\mathbb{W}^s(\mathbf{x}_s^{\text{unc}})$ earlier along the manifold - see the magnification in Fig. 4.5B2. The stronger coupling also affects the shape of the attractor. This is most visible close to $\mathbf{x}_s^{\text{unc}}$, which is considerably shifted rightward and upward if compared to the smaller ϵ in Fig. 4.5A1-A2. This region has the slowest dynamics, and is thus the one most sensitive to the coupling. Furthermore, similarly to the argument leading to the bulge in Fig. 4.5A1-A2, while unit i is in this slow region, unit j eventually becomes diametrically opposite it, and the coupling amplitude grows significantly. This increase, combined with the slow dynamics, pulls the units upward and rightward, explaining the shift. This decreases the amplitude of the oscillation, consistent with the behavior seen for larger networks (Figs. 4.2B-H), in which the amplitude of the oscillation is inversely proportional to the number of neighbors a unit has.

So far we have considered what happens in the case that the x and y directions are coupled with the same intensity, i.e., when $\epsilon = \epsilon_1 = \epsilon_2$. However, this is not required for new attractors to emerge. In particular, the LA-LA attractor still emerges when only the x -component of the coupling is kept (i.e., when $\epsilon_1 = \epsilon$ and $\epsilon_2 = 0$). The reinjection occurs similarly to before, as shown in Figs. 4.5C1-C2, where an illustrative trajectory of the coupled system can again be seen to cross $\mathbb{W}^s(\mathbf{x}_s^{\text{unc}})$. In fact, the y -component of the coupling is not necessary to generate the LA-LA attractor, although it helps. Decreasing ϵ_2 from $\epsilon_2 = \epsilon$ to $\epsilon_2 = 0$ has the effect of increasing the critical value of ϵ_1 for the saddle-node bifurcation of limit cycles that creates the attractor, effectively postponing its emergence, but not inhibiting it. The example in Figs. 4.5C1-C2 occurs soon after the LA-LA attractor emerges. Note that the coupling is much bigger than it was for Figs. 4.5A1-A2. Conversely, decreasing ϵ_1 from $\epsilon_1 = \epsilon$ to $\epsilon_1 = 0$ can either destroy the LA-LA attractor through a SNLC bifurcation or cause it to lose stability. Therefore, the x -component is necessary to generate this attractor.

In Fig. 4.5D1 we return to the case $\epsilon_1 = \epsilon_2 = \epsilon$ and examine the asymmetric attractor LA-SA. Its geometry differs from the previous cases, since now there is an asymmetry between the units. As in the previous cases, unit 1 oscillates in the excitability region with a large amplitude. Meanwhile, unit 2 (squares) is positioned, in the $x_2 - y_2$ projection, between the stable equilibrium (green cross) and the saddle point $\mathbf{x}_s^{\text{unc}}$ of the uncoupled dynamics (red cross). Both units can be seen in Figs. 4.3D1, represented

respectively as circles and squares. Their colors denote different time points along the trajectory. In this configuration, unit 1 is pulled downwards and to the left by unit 2, as illustrated in Fig.4.3D2, which shows $\epsilon\mathbf{g}_1$. This pull is capable of causing unit 1 to cross $\mathbb{W}^s(\mathbf{x}_s^{\text{unc}})$ and to be reinjected into the excitability region, as shown in Figs. 4.5D1-D2. Meanwhile, unit 2 is pulled rightwards and upwards by unit 1. This pull is counteracted by the attraction it feels towards the stable equilibrium, with the result being a small-amplitude oscillation. This competition is illustrated in Fig.4.3D3, where two arrows are associated with unit 2 for a representative time point of the trajectory: the upward and rightward arrow is $\epsilon\mathbf{g}_2$, which pulls unit 2 towards unit 1; the downward and leftward arrow is \mathbf{f}_2 , which pulls unit 2 towards the stable equilibrium.

With this configuration of the units in the LA-SA attractor, the x -direction is actually counter-productive. To see this, we can focus on the region to the right of the saddle point - in Fig. 4.3D1, several instances of unit 1 can be seen accumulated in this region with light blue colors. This accumulation is a result of the slow dynamics of trajectories moving near the saddle point. In this region, unit 1 is pulled leftwards back towards $\mathbb{W}^s(\mathbf{x}_s^{\text{unc}})$. The x -direction is thus acting against the reinjection mechanism, and so may be impeding the emergence of the LA-SA attractor. We can verify this qualitative claim by decreasing ϵ_1 from $\epsilon_1 = \epsilon$ towards $\epsilon_1 = 0$. By doing this, we see that indeed the critical value of ϵ_2 that leads to the emergence of the attractor decreases. If $\epsilon_1 = 0$ the attractor can still emerge. Therefore, the LA-LA and LA-SA attractors exhibit different dependencies on the x - and y -components of the coupling, due to their distinct geometries. This distinction is crucial in various applications where coupling can model diverse phenomena. For example, in ecology, coupling in the x -direction might represent migration between prey species, while coupling in the y -direction could denote migration among predator species.

Another intriguing attractor is the torus that emerges from the LA-LA attractor (cf. Fig. 4.3F), in which the two units continue to oscillate with a large amplitude, but quasi-periodically. Its geometry resembles that of the LA-LA attractor, but the increased coupling strength causes the units to exert a stronger mutual influence. Consequently, the reinjection still occurs, but now one unit pulls on the other so forcefully that the trajectory no longer follows a closed curve. Indeed, as ϵ increases, the torus expands, becoming wider.

Therefore, the reinjection mechanism, which acts to trap units in the excitability region of their uncoupled dynamics, underlies the emerging attractors we observe. This is true for the two distinct geometries: LA-LA and LA-SA, which emerge from different bifurcations. The mechanism also occurs for different dynamics: periodic and quasi-periodic.

4.4 Discussions

In this chapter we have shown that diffusive coupling acting on excitable dynamics can create multistability of oscillations. The variety of coexisting attractors, which can be periodic, quasiperiodic, and even chaotic, emerge in a similar way: through the trapping of units in the excitability region of their local dynamics. This local dynamics consists of three equilibria living in the units' state space: an unstable focus, a saddle point $\mathbf{x}_s^{\text{unc}}$ and a stable equilibrium, which is the only attractor in the uncoupled system. The stable manifold $\mathbb{W}^s(\mathbf{x}_s^{\text{unc}})$ of $\mathbf{x}_s^{\text{unc}}$ is extended in state space and has one branch that spirals out of the unstable focus. As a consequence, it separates the nearby state space

into two regions: one that directly converges to the stable node and another that has to go on a long excursion around the stable manifold before converging to the node. On top of this, the units feel the attractive diffusive coupling, which pulls one unit toward the other. The dynamics of the coupled units is determined by the interaction of these two effects: the local dynamics attempting to pull the units towards the stable node and the diffusive coupling attempting to pull the units towards each other.

This competition is controlled by the coupling strength ϵ . As already described in the literature for similar systems, there are two extremes [132]. For sufficiently small ϵ , the local dynamics dominates, and the only attractor is the stable node. For sufficiently large ϵ the coupling dominates, and the units converge to each other. When they do so, the coupling becomes zero, and then they again follow their uncoupled dynamics and converge to the stable node only. It is in between these extremes that interesting dynamics can occur [132]. In this case, the coupling is strong enough to impact the trajectory of the uncoupled system, but not enough to completely overrule it. Because of the geometry of state space, the coupling can manage to pull the units away from the stable node and into the excitability region. The units find a stable configuration in which they are repeatedly reinjected into the excitability region, generating permanent oscillations. The type of these oscillations depends on the coupling strength, the number of interacting units, and the network's topology.

It has been known that diffusive coupling on units with a single stable equilibrium in a region of state space can create oscillations. These oscillations can be periodic, originating from a Hopf bifurcation of the equilibrium [42, 149] or chaotic oscillations [150] originating from a Shilnikov homoclinic bifurcation [151]. However, as we have shown, the scenario for an excitable system, with the additional interaction of two unstable equilibria, has important differences to the single equilibrium case. First, for $N = 2$ coupled units, we have shown that periodic attractors can coexist with other periodic attractors and with the stable equilibrium, leading to a multistable coupled system. Further, these periodic attractors are qualitatively different: in one attractor, both units oscillate with a large amplitude (LA-LA attractor); in the other attractor, one unit instead has a very small amplitude oscillation, almost stationary (LA-SA and SA-LA attractors). The $N = 2$ case also supports the emergence of a quasiperiodic oscillation, which coexists with the stable equilibrium. The bifurcations giving rise to the periodic attractors also differ: the periodic attractors emerge either through a saddle-node bifurcation of limit cycles (SNLC) bifurcation or through a homoclinic (HOM) bifurcation.

In the bigger network, with $N = 10$ units, we have shown that the multistability becomes even richer. In this case, all these types of dynamics can coexist. The sheer number of coexisting attractors is also large (we observed up to 84 attractors for only $N = 10$ units), with a dominance of periodic solutions. Since units can be either trapped in the excitability region, with large amplitude oscillations, or oscillate with low amplitude near $\mathbf{x}_s^{\text{unc}}$, adding more units leads to a higher number of possible combinations of which units are placed in which position. Not all of these combinations are necessarily invariant solutions; and the ones that are invariant are not necessarily stable. The invariance and stability are controlled by the topology of the network, and more research in the future is needed to understand how exactly. It would be interesting to understand which topologies maximize the number of attractors, and which minimize them. This could provide further insights into other systems, for which a scaling of the number of attractors with the size of the network has been observed [140, 27, 32].

By studying the attractors from the point of view of the local dynamics competing

with the coupling, we identified an impact that the topology has on the attractors of the coupled system. Units that receive more connections tend to have a stronger coupling term than units with fewer connections. A stronger coupling term pulls the units more strongly towards the excitability region. This effect is stronger in the slower region of the oscillation, close to $\mathbf{x}_s^{\text{unc}}$, where the local dynamics is weaker. Thus, one could expect the oscillation of the units with more connections to be pushed away further from $\mathbf{x}_s^{\text{unc}}$, and thus have a smaller amplitude than units with fewer connections. This is indeed what we observe: units with more neighbors have smaller amplitudes.

On the attractors, the units are permanently reinjected into the excitability region by the coupling. In this sense, they are trapped in a transient region (transient for the uncoupled dynamics). Trapping in transient regions due to coupling appears to be a common mechanism for creating new attractors in networked systems. We have observed a similar behavior in an excitable model of an ecological predator-prey system based on the Truscott-Brindley model [166]. There, new equilibria are created by the coupling. On the equilibria, the coupling exactly balances out the local dynamics, and the units reach an equilibrium. Another example of trapping has been elucidated in units with chaotic saddles in their local dynamics [40, 41, 152]. Chaotic saddles are non-attracting invariant chaotic sets. Under some circumstances, when a sufficiently large number N of units are coupled diffusively, they can get trapped in this chaotic saddle and form a chaotic attractor [40, 41]. Another example has been recently elucidated in a system with a canard [153].

Interestingly, in the neuronal system we have studied, the trapping also works if the coupling is present in only one of the directions x or y . These directions have different effects in generating new attractors, due to the geometry of state space. If only the x -direction of the coupling is present, only the LA-LA attractor emerges, not the LA-SA or SA-LA. For coupling in the y -direction the reverse is true: LA-LA does not emerge, but LA-SA and SA-LA do. This coupling in y is not biophysically relevant for the neuronal system we study here, but is important in ecological systems. There, this may represent the difference between migration of predators or the migration of prey species. In particular for the x -direction, we also mention that multistability is still maintained in a bigger networks with $N = 10$ units. The coexisting oscillating attractors, with a mixture of some units oscillating at large amplitude and some at low amplitudes still occur, with more units in high-amplitude oscillations than in the case with the x and y -couplings. We believe our study could serve as inspiration for future studies in other systems, such as in ecological ones, to investigate these effects of the coupling in more detail. Furthermore, it also serves as simple yet powerful example of the more general phenomenon of multistability through trapping of units in transients.

Acknowledgment

K.L.R. was supported by the German Academic Exchange Service (DAAD). E.S.M and U.F. acknowledge the support by the Deutsche Forschungsgemeinschaft (DFG) via the project number 454054251 (FE 359/22-1) and by The São Paulo Research Foundation (FAPESP) via the project number 2023/15040-0. The simulations were performed at the HPC Cluster ROSA, located at the Carl von Ossietzky Universität Oldenburg (Germany) and funded by the DFG through its Major Research Instrumentation Programme (INST 184/225-1 FUGG) and the Ministry of Science and Culture (MWK) of the state of Lower Saxony.

Additional information

Attractors for different local dynamics of the neurons

In the main text we study the behavior of the coupled neuronal units with fixed parameters. One important parameter we can vary is I . Taking it as a bifurcation parameter and increasing it, the manifolds of the saddle approach each other to form a homoclinic orbit at $I = I_{\text{HOM}} \approx 3.09$. At $I > I_{\text{HOM}}$, a stable limit cycle emerges from the homoclinic orbit, and now the unit is bistable. Increasing I further, the saddle and the node approach each other and a saddle-node bifurcation occurs at $I = I_{\text{SN}} \approx 4.8$, and the neuron goes back to being monostable, with only the stable limit cycle remaining.

To recall the attractors emerging at $I = 2.0$ and to provide a complementary view, we show in Fig. 4.6 a three-dimensional version of Fig. 4.3. One can notice the emergence of the LA-LA attractor, and its eventual replacement by a torus. Also one can see the emergence of the LA-SA attractors, which emerge touching the red circles, that denote saddle points of saddle-node type.

To understand how these attractors depend on the local dynamics of the units, particularly how they change when the units go through the homoclinic and saddle-node bifurcation, we have studied a two-parameter continuation curve of the bifurcations giving rise to both the LA-LA and the LA-SA attractors. This is shown in Fig. 4.7.

The SNLC bifurcation generating the LA-LA solution converges to $(\epsilon, I) = (0, I_{\text{HOM}})$. For $I > I_{\text{HOM}}$ the LA-LA seems to occur for any value $\epsilon > 0$ that we tested. Therefore it seems that the LA-LA SNLC curve becomes vertical for $I > I_{\text{HOM}}$ at $\epsilon = 0$. The SNLC bifurcation destroying the LA-SA attractor converges to $(\epsilon, I) = (0, I_{\text{SN}})$.

The attractors therefore exist for a wide range of parameters in the local dynamics of the units. Further, for $I > I_{\text{HOM}}$, another attractor emerges, in which both units synchronize completely in the limit cycle that is now stable in the local dynamics.

Simple local dynamics: polynomial model

In the neuronal system, new attractors are created by an interplay between the coupling and the uncoupled vector field. There, units are trapped in a large excitability region wherein they oscillate. Trapping can occur more broadly in other systems. To illustrate this, we study a much simpler system. The basic result is that new attractors also emerge from this interplay. In particular, similarly to before, stable equilibria or limit cycles can appear for a finite interval of positive coupling strengths.

We take the uncoupled system as $f(x) = -(x + 2)(x + 1)x(x - 1)(x - 2) + d = -x^5 + 5x^3 - 4x + d$ for $d = 2$, such that it has 3 equilibria. The coupled system is then

$$\dot{x}_1 = -x_1^5 + 5x_1^3 - 4x_1 + d + \epsilon(x_2 - x_1) \quad (4.8)$$

$$\dot{x}_2 = -x_2^5 + 5x_2^3 - 4x_2 + d + \epsilon(x_1 - x_2). \quad (4.9)$$

For $\epsilon = 0$ it therefore has 3^2 equilibria. By plotting the system's nullclines, it is easy to verify that an increase in ϵ causes them to move toward each other such that at $\epsilon \approx 0.2419$ a saddle-node (SN) bifurcation occurs that generates a new attractor. In fact, because of the permutation symmetry between the units, two SN bifurcations are happening, generating two new stable equilibria. These new intersections live until $\epsilon \approx 0.94$, when another SN bifurcation destroys them. These equilibria exist as the coupling term $\epsilon(x_2 - x_1)$ exactly balances out the local dynamics $f_1(x_1)$ of unit 1 (and

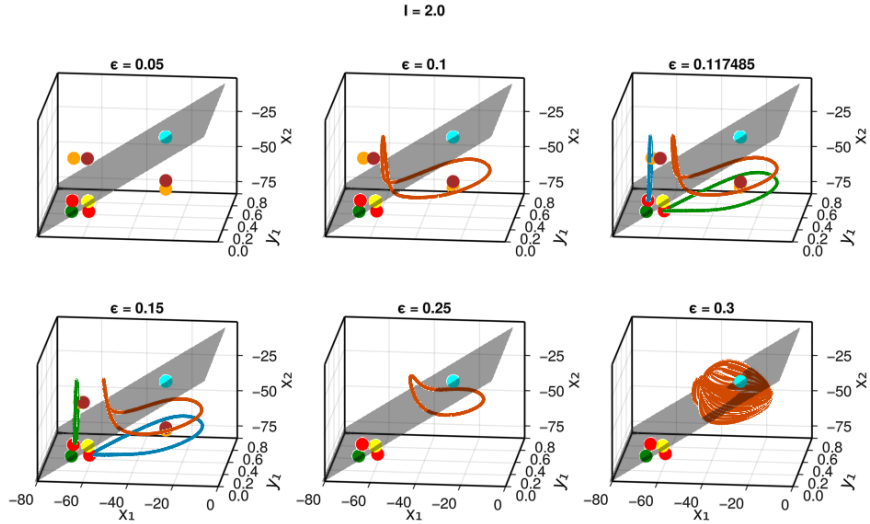


Figure 4.6: **Attractors transformed or created by the diffusive coupling for $I = 2.0$.** Each panel is a projection onto 3D space spanned by $x_1 - y_1 - x_2$. The gray plane denotes the plane with $x_1 = x_2$. The circles' colors denote types of equilibria. These equilibria are formed as combinations of the three equilibria in the single units, and are labeled according to this combination: green for stable node, yellow for saddle-saddle (two positive, two negative eigenvalues), cyan for focus-focus (two pairs of complex conjugate eigenvalues with positive real part), red for saddle-node (three positive, one negative eigenvalue), orange for node-focus (one pair of complex conjugate eigenvalues with positive real part, two negative eigenvalues) and brown for saddle-focus (one pair of complex conjugate eigenvalues with positive real part, one positive and one negative eigenvalues). One attractor emerges at $\epsilon \sim 0.065$ corresponding to two units oscillating with large amplitude. Two (symmetric) attractors emerge at $\epsilon \sim 0.117485$ corresponding to one unit oscillating with small amplitude around the saddle-node point and the other oscillating with large amplitude. The symmetric attractors die out at $\epsilon \approx 0.22$. A torus emerges at $\epsilon \sim 0.25$. More bifurcations keep happening until all new attractors die out, and only the stable equilibrium is left.

equivalently for unit 2). In this sense, on the equilibria, the units are also trapped. These two new attractors therefore emerge (and disappear) due to the coupling. We summarize this behavior in a continuation curve performed using XPPAUT [156].

These equilibria become limit cycles if one introduces a rotation in the system. To do this, one can modify the uncoupled dynamics, defining x as a radial variable r in polar coordinates and introducing an angular variable θ :

$$\dot{r} = -r(r+2)(r+1)(r-1)(r-2) + d \quad (4.10)$$

$$= -r^5 + 5r^3 - 4r + d \\ \dot{\theta} = \omega. \quad (4.11)$$

This system can be viewed as the first system with a rotation. In this case, the equilibria we observed before become limit cycles, and they now emerge through a saddle-node bifurcation of limit cycles (SNLC) at the same parameter values as before. Also, similarly to the equilibria, the units on these emerging limit cycles are trapped by the

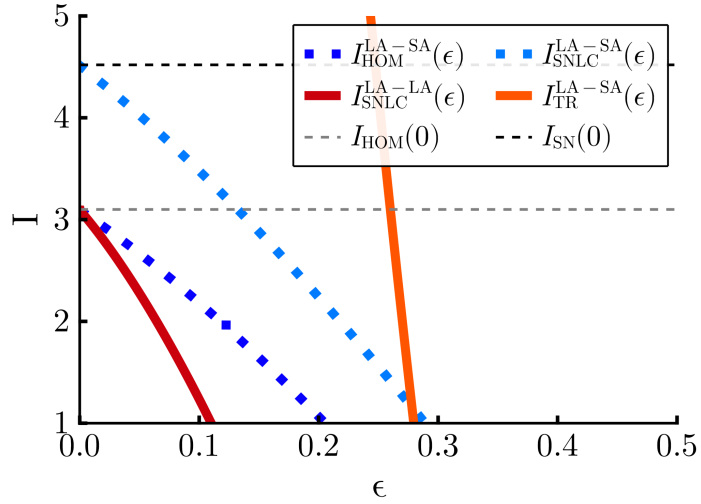


Figure 4.7: **Two-parameter continuation curves across I and ϵ .** The curves denote the $I(\epsilon)$ combinations that lead to each labelled bifurcation. The red and orange solid curves denote the bifurcations for LA-LA attractors, born through a SNLC bifurcation and de-stabilized through a torus (TR) bifurcation. The LA-LA is thus stable in between those curves. The blue and cyan dotted curves denote bifurcations occurring for the LA-SA attractor, born through a homoclinic (HOM) bifurcation and disappearing through a saddle-node bifurcation of limit cycles (SNLC). The LA-SA exists in between those curves. The homoclinic and saddle-node of equilibria (SN) bifurcations occurring in the uncoupled ($\epsilon = 0$) case are respectively shown in grey and black dashed lines. Continuations were done using XPPAUT [156]

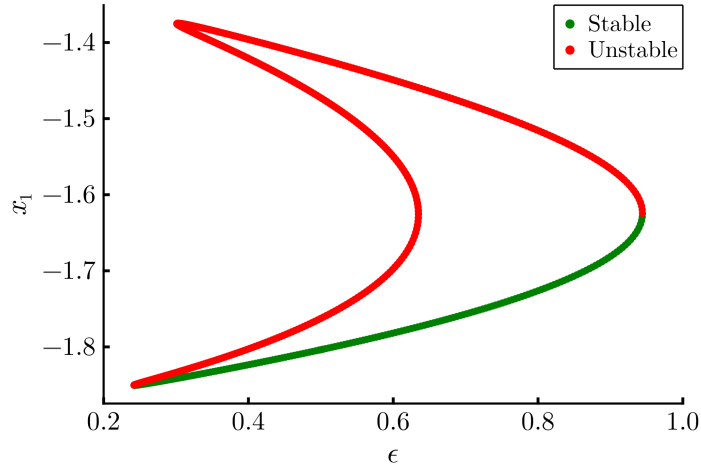


Figure 4.8: **Continuation of stable equilibrium emerging due to diffusive coupling in the simple algebraic system.** Similarly to the stable limit cycles we see in the neuronal system, the emerging attractor exists for an interval of coupling strengths, here approximately $[0.24, 0.94]$. It emerges and disappears in a saddle-node bifurcation.

coupling in a transient region of their uncoupled dynamics.

Chapter 5

Dynamical properties and mechanisms of metastability

Abstract

Metastability, characterized by a variability of regimes in time, is a ubiquitous type of neural dynamics. It has been formulated in many different ways in the neuroscience literature, however, which may cause some confusion. In this chapter¹, we discuss metastability from the point of view of dynamical systems theory. We extract from the literature a very simple but general *definition* through the concept of *metastable regimes* as long-lived but transient epochs of activity with unique dynamical properties. This definition serves as an umbrella term that encompasses formulations from other works, and readily connects to concepts from dynamical systems theory. This allows us to examine general dynamical properties of metastable regimes, propose in a didactic manner several *dynamics-based mechanisms* that generate them, and discuss a theoretical tool to characterize them quantitatively. This work leads to insights that help to address issues debated in the literature and also suggest pathways for future research.

5.1 Introduction

Time-series of neural activity often reveal series of transitions between experimentally observable regimes with unique dynamical properties. For example, as subjects fall asleep, their brains progress through a series of well-defined patterns, from the 11–15 Hz sleep spindle [167], to the large low-frequency rhythms of deep sleep [168], and to waking-like activity during rapid eye movement (REM) sleep [169]. These sleep stages, or regimes, can also occur on shorter timescales, as subjects transition from passive rest to active perception [170]. This ubiquitous phenomenon of regime switching has prompted connections to the concept of *metastability* in physics and dynamical systems theory. Many works have demonstrated metastability in neural systems across different spatiotemporal scales and species [171, 172, 173, 52, 53, 174, 175, 51, 176, 177, 178, 179, 180, 181, 182, 183, 184, 50, 185, 186, 187, 188, 189].

Understanding the mechanisms based on dynamical systems theory that can generate such metastable regimes is crucial, especially as this knowledge can aid in the development of techniques to predict transitions between regimes and to possibly control them. The literature in neuroscience has made crucial advancements in this regard [50, 190, 54, 191, 51, 192, 193], but differences in formulation between works can lead to some confusion. For instance, the explicit definition of metastability is not totally clear in the neuroscience literature (see Sec. 5.2.2 for more). Further, discussions on

¹This chapter is a modified form of a manuscript under review: Kalel L. Rossi, Roberto C. Budzinski, Everton S. Medeiros, Bruno R. R. Boaretto, Lyle E. Muller, and Ulrike Feudel. Dynamical properties and mechanisms of metastability: a perspective in neuroscience.

the dynamics-based mechanisms for metastability are usually restricted to only a few possible mechanisms, depending on the context and formulation of each work.

In this chapter, we aim to address these issues by discussing the neuroscience literature through the lens of dynamical systems theory. First, we extract from the literature a very simple but general definition of metastability, based on *metastable regimes*. Regimes are epochs of a time-series identified in each work that have unique dynamical properties. They are considered metastable when they are *long-lived but transient*. This idea is widespread among works not only in neuroscience, but is also similar to the well-defined view in physics and dynamical systems theory [194, 195, 196]. The characterization as long-lived is specific to the system being studied, and discussed in details later. We argue that all metastable regimes share a crucial defining property in state space, which is the space spanned by all variables of a system (explained in detail in Sec. 5.3.1). Simply put, metastable *regimes* correspond to metastable *regions* in state space, in which trajectories have a high probability of remaining inside. This idea can be formulated theoretically through the concept of almost-invariant regions [56, 55] (see Sec. 5.3.2 for details).

Associating metastable regimes in time to metastable regions in state space, which in turn are defined as almost-invariant [56, 55], allows for a single coherent view on metastability. It also allows for a direct connection to well-known dynamics-based mechanisms from dynamical systems theory. Here, we discuss and compare several of these mechanisms in a didactic manner. By looking into them together through a general definition, we are able to add important insights into issues debated in the literature and propose new research directions to generate experimentally testable and falsifiable hypotheses about metastability in the brain, potentially including phenomena such as sleep, seizures, and computations in neural circuits.

5.2 Short summary of metastability in the brain

5.2.1 Observations of metastability

We now review key observations that have helped to establish metastability as an important dynamical phenomenon. We focus on examples of metastability characterized by the switching between long-lived regimes of activity. These regimes are epochs of observations with unique dynamical properties identified by the authors of each work, and their characterization as long-lived depends on the specific application being considered. Further, as a note of terminology, these regimes are often called states in the neuroscience literature, but we avoid this here because it conflicts with already well-established terminologies in other fields of science. Instead, we believe regime is equally descriptive, and less ambiguous. In this section, we only maintain state as a synonym for regime when it refers to a well-established name, such as EEG microstates.

Figure 5.1 illustrates some observations showing time-series with metastable regimes, along with two corresponding characteristics: (i) whether the transitions between the regimes occur during resting conditions (spontaneously) or if they are evoked by some stimulus; and (ii) whether the metastable regimes occur more than once in the observation (repeat) or not.

As a first example, Fig. 5.1A shows time-series of electroencephalography (EEG) measurements performed in resting humans with eyes closed (taken from Ref. [171]). Colors indicate **EEG microstates**, identified from the spatial configuration of the elec-

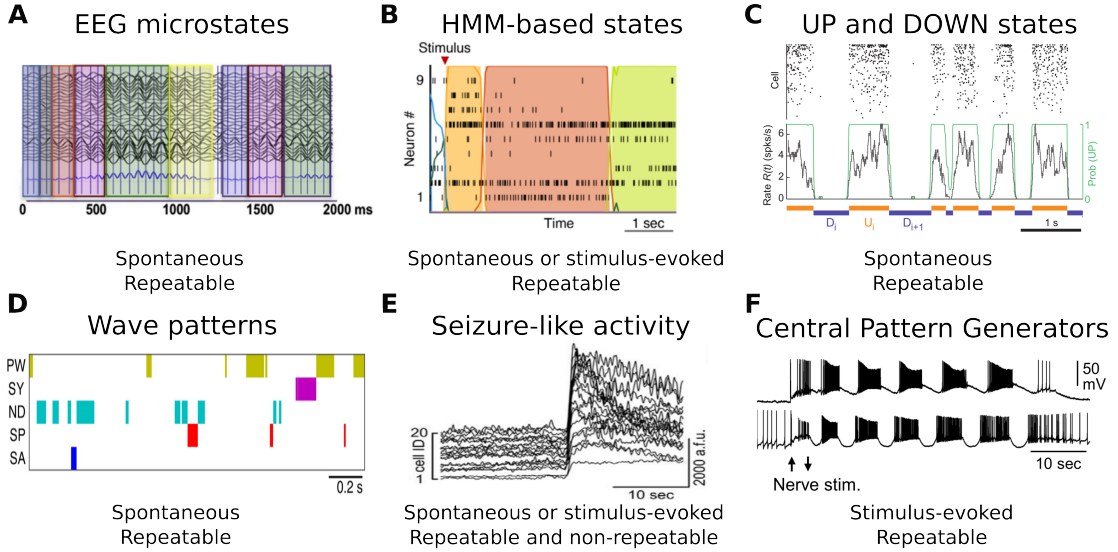


Figure 5.1: Brain activity typically evolves as a sequence of well-defined regimes that are transient but long lived. The panels illustrate observations taken from the literature, namely EEG microstates [171] (A), firing rate states identified via hidden-Markov-modelling (HMM) [51] (B), UP and DOWN states [178] (C), cortical wave patterns [197] (D), seizure-like activity [198] (E), and bursting in central pattern generators [199] (F). Each observation is explained in detail in the main text, and is classified into subtypes of metastability that we define in the Sec. 5.3.4.

tric potential amplitude of each electrode. These microstates remain almost constant for roughly 100 ms [172, 173], and then give way to other microstates.

Figures 5.1B-C show results based on firing rates of neurons. In particular, Fig. 5.1B shows exemplary sequences of regimes adapted from Ref. [51]. The regimes are characterized by roughly stationary behavior in the firing rates of neurons in the gustatory cortex of rats, and are identified via the technique of **hidden Markov modelling** (HMM). Each regime lasts for roughly an order of magnitude longer than the transitions between any regime [52, 53, 174, 175, 51]. This is observed during both spontaneous and stimulus-evoked activity, and the sequence of such regimes is shown to encode the stimuli presented to the animals [53, 174]. These regimes are proposed to serve as a “substrate for internal computations” in the brain [53]. Similar results have also been reported in the frontal cortex of monkeys during a delayed localization task [176, 177].

Figure 5.1C shows sequences of sustained firing (significant activity, **UP states**) and silence (**DOWN states**) in the firing rates of the deep layers of the somatosensory cortex of urethane-anesthetized rats (adapted from Ref. [178]). Each regime lasts for a significant time, with quick transitions between them [178]. These regimes are ubiquitously observed in spontaneous activity [179, 178].

Figure 5.1D shows a sequence of complex **wave patterns** identified in the cerebral cortex of anesthetized marmoset monkeys, taken from Ref. [197]. Starting from local field potential data from multiple electrodes, the authors created a spatial map for the phases of the oscillations, filtered at the δ band (1 – 4 Hz), from which they identified different spatiotemporal patterns, classified as plane waves (PW), synchrony (SY), node (ND), spiral (SP), and saddle (SA) [197]. These patterns repeat across the time series,

but the probability of switching from one pattern to another differs from pattern to pattern, i.e., there is preferential switching between patterns [197].

Mazor and Laurent [180] (not included in the figure) measured the firing rate of neurons in the antennal lobe of locusts as the animals were presented with a variety of odor pulses. Their results suggest that, for long pulses (lasting more than 2 s), spiking activity in the antennal lobe switches between a baseline fixed point and an odor-specific fixed-point, which can last for a few seconds. Interestingly, the transition epochs between the two fixed points were found to contain the most amount of information about the stimuli, suggesting an important role for them in neural computations [180, 200]. This suggests a functional role of transitions between metastable regimes for information processing [180, 201].

Figure 5.1E shows the neural activity recorded by two-photon calcium imaging in mouse neocortex [198] (Copyright 2019 Society for Neuroscience). The neural population is being invaded by a propagating **seizure-like activity**, which appears in the middle of the time-series, and is characterized by sustained firing of a large number of neurons. Traveling as a wave, it transiently replaces the baseline regime, in which firing is more sparse and distributed. In this study, a pharmacological agent was applied to a specific region of the cortex to induce the seizure-like activity.

Figure 5.1F shows the swim motor pattern in intracellular recordings of two neurons that belong to the swim central pattern generator of the mollusk *Tritonia* [199] (adapted from Ref. [199]). These neurons respond by **bursting** when nerve PdN3 is stimulated. These bursts are phenomenologically similar to those shown later in Fig. 5.4E (though their mechanisms might differ), and demonstrate the alternation between periods of sustained firing and periods of silence. The dynamics of central pattern generators often include metastable regimes [202].

Another work (not included in the figure) has also found that the power spectrum of local-field potential (LFP) recordings in rats progresses as a sequence of relatively stationary regimes lasting for some time before rapidly transitioning to other regimes [184] (see e.g. Fig. 2 of Ref. [184]). This was observed as the rats recovered consciousness, when the concentration of anesthetic was progressively decreased. The authors argue that the existence of well-defined metastable regimes is crucial for the fast recovery of consciousness [184].

Additionally, we remark that several other regimes could be mentioned in this section, such as other types of seizures [186, 203]; sleep spindles [187], transient patterns of circular waves that repeatedly travel across the cortex during sleep and may aid the consolidation of memories [204], and the phases of local-field potentials in cats at rest [50, 185]. For further reviews on this topic, we refer the reader to Refs. [50, 51, 191, 205].

5.2.2 Current formulations of metastability

Several theoretical formulations have been employed to study the observations of metastability in the brain, but they have remained focused mostly on the specific context of their observations, and a general view is currently lacking. To illustrate this issue, we depict in Figs. 5.2A-F the main formulations of metastability that we have identified in the neuroscience literature.

We can generalize the formulations in Figs. 5.2A-E as considering metastability to be a behavior with a type of variability in the dynamics. This variability can be directly observed as different *patterns of activity* (Fig. 5.2A) [206, 207, 77, 208]; or *patterns of*

synchronization (Fig. 5.2B, where activity shifts between in-phase and out-of-phase) [81, 209, 193, 80, 210]. As mentioned in the previous section, abstract regimes can be identified through techniques such as Hidden-Markov model [211, 53, 51] or Principal Component Analysis (PCA) [181]. Then, metastability is simply said to be the variability of these regimes (Fig. 5.2C, with each circle representing one distinct regime) [211, 53, 212, 213, 214, 215, 216, 217, 218, 191, 219, 220]. In other works, metastability is said to occur due to variability of trajectories along different *regions of state space* [221, 54]; see Fig. 5.2D, where the black curve represents a trajectory passing through equilibria in colored circles, with their stable and unstable manifolds in dark green and red, respectively. For a detailed explanation of these concepts, we refer the reader to Sec. 5.3.1. Metastability has also been defined as a variability along different positions on an *energy landscape* (Fig. 5.2E) [222, 191, 210, 221]. Another, more distinct, formulation of metastability is that of a behavior with *integration-segregation*, in which neural assemblies transiently synchronize and desynchronize (Fig. 5.2F, where the nodes represent assemblies whose anatomical or functional connections correspond to lines, and their activity to colors, which alternate between synchronized and desynchronized) [120, 223, 50, 224, 225, 226, 227].

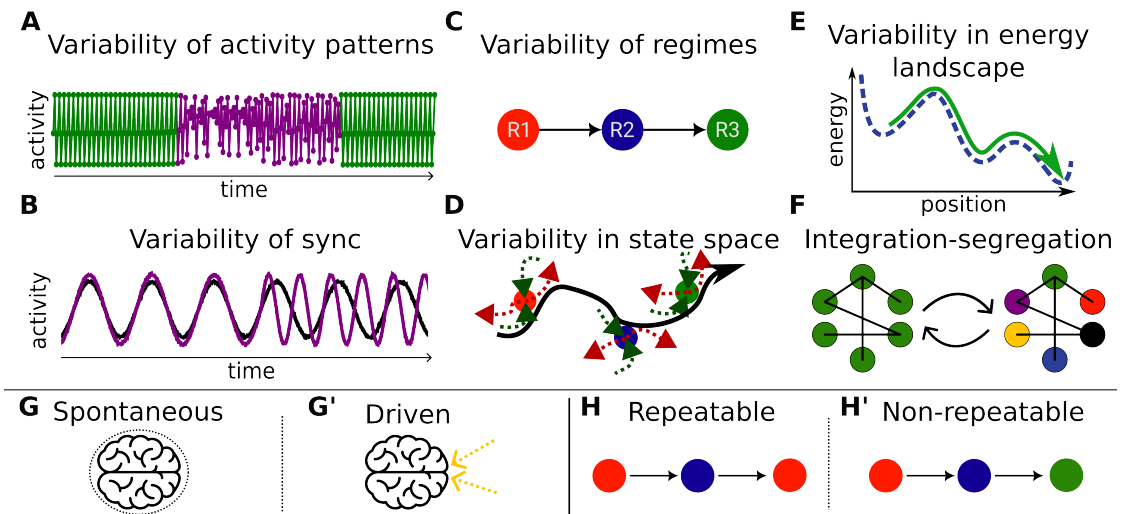


Figure 5.2: **Formulations of metastability in the neuroscience literature.** A common theme among these is the presence of transitions between certain aspects of the system’s dynamics (e.g., between activity patterns). The upper part of the figure (A-F) illustrates what these aspects are in each formulation, and the bottom part (G-H') shows characteristics of the transitions. Further details are available in the main text.

Furthermore, we remark that, while some works explicitly mention a time-scale separation in metastability [221, 51], others do not. Works also differ in regard to the possible mechanisms giving rise to metastability. Some consider that the variability in the dynamics needs to be spontaneous, occurring in autonomous systems (Fig. 5.2G) [181, 226, 208, 228, 191], while others argue that the variability must be externally induced, occurring in non-autonomous systems (Fig. 5.2G') [178, 221]. A combination of both is also found in Refs. [51, 207, 53]. Finally, another source of difference is in the repeatability of metastable regimes: some works consider metastable regimes only when they are repeatable (Fig. 5.2H) [54], while others also consider non-repeatable

(Fig 5.2H') regimes [51]. Examples of these types of metastability are shown in the observations in Fig. 5.1.

5.2.3 The common thread

As we have seen in the previous sections, the explicit formulation of metastability can vary considerably depending on context. However, there is a common thread across all the observations and formulations. It starts with the notion of regimes as epochs of a time-series with unique dynamical properties. For instance, unique spatial configurations of the EEG electric field define unique EEG microstates [171], and UP states have an above-threshold firing rate, while DOWN states do not [178]. Further, these regimes often have constant, or almost-constant properties throughout their duration.

Then, regimes are characterized as long-lived, even if only qualitatively, establishing thus the common thread across works: **metastable regimes are long-lived but transient**. Although sometimes implicit, we believe this common thread is the fundamental aspect of metastability as a dynamical behavior. This is also the view that has been held generally in physics [194, 195].

In this chapter, we look into dynamics-based mechanisms that generate such metastable regimes, connecting these ideas with dynamical systems theory. To achieve this, we introduce some crucial concepts from this theory in the next section.

5.3 Metastability in state space

5.3.1 Stability and invariance - initial concepts

A dynamical system is a set of N variables together with the rules that dictate their time evolution. These variables may be observables identified from experiments, for instance. At each instant, the values of these N variables define the *state* \mathbf{s} of the system. The N -dimensional abstract space containing all possible states of a system is called the *state space*. In this space, each dimension corresponds to a variable of the system.

For example, consider a ball moving in a landscape with two wells separated by a hill (cf. Fig. 5.3A). When released, the ball rolls downhill in this landscape. Appropriate variables defining the state of the ball at any given time are its position x and velocity v , such that we can write the state \mathbf{s} of the ball as a two-dimensional vector $\mathbf{s} = (x, v)$. So the state space for the ball will have two dimensions: one for x , another for v , as represented in Fig. 5.3A'. We can initialize this system by releasing the ball from a certain height with some speed, defining an initial state $\mathbf{s}_0 = (x_0, v_0)$.

This initial state, also called initial condition, is one point in state space. Once released, that ball will evolve in time, going through a continuous sequence of different states, revolving around the well until it eventually comes to rest at the bottom of one well. This sequence of states representing the movement of the ball is called a *trajectory* of the system, and corresponds to a path in state space. Equivalently, a trajectory is a set of points (a set of states). There are infinitely many trajectories in state space; one of them is represented in Fig. 5.3A' as the black curve.

Dynamical systems theory shows that the time evolution of the infinitely many trajectories is governed by the properties of certain structures present in state space. It then becomes crucial to understand these structures.

To start, notice that in the example the ball eventually converges to the bottom of one of the wells because it loses energy due to friction. In general, any system

characterized by energy losses will converge to *attractors*, which are attracting sets of points in state space. The state of the ball at rest on the bottom of each well is an equilibrium attractor, as the trajectories converge to that state and stay on it indefinitely. The equilibrium thus does not change under the time evolution of the system, and is called *invariant*. If one were to periodically kick the ball, it may start to draw a periodic motion: instead of converging to a single point, it revolves around the well and repeats its motion every certain period. In state space this corresponds to a closed loop, also an invariant set. Other invariant sets are also possible, such as chaotic sets, in which the long-term behavior of a trajectory is highly sensitive to changes in its initial conditions.

Attractors are said to be locally stable in state space: any small perturbation away from an attractor leads to a trajectory that eventually returns to it. An important remark is that this double well system has two stable equilibria, i.e. two attractors, so it is called bistable (in general, for more attractors, it would be called *multistable* [1, 126]). To which of the two attractors the ball converges depends on its initial state.

Another class of important structures are unstable sets. We have one such structure in the double well: the top of the hill. If a trajectory starts exactly on top of the hill, it will stay there for an infinitely long time; again, the top of the hill is invariant. If we perturb the ball, even slightly, it will leave the top and converge to one of the wells.

The stability of invariant sets can be understood from a geometrical point of view in state space. While the stable equilibrium attracts trajectories from all directions near it, the unstable equilibrium has specific attracting and repelling directions. In this case, the unstable equilibrium is said to be of saddle type [229], in reference to saddles (e.g. a horse-riding saddle), which also have such attracting and repelling directions. These directions are called the stable and unstable manifolds of the equilibrium, respectively. Figure 5.3A' shows the saddle equilibrium in a red circle, with its stable and unstable manifolds as green and red curves, respectively. Saddle-points, or in general saddle invariant sets, play an important role in several deterministic mechanisms leading to metastability, as we show in Sec. 5.3.3.

Before proceeding, we remark that an alternative introduction to many of these concepts is provided in Ref. [230].

5.3.2 Metastability and almost-invariance - definition

In the previous section we introduced a common notion of stability, which requires that a set is invariant, such that trajectories reaching it remain on it for infinitely long times. Now let us imagine a different scenario in the double well landscape: suppose the ball has a small demon that is constantly kicking it in randomly chosen directions with randomly chosen strengths, as illustrated in Fig. 5.3B. This effectively adds noise to the ball's evolution, creating a *noisy* system. The landscape of course has not changed, so the *noiseless* system is still the same. Therefore, the ball still tends to roll downhill, attracted towards the bottom. But the noise often kicks it away, repelling the ball from the bottom. As a result of this interplay between attracting and repelling tendencies, the ball is always in motion, revolving randomly around the bottom of one well, but never gets stuck to it.

Eventually, by chance, the demon will give the ball successive kicks up the hill in such a way that it overcomes the top and falls onto the other well. How many kicks are needed depends, on average, on the noise strength: lower noise requires on average more kicks, such that the ball can stay around one well for very long epochs (see Ref. [231]

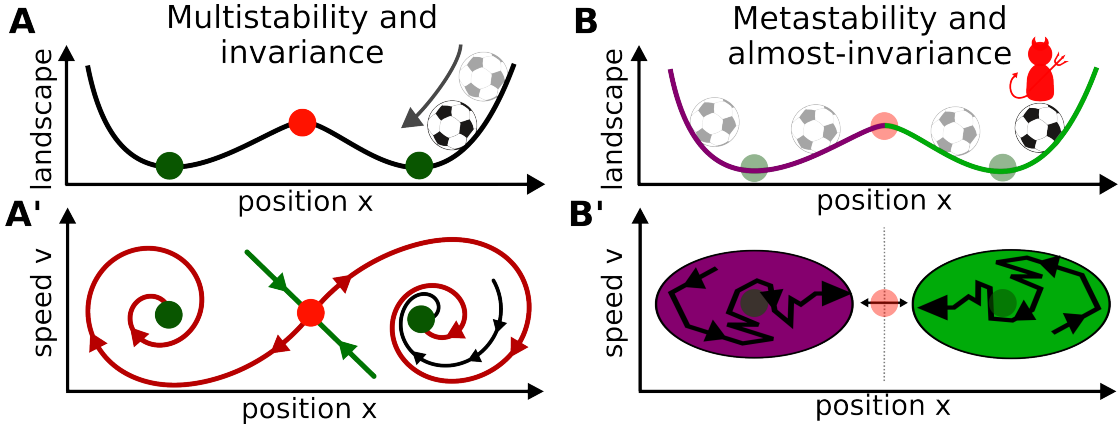


Figure 5.3: **Illustration of multistability versus metastability.** Panels A and A' illustrate the behavior of a ball on a double-well landscape, representing a multistable system. The stable and unstable equilibria are represented by green and red circles, respectively. In A, the ball is shown on the landscape to converge to the equilibrium on the right, where it stays indefinitely (equilibria are invariant). In A', a possible corresponding trajectory is shown in state space. The green curves leaving the unstable equilibrium denote its stable manifold, while the red curves denote the unstable manifold. In B, we suppose there is a demon kicking the ball and thus introducing white noise to its dynamics. This now makes the ball switch eternally between the two wells, and effectively transforms the previous equilibria (not invariant anymore, represented as faded circles) into metastable regions (which are almost-invariant), represented illustratively in B' by the purple and green ellipses.

for more details).

So the ball with noise never converges to an attractor - instead, it moves for potentially very long times inside a region close to where the noiseless attractor is located, and eventually leaves. The noise transforms the ball's dynamics from stable equilibria into metastable regimes, *from multistability into metastability*, in the sense of long-lived but transient regimes that we discussed in Sec. 5.2.3 [231, 3, 232, 233, 234, 235, 1]. This idea is illustrated in Figs. 5.3B and B'. It should be noted that these remarks are valid as long as the noise strengths are not large enough to create purely noisy trajectories, which just diffuse through the state space.

In the noiseless system, the bottom of each well forms an invariant set. In the noisy system, we have seen that two regions emerge in which the ball spends a long time. These regions are *almost-invariant*, in the sense that trajectories inside them have a high probability of remaining inside as they evolve [56, 55]. An almost-invariant region R can be defined such that the probability of staying inside it after some time evolution is large enough that trajectories stay inside for long periods of time. The higher the probability, the longer they stay. These concepts have been nicely formalized in previous works [56, 55], so we refer the reader to those references for more details. We provide a brief summary in the Supplementary Material.

Importantly, note that noise is, in general, not necessary for generating almost-invariant regions - as we see later in Sec. 5.3.3, there are also several mechanisms that lead to almost-invariant regions in deterministic, autonomous systems. The case with

noise was used here only as a simple concrete example.

Therefore, we can say in general that a region R of state space is metastable if it is almost-invariant, that is, if trajectories, once in R , tend to stay in R for a long time before leaving. This is a key point in our work: **metastability is observed through long-lived but transient (metastable) regimes, and underlying any metastable regime is an almost-invariant (metastable) region of state space.**

This view formalizes the notion of long-lived but transient regimes and reformulates them into properties in state space, associating a dynamical regime to its corresponding region, and associating that region to an interpretable quantity, namely the probability of trajectories remaining inside. The concept of almost-invariance is crucial for this, and serves as a theoretical tool to quantitatively characterize metastability.

In some applications, one might be concerned with the minimum duration of metastable regimes, i.e., how long regimes need to be in order to be metastable. This question requires an arbitrary decision on a threshold, which cannot be objectively decided in general; it depends on the specific application. The advantage of this definition is that it is agnostic to a minimum duration and thus flexible to this decision. Another advantage is that the decision can be made not in terms of a duration, but in terms of a probability, which may have a clearer interpretation.

Beyond their characterization, the identification of metastable regimes is also an important problem, which has seen several solutions in the neuroscience literature, as discussed in Sec. 5.2.1. An interesting approach is through optimization procedures that aim to maximize the probability of trajectories remaining inside the almost-invariant regions [236, 56, 55]. This can identify maximally almost-invariant regions, on which regimes will be maximally long, on average. These regions have been shown for some systems to have a particular geometrical property: they are partially separated in state space by invariant manifolds, which gives further insight into their structure and localization [237]. The technical details of how this identification can be done for observed time-series, however, go beyond the scope of this work, and is the subject of ongoing research [238].

Further, it is worth remarking that metastability of a regime does not fully define its dynamics. As we see in the next section, metastable regimes can be, for instance, periodic or chaotic, generated by deterministic or by noisy mechanisms, etc. A deeper analysis is required to fully characterize metastable regimes.

5.3.3 Dynamics-based mechanisms for metastability

The definition of metastability encompasses the observations and formulations previously reported in neuroscience. Furthermore, and crucially, it also allows one to study concrete mechanisms that generate metastable dynamics. These are known from dynamical systems theory. Some have been proposed in the context of metastability [54, 191, 51], but others have not yet so far, to our knowledge.

Before we proceed to the mechanisms, we remark that around any metastable region there is a *coexistence of attracting and repelling tendencies* [50, 239]. The ability of metastable regions to retain trajectories is due to their attracting tendencies, and their finite duration is due to their repelling tendencies that push the trajectories away - for instance, in the double-well example, think of the attraction towards either of the two wells versus the repulsion due to the noise.

The double-well landscape with noise is a simple example of the general behavior

of noise in a multistable system. As we have discussed before, trajectories spend considerable time around one well, then hop to the other well, and repeat this behavior indefinitely. This phenomenon is called *attractor hopping* [234]: the system now has two metastable regimes, each corresponding to the dynamics around one well. In this sense, *noise replaces the stable equilibria with metastable regions*. The regimes can be seen in the time-series of the ball's position x in Fig. 5.4A and the regions in the ball's state space, spanned by its position x and velocity v , shown in Fig. 5.4A'. The times spent on each metastable region (called residence times or dwell times) follow a probability distribution, such as an exponential distribution for Gaussian white noise [240] (Fig. 5.4A''). This mechanism of noise-induced transitions in multistable systems has been proposed for several observations of metastability in the brain [51, 221].

We introduced metastability with the example of a noisy system in Figs. 5.3B-B' and 5.4A-A'', but metastability can also occur without any noise or external input, due to several possible *deterministic* mechanisms. We concentrate now on some of these, starting with a **stable heteroclinic cycle**, which is demonstrated here by a firing-rate model derived from three synaptically-coupled Hodgkin-Huxley neurons [241]. Figure 5.4B shows the time-series of a trajectory on such a cycle, performing a sequential alternation between three distinct regimes, each with a unique color. These regimes correspond to the vicinity of specific points in state space, as highlighted in Fig. 5.4B'. They are saddle-points, like the red circle shown in Figs. 5.3A-A', which have coexisting attracting directions (stable manifold) and repelling directions (unstable manifold). The stable manifold of one saddle is connected to the unstable manifold of the next, in what is called a heteroclinic connection [229]. Furthermore, this cycle is stable: trajectories approach one of the saddle-points along its stable manifold and potentially spend a long time near it - then, they depart along its unstable manifold to the next saddle, and so keep cycling through them, converging ever closer to the saddles and their manifolds. This can be seen in the increasing residence times in Fig. 5.4B''. Trajectories in the neighborhood of each saddle-point stay inside for considerable durations, so the neighborhood is a metastable region (even though the saddle-point itself is invariant and unstable).

Importantly, it can be shown that such heteroclinic cycles can globally attract trajectories [242] and are also conserved under small parameter changes (they are structurally stable) [218]. Moreover, it has been shown in neural networks that heteroclinic cycles depend on the inputs to the neurons, such that the cycle is sensitive to the stimulus to the network [243]. Once the stimulus is applied, and the cycle is defined, it is robust against noise. So this mechanism can allow for robustness to noise while keeping sensitivity to inputs [243, 218]. This, on top of the cyclic behavior, means that heteroclinic cycles are important structures to perform sequential *computations* [192]. An example of this is chunking dynamics, in which a trajectory coding for a memory alternates along a heteroclinic cycle composed of further heteroclinic cycles, each corresponding to chunks of a memory [192]. As such, stable heteroclinic cycles have also been proposed as the mechanism behind experimental observations [218, 200, 244] and theoretically hypothesized as a mechanism for cognition [192, 245]. Heteroclinic cycles can be extended to heteroclinic networks; for a review, see [246].

Now we move to another example, which involves a *chaotic attractor* that originates from an **attractor-merging crisis** [247]. In this case, the chaotic attractor can be decomposed into two distinct sub-regions. For a different parameter value of the system, these sub-regions are separate chaotic attractors. Starting from some critical parameter value, they merge together into a combined chaotic attractor, with a specific pathway

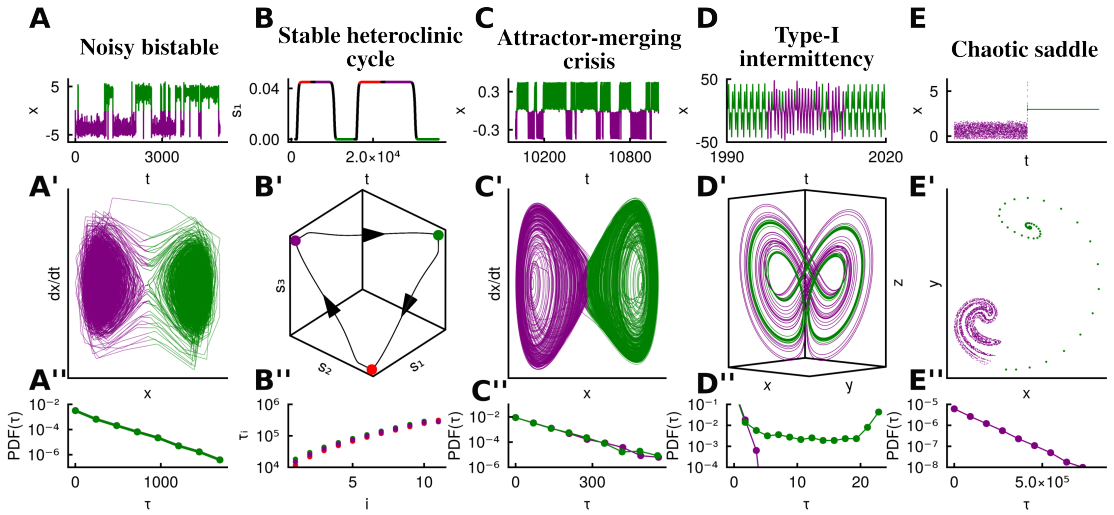


Figure 5.4: Dynamics-based mechanisms of metastability. Each column corresponds to a distinct mechanism. The first row (A-E) shows a representative time-series, with alternations between metastable regimes, each receiving a distinct color. The second row (A'-E') shows the state space of each system with the trajectory corresponding to the time-series above. The third row (A''-E'') shows the distribution of residence times in each metastable region for several trajectories. Further details are discussed in the main text and Supplemental Material.

connecting them. Then, trajectories in each sub-region oscillate chaotically for a long time, on average, before they switch to the other sub-region, and repeat this process indefinitely. Figures 5.4C-C' illustrate these two intermittent regimes in a time-series and their corresponding regions in state space, respectively, colored green and purple in both. The specific pathway guiding the transitions between each sub-region is a particular periodic trajectory of type saddle (having stable and unstable manifolds) - trajectories on one sub-region approach this trajectory and then are taken to the other sub-region. It thus acts as the repelling tendency mediating the transitions between the sub-regions. The probability distribution of residence times on each of these metastable regions is exponential (Fig. 5.4C'').

It is interesting to note that the trajectories for this mechanism look similar to those for the noisy bistable systems (compare Figs. 5.4A and 5.4C). The key difference is that the transitions in the former are caused by noise, and in the latter they are caused purely by the deterministic dynamics of the system on the attractor, with the mediating saddle periodic trajectory. Still, this highlights the often apparent similarity between noisy and chaotic dynamics, and the need for deeper analysis to distinguish between both [248].

Similar dynamics occur as a result of another mechanism, an **interior crisis** [249, 229]. Also in this case, trajectories intermittently switch between two sub-regions of the same chaotic attractor. But the underlying structures are different from the attractor-merging crisis: a change of parameters causes a chaotic attractor to connect to a chaotic set that is unstable (a chaotic saddle, which we see more in Fig. 5.4E-E''). This connected chaotic attractor now includes both regions, but trajectories stay inside each sub-region for long times, before switching to the other. These transitions are again mediated by a special pathway, a periodic trajectory of saddle type, which acts as the repelling tendency.

The distribution of times on the region occupied by the original chaotic attractor is again exponential. See Ref. [229] for more details.

Another example of a chaotic attractor that can be decomposed into two metastable regions occurs in **type-I intermittency**. We show in Fig. 5.4D an example in a 3-dimensional system. The trajectory alternates between metastable regimes: one with clear chaotic dynamics (in purple) and another with seemingly periodic dynamics (green). Looking at the state space in Fig. 5.4D', we note that the purple regime corresponds to a region that looks clearly chaotic (fractal-like structure), while the green regime corresponds to a region that looks like a periodic orbit (a closed loop). Trajectories can spend a considerable amount of time on the green region, looking periodic. When they leave it, they can then spend a long time in the purple region, leaving it when they approach the green region again. Mechanistically, the green region is actually the *ghost* of a stable periodic orbit that exists for different parameter values [250, 251, 57]. That stable periodic orbit is destroyed by a collision with an unstable periodic orbit at some critical parameter value, leaving behind only the ghost, which is not an invariant structure [252]. The bifurcation giving rise to this behavior is a *saddle-node bifurcation of periodic orbits*. It can also occur analogously for equilibria, and we refer the reader to Refs. [253, 254] for further work and illustrations. Importantly, the two metastable regions in our example belong to the same chaotic attractor, and the trajectories near the ghost merely *appear* to be periodic. Further, the time spent near the ghost can be considerably long, but is finite for any fixed parameter [251] (see the distribution of times in Fig. 5.4D'').

The type-I intermittency mechanism, along with the two crises discussed before, are three of many concrete instances of an idea proposed by Friston [207], who argues that different metastable regimes can correspond to different sub-regions of a same invariant set (usually attracting).

An important remark is that this mechanism does not require a chaotic attractor, as it occurs whenever a saddle-node bifurcation is nearby in parameter space. The chaotic attractor in the example only acts to re-inject the trajectories that leave the neighborhood of the ghost back onto it, creating a repeatable metastability. This re-injection can also occur due to noise, not only chaos [252]. But if there is no re-injection mechanism, nearby trajectories will pass the neighborhood of the ghost only once, and then this is an example of non-repeatable metastability.

This saddle-node mechanism has been proposed by Kelso and colleagues as a mechanism for metastability in the brain [255, 50]. Ghost structures have also been shown to play a role in the dynamics of recurrent neural networks performing particular computations [254]. Further, similarly to the idea of cycles of saddle-points (Figs. 5.4B-B''), cycles of ghost structures can also be constructed, and have been shown to generate sequences of metastable regimes that are robust in the presence of noise, having potential advantages over cycles of saddle-points [253].

Another mechanism that leads to metastable regimes is due to a **chaotic saddle**. A chaotic saddle is similar to a chaotic attractor, with the distinction that it also has repelling directions - it is thus the analogue of a saddle equilibrium for a chaotic set [256]. As a consequence, trajectories can stay near the chaotic saddle for potentially very long times, displaying chaotic dynamics, but are eventually expelled from it [196]. Figure 5.4E shows a trajectory switching from a regime near a chaotic saddle (in purple) to one on an equilibrium (in green); the corresponding regions in state space are shown in Fig. 5.4E'. Note that the trajectories leave the chaotic saddle because they are not

on it exactly; they are only near it. These are the typical trajectories, which are the ones numerically and experimentally observed. They form a metastable region even though the chaotic saddle itself is invariant and unstable. Ultimately, the trajectories converge to the stable equilibrium and remain on it infinitely long. The residence times for different initial conditions near the chaotic saddle follow an exponential distribution [249] (Fig. 5.4E'').

A chaotic saddle has been reported in networks of spiking neurons [148], in which, interestingly, it can be subdivided into three distinct dynamical regimes, corresponding to three distinct sub-regions, which are all intermittently visited for considerable durations. Therefore, also every sub-region of that chaotic saddle can be considered metastable. That is thus an example of *hierarchical metastability*, in which metastable regions contain inside more metastable regions, and the dynamics progresses through a hierarchy of metastable regimes [191]. Chaotic saddles have also been observed in other networks of spiking neurons [257, 258, 259, 260], and may play a key role in synchronization processes [40, 41].

There are several other dynamics-based mechanisms for metastability beyond the ones discussed previously. One example is **on-off intermittency**, which is common, for instance in systems that can completely synchronize [261, 262], and occurs during transitions from synchronization to desynchronization induced by changing the coupling strength between units. During these transitions, systems with on-off intermittency have trajectories that intermittently switch from a synchronized regime to a desynchronized one and back. The mechanism for this intermittency, and its statistical scaling, has been studied in detail [263, 264, 265, 266]. It is one out of many possible mechanisms that can realize the coexistence of integration (synchronization) and segregation (desynchronization), often mentioned as a crucial need for the brain [223, 50, 224, 120]. It is also a possible mechanism for the intermittent switching between UP and DOWN states exemplified in Fig. 5.1C. Furthermore, evidence for on-off intermittency has been reported for EEG data of non-convulsive paroxysmal (high-amplitude) activity in rats with genetic absence epilepsy [267]. The study identified a power-law distribution of residence times characteristic of on-off intermittency in regular brain activity, which alternated with the epileptic paroxysms. A very similar mechanism is in-out intermittency [268, 269, 270, 271]. In addition, evidence for yet another type of intermittency, known as type-III intermittency [250], has been reported in [272].

Metastability can also manifest as **mixed-mode oscillations**, in which trajectories alternate between regimes of small and large amplitude oscillations [273]. There are various mechanisms for mixed-mode oscillations, which can involve forcing the system to induce changes in parameters or through an adaptation variable that enables the switching between the two modes [273, 274]. A particular example of mixed-mode oscillations is *bursting* behavior occurring in neurons, characterized by quick firing of spikes followed by a quiescent period (as in Fig. 5.1F). Bursting is a ubiquitous mode of firing in neurons [275], and can have important functional roles due to its ability to generate more robust responses [276]. A simple model displaying bursting is the Hindmarsh-Rose neuron [277]. In it, an adaptation current causes the switching between the tonic spiking and the silence [277]. The whole trajectory is on a stable limit cycle, but can still be decomposed into the tonic spiking and the silence, each of which can be considered metastable. This is yet another example of the idea proposed by Friston in [207]. Beyond this model, bursting behavior occurs in systems with a period-adding cascade [278]. Mixed-mode oscillations can also occur as neuronal avalanches, which are cascades of activity occurring

in varying sizes and durations, and across different scales, seen in local-field potential activity [279]. An example of a dynamics-based mechanism generating avalanches has been recently elucidated in [153]. The onset of these avalanches may be associated with critical phenomena in the brain (see Ref. [280] for a recent review).

Moreover, an important example of metastable behavior is **chaotic itinerancy** [239]. This phenomenon has also been discussed in the context of neuroscience [281, 205, 282], and can include several specific mechanisms, and thus is also an umbrella term, but more specific than metastability as we define it here.

5.3.4 Subtypes of metastability

The definition of metastability proposed in Sec. 5.3.2 acts as an umbrella term encompassing several distinct observations, formulations, and mechanisms. More specific formulations, which restrict the phenomenon to particular contexts, can be defined as subtypes of metastability.

As a first example, we may think of **spontaneous and driven** metastability (illustrated in Figs. 5.2G-G' respectively). They differ in regards to how transitions between metastable states are generated. In *spontaneous* metastability, the mechanism behind transition is intrinsic to the system, and thus occurs without the need of external perturbations - such as noise, or stimuli. This is the case for Figs. 5.4B-E''. Driven metastability is the opposite: transitions occur because of external perturbations, as in Fig. 5.4A-A''. Each subtype has distinct but important functional roles: spontaneous metastability enables transitions between regimes without the expenditure of additional energy to stimulate the transitions [50], and guarantees that a system does not get stuck in the same regime [283]; driven metastability is important for direct control of the transitions, such as in stimulus-evoked scenarios.

A second important pair of subtypes is **repeatable versus non-repeatable metastability** (Figs. 5.2H-H'). These are characterized by whether the metastable regimes eventually repeat in the time series or not. If the metastable regimes repeat along observations, the metastability is repeatable; if they do not, it is non-repeatable. The case of non-repeatable regimes is sometimes called metastability en route to ground state [51]. Note that the observations in Fig. 5.1 and the mechanisms in Fig. 5.4 are already classified into these subtypes.

5.4 Conclusions and outlook

In this chapter we have provided a discussion on metastable brain dynamics in a way that is consistent across observations and theory in both neuroscience and dynamical systems. With this, we have looked into several dynamics-based mechanisms that generate metastability, and compared them to obtain insights into their commonalities, distinctions, and connections to previous literature.

The first step was to extract a general definition of metastability from the literature: metastable regimes are long-lived but transient. This serves as an umbrella term encompassing the other formulations in the literature, is useful to interpret observations, and readily connects to dynamical systems theory. We then looked deeper into how these metastable regimes behave in state space. To achieve this, we introduced the notion of almost-invariant regions of state space, characterized by a high probability (smaller than one) that trajectories, once inside them, remain inside [56, 55]. Trajectories can

enter an almost-invariant region, stay inside for a long time, and eventually leave. While inside such a region, trajectories exhibit time-series containing long-lived but transient epochs with unique dynamical properties, i.e. metastable regimes. The dynamics of the regimes corresponds to the dynamics in the regions (e.g., periodic or chaotic). Thus, almost-invariant regions, which we identify as metastable regions, underlie the dynamics of metastable regimes.

With this view, we have then discussed the *dynamics-based mechanisms* for metastability, i.e. how metastable regions and regimes are generated, and how they behave. Dynamical systems theory provides several concrete possibilities. Some of these have been previously discussed in the neuroscientific context [54, 191, 51], but some are also new, to the best of our knowledge. Though not a comprehensive list, we believe it serves as a good starting point for researchers both in neuroscience and dynamical systems intending to study metastability.

Looking at so many different mechanisms together provides several insights. To start, it provides concrete examples of metastable regimes corresponding to trajectories visiting metastable (almost-invariant) regions. Further, it becomes clear that around each metastable region there is a *coexistence of attracting and repelling tendencies in state space*, as has been discussed in Refs. [50, 239]. These realizations further validate the definition, which is general but still meaningful to allow for common underlying principles.

With this rich list of possible mechanisms, we have been able to provide several concrete instances of an idea that was abstractly proposed by Friston in Ref. [207]: that the same attractor can have multiple sub-regions, each corresponding to one metastable regime. An interesting instance of this has been reported in Ref. [148], in which networks of spiking neurons display a chaotic saddle (its neighborhood a metastable region) that can be further subdivided into three sub-regions, each metastable and corresponding to different patterns of activity.

We have also suggested more dynamics-based mechanisms that can account for the important behavior of coexistence of segregation and integration: besides the important saddle-node bifurcation of fixed points that often occurs [50], we also mention in-out and on-off intermittency as mechanisms that lead to variability of synchronization [261, 270].

The solid theoretical background offered by the idea of almost-invariant regions allows us to provide objective answers to issues debated in the literature. The distinction between attractors and metastable regions, and hence between *multistability* and *metastability* becomes clear. As discussed in Sections 5.3.1 and 5.3.2, attractors are invariant: trajectories on them remain on them infinitely long; meanwhile, metastable regions are only almost-invariant: trajectories eventually leave them. A system is called multistable when it has multiple coexisting attractors for fixed parameters, a typical behavior in nonlinear dynamical systems [1, 126]. In a multistable system, trajectories converge to one of the attractors, selected by their initial conditions, and remain on this attractor forever. There are no transitions between attractors in a multistable system. If external perturbations such as noise are introduced to a multistable system, the trajectories do not stick to attractors anymore, but can hop between them [231]. In this case, multistability is *substituted* by metastability [3]. An important remark is that, when the noise is too strong, it can overpower any dynamics of the system and then there is neither multistability nor metastability observable, only a random motion [234]. Crucially, however, stability (and multistability) can *co-occur* with metastability in autonomous systems, without noise. For instance, an attractor can be in some

cases decomposed into two or more metastable regions, as discussed previously and in Sec. 5.3.3. Then, trajectories remain eternally inside an attractor, but with transitions between its metastable regions.

Another point that is often debated is whether both *spontaneous* and *noise-induced* cases should be considered as metastable [226, 191, 221]. Here, we provide an objective answer: since there are almost-invariant regions underlying the dynamics in both cases, both are metastable. This is exemplified through the motion in the double-well landscape with noise (Figs. 5.4A-A'') and the intermittency due to an attractor-merging crisis (Figs. 5.4C-C''), in which also the phenomenology in the time-series, in state space, and in the distribution of residence times is strikingly similar. This means that many dynamics-based mechanisms may underlie the same observation. Therefore, the characterization of regimes as metastable is only part of the story: they possess other dynamical properties that also need to be studied. Developing methods to achieve this and properly distinguish between various mechanisms is still a subject of future research.

Understanding dynamics-based mechanisms is an important first step for *predicting* transitions between metastable regimes. This is particularly important in the context of seizure prediction, an area that has deservedly received a lot of attention but which still has many open questions [284]. Knowledge of the dynamics-based mechanism underlying transitions from normal brain activity to seizures has been recognized as a key development in the field [284], but that alone may not be enough: part of the difficulty may be the co-existence of several mechanisms, not just one. A more comprehensive understanding of the mechanisms for metastability, extending the ideas proposed here, could prove useful to address these difficulties through a better understanding of the precursor dynamics of transitions [285]. A possible future path can also aim to determine mechanisms underlying observations through the use of techniques to identify system equations from data [286, 287, 288, 289, 290].

Finally, we believe it is worth mentioning that transient or metastable dynamics have been recognized as important mechanisms for *computations* in the brain [192, 53, 291, 292, 180, 254] and other biological systems [293, 49]. Research has shown that systems can successfully perform computations with attractors [230] or with transient regimes [180, 294, 292, 230, 295, 296, 297]. This, allied with the observations of complex metastable dynamics in the brain [51], brings up the question: what advantages can spontaneous metastable regimes provide for computations, in contrast to stable regimes? This is a crucial question that needs to be addressed in future works, and may use the ideas proposed here as a starting point.

Therefore, we believe that the perspective we provide here connects observations, formulations, and mechanisms of metastability in neuroscience with the goal of understanding metastable brain dynamics.

Acknowledgments

We would like to thank Klaus Lehnertz, James A. Yorke, Niccolò Zagli, Nicolás Rubido, and Péter Koltai for inspiring discussions. In particular we would like to deeply thank Klaus Lehnertz for comments on this manuscript. K.L.R. was supported by the German Academic Exchange Service (DAAD). E.S.M and U.F. acknowledge the support by the Deutsche Forschungsgemeinschaft (DFG) via the project number 454054251. B.R.R.B. acknowledges the support of the São Paulo Research Foundation (FAPESP), Brazil, Proc. 2018/03211-6 and 2021/09839-0. This work was partially supported by

BrainsCAN at Western University through the Canada First Research Excellence Fund (CFREF), the NSF through a NeuroNex award (#2015276), the Natural Sciences and Engineering Research Council of Canada (NSERC) grant R0370A01, and the Western Academy for Advanced Research. R.C.B gratefully acknowledges the Western Institute for Neuroscience Clinical Research Postdoctoral Fellowship.

Additional information

Models

The code used to generate Figure 4.4 in the main text is available in the GitHub repository [298]. The data used can be made available upon request. All the code is done in the Julia computational language [98]; integration was done with the package DifferentialEquations.jl [97], with the aid of packages DynamicalSystems.jl [157] and DrWatson.jl [100]. Plots were made with Makie.jl [158].

Noisy bistable system

The noisy bistable system, also known as the noisy Duffing oscillator [57], is given by:

$$dx = v + \eta_1 dW \quad (5.1)$$

$$dv = -ax^3 + bx - c - dv + \eta_2 dW, \quad (5.2)$$

with dW describing a white Gaussian noise. The equations describe the evolution of a particle on a double-well (quartic) potential $U(x) = ax^4/4 - bx^2/2 + cx$ being periodically driven and with noise. The parameters used were $a = 0.5$; $b = 8.0$, $c = 0.0$, $d = 0.2$, $\eta_1 = \eta_2 = 0.18$, with initial condition $(0, 0)$.

The heteroclinic cycle

The heteroclinic cycle occurs in a rate model derived from Hodgkin-Huxley type neurons with synaptic coupling [241]. The equations are given by:

$$\tau \dot{s}_i = (r_i - s_i/2) \frac{S_{\max} - s_i}{S_{\max}} \quad (5.3)$$

$$\tau \dot{r}_i = x_0 F \left(I - \sum_{j=1}^N g_{ij} s_j \right) \tau - r_i \quad (5.4)$$

for $i = 1, 2, 3$, with

$$F(x) = \exp(-\epsilon/x) [\max(0, x)^\alpha]. \quad (5.5)$$

The matrix g is constructed such that $g_{21} = g_{32} = g_{13} = g_1$, $g_{12} = g_{23} = g_{31} = g_2$ and $g_{11} = g_{22} = g_{33} = 0$. The parameters are $\tau = 50$, $\epsilon = 10^{-3}$, $I = 0.145$, $S_{\max} = 0.045$, $g_1 = 3.0$, $g_2 = 0.7$, $x_0 = 2.57 \times 10^{-3}$, and $\alpha = 0.564$.

The numerical integration is best done with a change of coordinates $z_i \equiv \log(S_{\max} - s_i)$, which reduces the numerical precision difficulties associated with the trajectory getting too close to the stable manifold of the fixed points. The initial condition was $(0.5, 0.2, 0.4, 0.9, 0.5, 0.6)$.

Attractor-merging crisis

We have provided an example of attractor-merging crisis for the Duffing oscillator, whose dynamics is described by [299]:

$$\dot{x} = v \quad (5.6)$$

$$\dot{v} = -ax^3 + bx - dv + f \cos(\omega t), \quad (5.7)$$

with parameters $a = 100$, $b = 10$, $d = 1.0$, $f = 0.852$, $\omega = 3.5$ and initial condition $(x, v) = (0.11, 0.11)$.

Type-I intermittency

The system used to obtain the type I intermittency is the Lorenz63 model [300]. The equations are given by

$$\dot{x} = \sigma(y - x) \quad (5.8)$$

$$\dot{y} = x(\rho - z) - y \quad (5.9)$$

$$\dot{z} = xz - \beta z. \quad (5.10)$$

The parameters used in the figure are $\sigma = 10$, $\beta = 8/3$ and $\rho = 166.1$, based on [196]. The parameter used to obtain a stable limit cycle (before the saddle-node bifurcation) was $\rho = 166.06$. The initial condition was $(0.1, 0.1, 0.1)$.

Chaotic saddle

The chaotic saddle shown in the Fig. 4E-E'' occurs in the Ikeda system [301], which has discretized time:

$$x_{n+1} = a + b(x_n \cos(t_n) - y_n \sin(t_n)) \quad (5.11)$$

$$y_{n+1} = b(x_n \sin(t_n) + y_n \cos(t_n)), \quad (5.12)$$

with

$$t_n = c - \frac{d}{1 + x_n^2 + y_n^2}. \quad (5.13)$$

The parameters used for the chaotic saddle were $b = 0.9$, $c = 0.4$, $d = 6.0$, $a = 1.003$. The saddle exists due to a boundary crisis, which occurs for a slightly smaller a . For reference, the value of a used to obtain a chaotic attractor was $a = 0.997$. The initial condition was $(2.97, 4.15)$. This is the only mechanism in the figure where the initial condition is important: to reproduce the behavior, the trajectories need to be initialized near the chaotic saddle.

Brief notion of almost-invariant sets

Following Ref. [56], we provide a brief notion of almost-invariant sets for a mapping $T : X \rightarrow X$, with X being the state space, but it can also be formulated for flows [237]. To formalize the notion of almost-invariant sets, we need to first define a natural measure on any set A . This corresponds to the fraction of time that typical trajectories, starting in $x \in X$, spend on that set along their evolution:

$$\mu(A) = \lim_{N \rightarrow \infty} \frac{\#\{i \in [0, N-1] : T^i x \in A\}}{N} \quad (5.14)$$

The probability of trajectories, once inside A , to remain in A , is computed as

$$\rho(A) = \text{Prob}(Tx \in A | x \in A) = \frac{\mu(T^{-1}A \cap A)}{\mu(A)}. \quad (5.15)$$

A set A is then said to be almost-invariant if $\rho(A)$ is high but not 1, meaning that trajectories, once inside R , have a high probability of remaining in R . Suppose that the state space can be divided into disjointed almost-invariant sets $\{R_1, R_2, \dots, R_N\}$. One can obtain maximally almost-invariant sets by maximizing the mean probability $\frac{1}{N} \sum_{i=1}^N \rho(A_i)$ [56, 236].

Chapter 6

Conclusions

Science is typically reductionist [302]. We break a hard problem into smaller parts that are easier to understand separately. We have achieved tremendous success with this effort, but we have not solved everything; indeed, we have found out that putting everything back together can be quite complicated: the interactions between the parts can generate complex behavior that is not present in any one of the parts alone. The field of complex systems arose from the need to understand this *emergent phenomena* - to (re)construct the full system's behavior from knowledge of its parts. In the case of networked systems, studied in this thesis, the challenge can be phrased as the need to understand how the whole system's behavior arises from the coupling between the units. A major challenge still today is to develop tools that allows us to characterize and understand complicated emergent behavior.

One such complicated behavior in networks is the coexistence of multiple stable solutions to the same equations with the same parameters - *multistability*! How do these solutions come about, where are they situated and how are they separated in state space - these are all questions under active research [1, 2, 36].

Some of these stable solutions may correspond to synchronized regimes, which brings into light another important phenomenon: *synchronization*. Here again the field of complex systems has to contend with another problem: how individually distinct units can cooperate together and start to operate in unison, in a beautiful example of an emergent phenomenon. The study of synchronization - both frequency and phase synchronization - also has important practical motivations, for instance in the study of power grids. In power grids, and other complex networks, understanding the robustness of solutions, in particular of synchronized solutions has been an object of active research.

Combining these two research areas, Chapter 3 investigated the robustness of solutions in a complex network of Kuramoto oscillators, a paradigmatic model for studies on synchronization phenomena and complex networks in general. The idea was to investigate how the network behaves - how the solutions change - when we alter the parameter of a single unit in the network. We found that the *dynamical malleability* of the network depends on how strongly coupled the units are, and the topology of the connections. Roughly, we showed that for very weak coupling strength the individual tendencies of the oscillators win and most of them oscillate incoherently. For sufficiently strong coupling, most of the oscillators become phase locked - they oscillate at the same frequency. This is the same behavior as in all-to-all networks (see Sec. 2.4). The spatial pattern of the phases, which we can measure via the degree of phase synchronization, was then determined by the topology. For several of the coexisting attractors, including the most phase synchronized attractor, the following tendency was observed: networks dominated by short-range connections tend to have attractors with short-range patterns (phase desynchronized), while networks dominated by long-range connections tend to have attractors with long-range patterns (phase synchronized). In parameter space, phase synchronization in these networks lives in the region of sufficiently high coupling strength and number of long-range connections. Changing the parameters toward this region therefore makes the system undergo a transition to phase synchronization. We showed that precisely during this transition their dynamical malleability increases con-

siderably. To the point that changing a single unit radically alters the pattern of phases in the network, potentially changing it from phase synchronized to phase desynchronized.

The mechanism for this dynamical malleability is two-fold. First, it is related to *increased sample-to-sample fluctuations* near a phase transition [28, 29]. This mechanism does not require multistability. In fact, suppose the systems have a single attractor, like the randomly connected networks. Each change to a parameter of a unit leads to a different dynamical system, which may have a different attractor. In particular, the transition to phase synchronization of this attractor may occur at different coupling strength values, earlier or later compared to the system before the change. If we enact this change but keep the coupling strength fixed, we switch to an attractor that has a smaller or larger value of phase synchronization - this is the fluctuation from one sample to another. If the systems have multiple attractors, this effect is still there, but there is the added possibility of switching to other attractors, which might be even more different. The *multistability* increases the possible fluctuations that may occur. This explains our observation that for Watts-Strogatz networks the malleability and multistability seem to go hand in hand. It can also explain why these networks have a considerably larger malleability than the distance-dependent networks, which do not seem to be multistable.

An important concept in the area of complex systems is that of global stability, typically taken to mean the relative size of the basin of attraction of each attractor. In this view, attractors whose basins occupy larger regions of state space are more globally stable [303]. The rough idea is that trajectories on attractors with bigger basins of attraction are more likely to require bigger perturbations in order to be kicked across the basin boundary and into another attractor. This is not necessarily the case, however, since the situation depends on the geometry of the basin of attraction [304], but it highlights the importance of studying perturbations applied to the state of a system. In general, more attractors means they are sharing state space more and therefore the global stability is smaller, meaning the system is less robust (or less resilient, depending on terminology [304]). In this work we show that multistability affects the robustness of the system in another way: by affecting its malleability. So not only is it dangerous to kick the state of the system, it is also dangerous to change its parameters - even the parameter of one single unit!

Another important observation was the study of how malleability, and multistability, depend on the topology of the system. Topologies that put the systems in the vicinity of a transition to phase synchronization, which were in the small-world range, made it very malleable. An important question that is left for future work is why these specific topologies lead to a higher number of attractors - which properties do they possess that lead to the emergence of the attractors, compared to, say, the random topologies, which do not induce multistability? The distance-dependent networks also do not seem to be multistable, a factor that would also be interesting to investigate.

A related question is about the generality of these results. Malleability due to sample-to-sample fluctuations is very common, being extensively described in statistical physics literature [113]. We also described it initially in a network of spiking neurons [26], and observed it in the Kuramoto model under different topologies of distributions of the natural frequency, and under other models, such as a simple model of excitable cells. We believe that the multistability results will also generalize somehow - supported by the available evidence from other works - but this is also object of future research. Understanding better the mechanisms generating the multistability will also help answer this.

In a similar vein, we also investigated in Chap. 4 how multistability emerges when excitable neurons are coupled diffusively. Excitability in the individual units here occurs due to the presence of a saddle and an unstable equilibrium in state space, which force part of the trajectories to go around on a long excursion before eventually converging to the stable equilibrium. This region where trajectories go through is called the *excitability region*. We showed that the coupling can trap trajectories in this excitability region by repeatedly reinjecting them there. This mechanism underlies all the emergent attractors we observed, even though they arise due to different bifurcations: saddle-node of limit cycles and homoclinic. For two units, it can create three coexisting periodic attractors, and can also create a quasiperiodic attractor. For more units, it can create a larger number of attractors, including potentially a chaotic attractor. Based on the trapping mechanism and preliminary results, we conjecture that the topology of the networks plays a key role in dictating which attractors emerge, and how many. This could be very similar to Kuramoto networks, and a more in-depth comparison is definitely warranted. It would be very interesting in the future to explore how exactly the size and topology of the networks control the emerging attractors.

In this initial work we decided to focus mainly on the pure dynamics of the system, so we showed most of the results in the case where the coupling is applied to both the x and y directions of the system. In some models, such as ecological models - where the diffusive term would model a migration of species - this might be very sound. For the neuronal case, however, only the x -coupling is biophysically sound. Motivated by this fact, we also investigated how the attractors change when the coupling is applied to only one variable. Interestingly, the mechanism is still present, but the two main types of attractors we observed split up when the coupling is split. The exclusive x -coupling leads to the attractor with two units trapped in the excitability region (LA-LA); the exclusive y -coupling leads to the one with only one unit in the excitability region (LA-SA or SA-LA). We confirmed this with a bifurcation analysis and also qualitatively explained it based on the geometry of the attractors and the trapping mechanism. This is important in terms of potential applications. First, it means that adding a gap junction between two otherwise silent neurons could make them bistable, with the possibility of periodic or even quasiperiodic spiking. In fact, there is some evidence that this seems to occur in neurons coupled under gap junctions in the motor cortex of fruit flies [23]. It is also interesting in the ecological direction, if we consider that only some species in an ecological niche might be migrating between patches.

Furthermore, we focused for simplicity on the excitable case, where the trapping mechanism creating the attractors is more easily seen. But attractors still emerge similarly in a bistable regime, where the stable equilibrium coexists with a stable limit cycle. We can achieve this by changing the input current I of the model. A difference in this case is that the uncoupled neuron already has an oscillating attractor. Therefore, when they are diffusively coupled they can also synchronize together in this oscillating attractor. This system thus has the possibility of achieving full synchronization on a periodic attractor. In this case, one could reframe the study in terms of the stability, global and linear, of the synchronized state, and how the coupling might create new attractors and thus reduce the relative size of the basin of the synchronized attractor.

We initially arrived at this problem when trying to understand the synchronization behavior of a network of bursting neurons [37]. The degree of phase synchronization in that system changes nonmonotonically as a function of the coupling strength: increasing the coupling initially increases the phase synchronization, then actually decreases it in a

certain region, before increasing it again for very strong coupling. This is also reminiscent of a behavior observed in networks with chaotic saddles in Ref. [40]. We also studied a network of bursting neurons following another model, and found that a chaotic saddle was important there but also a slow region of system's limit cycle was related to the multistability that emerged. From the work on excitable neurons, we understand that slowness can help generate attractors, at least for the reinjection mechanism we observed. It would be interesting in the future to go back and finish the initial studies.

When working on a project, I believe it is not an uncommon feeling to find an interesting paper, try to replicate its results and not quite manage. Then, to look at the source code that the authors hopefully provided, and to be underwhelmed. While working on a paper, it is often the case that people might want to spend as little time as possible implementing the algorithms they need, leading usually to confusing code, which might not be as efficient as it could, and not as well-tested - and thus, more susceptible to errors. One solution to this is to create a unified library that implements efficient code, tests and documents it. And to make it open-source, to share it with the whole community. Then, anyone can scrutinize the code, find improvements and test it further. Also, more importantly, everyone can use it. This saves implementation time, potentially run times due to improved code efficiency, and also re-implementation time for poor students aiming to replicate papers. This is the philosophy of the dynamical systems library [157], started by Dr. George Datseris, written in the Julia programming language. With this idea in mind, we also collaborated to implement algorithms related to finding attractors and their basins. In particular, I worked on the algorithm used in the two multistability works in this thesis. It is a brute-force algorithm that integrates trajectories, converts them into vectors of features, and selects attractors as unique groups of features [32, 45, 46]. Together with Prof. Alexander Wagemakers, we also implemented an algorithm that applies attractor-finding algorithms across a parameter range, in a continuation manner. The result of this work was the *Attractors.jl* package, also co-developed by more collaborators, and a publication describing this novel algorithm and improvements to previous literature [46].

So far on the study of dynamical systems we have mostly focused on attractors. The motivation for this is that attractors represent a system's long-term dynamics: after some *transient* time, trajectories converge to attractors. There is, however, a key assumption here: that the period of time during which we observe the system T_{obs} is longer than the convergence time T_{conv} to the attractor. It is a matter of time-scales: of the observation versus the relaxation to the attractor. Whether this can be guaranteed or not depends on the application. In power grids, for instance, one is generally interested in the long-term dynamics of the system. In the brain, however, changes may be occurring too fast, and there may not be enough time to wait for convergence to an attractor. The time-scales can also vary within the same system: as we saw in the excitable units, trajectories starting on one side of the state space converge rapidly to the attractor, whereas trajectories starting on the excitability region spend a relatively long time performing an excursion in space before reaching the attractor. This problem is made more complicated due to the fact that there are many mechanisms that can generate long - potentially arbitrarily long - transients. An example is chaotic saddles, wherein trajectories can stay indefinitely long [256]. Therefore, the behavior that is actually observed in some studies may be a transient. Moreover, some of these long-lived transients occur inside attractors. One example can be seen in ghost states inside chaotic attractors - such as for the Logistic map or the Lorenz system - where

the trajectories switch between clearly chaotic and seemingly periodic dynamics (cf. Chap. 5). Another example is the stable heteroclinic cycle: the cycle as a whole can be an attractor, but trajectories on it switch between the neighborhoods of saddle-points, describing sequences of metastable regimes. Yet another example is crawl-by motion, in which a limit cycle is in the proximity of a saddle-point. The region near the saddle-point may have very slow dynamics, and trajectories on the cycle take a long time to pass through (crawl-by) this region [305]. These examples illustrate the intricate relation between multistability - and attractors - and metastability.

Transients can play important roles. A specific example that illustrates the role of sequences of transient states is the Turing machine, the paradigmatic model for *computations* [306, 307]. It is a simple finite state machine with a head that stores a certain state and can read, write, and move along a tape. The tape is subdivided into cells containing symbols (e.g., 0's and 1's). The head represents a modern computer's central processing unit, while the tape represents the memory. Accordingly, the head follows a set of instructions that take the current state, currently read symbol on the tape and outputs the new state, the new symbol it writes on the tape, and the direction it moves. Computations are done by traversing a sequence of such state-symbol combinations. The machine may run forever - it is said to not halt -, in which case the computation is not completed. If the machine does halt, the computation is finished. From this point of view, therefore, the computation is only complete once the machine terminates the previous sequence of states. This sequence can therefore be seen as a type of transient behavior, which is crucial for the computation performed by the machine. This remark is not just an analogy - dynamical systems can be constructed that implement Turing machines [308].

More concretely, in the brain, transients have been shown to play important roles [201, 180]. There is a plethora of observations showing neural activity going through sequences of distinct states, which are all therefore transient [50, 51]. In several cases, these states are long-lived (i.e., metastable). Understanding the exact roles that *metastable regimes* play in neural circuits is crucial to understanding how they perform computations, a central question in neuroscience and also artificial intelligence [48, 309, 254]. Recent work, based on theoretical and experimental results, has shown that ghosts of saddle-node equilibria, which generate long transients, are a particularly important mechanism [48, 66, 49, 180]. It is expected, however, that other mechanisms are also present in circuits. For instance, a wide literature in neuroscience uses attractors to perform computations, and adds external perturbations to induce changes between regimes [128, 254, 51, 292]. It will be important in the future to contrast these two ideas to see the actual roles played by each of them.

To better understand the role of transients on computations in neural circuits, it is therefore important to have both an in-depth as well as a general understanding of metastable dynamics. Under this logic we developed a *general conceptual framework* for metastability, collecting and refining ideas from the neuroscience and dynamical systems literatures. As seen in Chap. 5, we proposed that the main concept behind metastability is that of long-lived transients, and showed many dynamical mechanisms capable of generating it. In the future, one can use this framework to actively compare the different mechanisms, with a view towards experiments - both biological as well as *in silico*, looking to understand how networks perform computations [48].

Besides the metastable regimes themselves, perhaps the actual *sequences* play an important role. This is the case in the Turing machine, but there is also evidence in

biological networks. An important example, already mentioned in the Introduction and in Chap. 5, showed in a series of works that sequences of metastable regimes are elicited when mice are fed tastants [52]. The sequence of regimes is unique to each tastant, suggesting they play an active role in encoding the stimuli [53]. Sequences of metastable regimes have been linked to computations in other experiments also [180, 53, 128]. In this case, a useful concept coming from dynamical systems theory is that of excitable networks by Ashwin and Postlethwaite [310, 311]. They developed methods that allow one to construct systems with prescribed connections between equilibria states. These connections may be spontaneously activated (as in connected ghosts) or via a perturbation (by perturbing across the basin boundary). This is an example of how the theory of dynamical systems is offering many tools and mechanisms that can be used to model and better understand how circuits are actually solving tasks and performing computations. This is an exciting area for future research.

Taking everything together, the field of complex systems is under intense research, with lots of us aiming to develop theory and tools to understand emergent dynamical phenomena like synchronization, the coexistence of multiple long-term solutions and the (transient) path to them. I believe that during my PhD we managed to provide some timely contributions in these directions, but there is still much to be done - with applications being very significant in biology, technology and even climate. I am very excited to help put all these pieces together.

Bibliography

- [1] Ulrike Feudel. Complex Dynamics In Multistable Systems. *International Journal of Bifurcation and Chaos*, 18(06):1607–1626, 2008.
- [2] Alexander N. Pisarchik and Alexander E. Hramov. Multistability in Physical and Living Systems, Characterization and Applications. *Springer Series in Synergetics*, 2022.
- [3] Alexander N. Pisarchik and Ulrike Feudel. Control of multistability. *Physics Reports*, 540(4):167–218, 2014.
- [4] Ronghui Zhu, Jesus M. del Rio-Salgado, Jordi Garcia-Ojalvo, and Michael B. Elowitz. Synthetic multistability in mammalian cells. *Science*, 375(6578):eabg9765, 2022.
- [5] Erzsébet Ravasz Regan and William C. Aird. Dynamical Systems Approach to Endothelial Heterogeneity. *Circulation Research*, 111(1):110–130, 2012.
- [6] Tahmineh Khazaei, Rory L. Williams, Said R. Bogatyrev, John C. Doyle, Christopher S. Henry, and Rustem F. Ismagilov. Metabolic multistability and hysteresis in a model aerobe-anaerobe microbiome community. *Science Advances*, 6(33):eaba0353, 2020.
- [7] Frank Hellmann, Paul Schultz, Patrycja Jaros, Roman Levchenko, Tomasz Kapitaniak, Jürgen Kurths, and Yuri Maistrenko. Network-induced multistability through lossy coupling and exotic solitary states. *Nature Communications*, 11(1):592, 2020.
- [8] Lukas Halekotte, Anna Vanselow, and Ulrike Feudel. Transient chaos enforces uncertainty in the British power grid. *Journal of Physics: Complexity*, 2(3):035015, 2021.
- [9] Hugh R. Wilson and Jack D. Cowan. Excitatory and Inhibitory Interactions in Localized Populations of Model Neurons. *Biophysical Journal*, 12(1):1–24, 1972.
- [10] Jennifer Foss, André Longtin, Boualem Mensour, and John Milton. Multistability and Delayed Recurrent Loops. *Physical Review Letters*, 76(4):708–711, 1996.
- [11] Mathieu Golos, Viktor Jirsa, and Emmanuel Daucé. Multistability in Large Scale Models of Brain Activity. *PLoS Comput Biol*, 11(12):1004644, 2015.
- [12] Andrew Flynn and Andreas Amann. Exploring the origins of switching dynamics in a multifunctional reservoir computer. *Frontiers in Network Physiology*, 4:1451812, 2024.
- [13] Alexander Robinson, Reinhard Calov, and Andrey Ganopolski. Multistability and critical thresholds of the Greenland ice sheet. *Nature Climate Change*, 2(6):429–432, 2012.

- [14] Ulrike Feudel, Celso Grebogi, Leon Poon, and James A. Yorke. Dynamical properties of a simple mechanical system with a large number of coexisting periodic attractors. *Chaos, Solitons & Fractals*, 9(1-2):171–180, 1998.
- [15] Miri Adler, Avi Mayo, Xu Zhou, Ruth A. Franklin, Matthew L. Meizlish, Ruslan Medzhitov, Stefan M. Kallenberger, and Uri Alon. Principles of Cell Circuits for Tissue Repair and Fibrosis. *iScience*, 23(2):100841, 2020.
- [16] Arkady Pikovsky, Michael Rosenblum, and Jürgen Kurths. *Synchronization: A Universal Concept in Nonlinear Science*, volume 70. Cambridge University Press, 2001.
- [17] Stefano Boccaletti, Alexander N. Pisarchik, Charo I. del Genio, and Andreas Amann. *Synchronization: From Coupled Systems to Complex Networks*. Cambridge University Press, 2018.
- [18] Alex Arenas, Albert Díaz-Guilera, Jurgen Kurths, Yamir Moreno, and Changsong Zhou. Synchronization in complex networks. *Physics Reports*, 469(3):93–153, 2008.
- [19] Steven H. Strogatz. From Kuramoto to Crawford: exploring the onset of synchronization in populations of coupled oscillators. *Physica D: Nonlinear Phenomena*, 143(1-4):1–20, 2000.
- [20] W Singer. Neuronal synchrony: a versatile code for the definition of relations? *Neuron*, 24(1):49–65, 111, 1999.
- [21] Pascal Fries. Rhythms for Cognition: Communication through Coherence. *Neuron*, 88(1):220–235, 2015.
- [22] Thilo Womelsdorf and Pascal Fries. The role of neuronal synchronization in selective attention. *Current Opinion in Neurobiology*, 17(2):154–160, 2007.
- [23] Silvan Hürkey, Nelson Niemeyer, Jan-Hendrik Schleimer, Stefanie Ryglewski, Susanne Schreiber, and Carsten Duch. Gap junctions desynchronize a neural circuit to stabilize insect flight. *Nature*, 618(7963):118–125, 2023.
- [24] Juan A. Acebrón, L. L. Bonilla, Conrad J. Pérez Vicente, Félix Ritort, and Renato Spigler. The Kuramoto model: A simple paradigm for synchronization phenomena. *Reviews of Modern Physics*, 77(1):137–185, 2005.
- [25] Francisco A. Rodrigues, Thomas K.D.M. Peron, Peng Ji, and Jürgen Kurths. The Kuramoto model in complex networks. *Physics Reports*, 610:1–98, 2016.
- [26] R. C. Budzinski, K. L. Rossi, B. R. R. Boaretto, T. L. Prado, and S. R. Lopes. Synchronization malleability in neural networks under a distance-dependent coupling. *Physical Review Research*, 2(4):043309, 2020.
- [27] Kalel L. Rossi, Roberto C. Budzinski, Bruno R. R. Boaretto, Lyle E. Muller, and Ulrike Feudel. Shifts in global network dynamics due to small changes at single nodes. *Physical Review Research*, 5(1):013220, 2023.
- [28] Hyunsuk Hong, Hugues Chaté, Hyunggyu Park, and Lei Han Tang. Entrainment transition in populations of random frequency oscillators. *Physical Review Letters*, 99(18):1–4, 2007.

- [29] Hyunsuk Hong, Hyunggyu Park, and Lei Han Tang. Finite-size scaling of synchronized oscillation on complex networks. *Physical Review E*, 76(6):1–7, 2007.
- [30] Franziska Peter and Arkady Pikovsky. Transition to collective oscillations in finite Kuramoto ensembles. *Physical Review E*, 97(3):032310, 2018.
- [31] Paulo F. C. Tilles, Fernando F. Ferreira, and Hilda A. Cerdeira. Multistable behavior above synchronization in a locally coupled Kuramoto model. *Physical Review E*, 83(6):066206, 2011.
- [32] Maximilian Gelbrecht, Jürgen Kurths, and Frank Hellmann. Monte Carlo basin bifurcation analysis. *New Journal of Physics*, 22(3):033032, 2020.
- [33] Max Potratzki, Timo Bröhl, Thorsten Rings, and Klaus Lehnertz. Synchronization dynamics of phase oscillators on power grid models. *Chaos: An Interdisciplinary Journal of Nonlinear Science*, 34(4):043131, 2024.
- [34] Daniel A. Wiley, Steven H. Strogatz, and Michelle Girvan. The size of the sync basin. *Chaos: An Interdisciplinary Journal of Nonlinear Science*, 16(1):015103, 2006.
- [35] Alex Townsend, Michael Stillman, and Steven H. Strogatz. Dense networks that do not synchronize and sparse ones that do. *Chaos: An Interdisciplinary Journal of Nonlinear Science*, 30(8):083142, 2020.
- [36] Yuanzhao Zhang and Steven H. Strogatz. Basins with Tentacles. *Physical Review Letters*, 127(19):194101, 2021.
- [37] K. L. Rossi, R. C. Budzinski, B. R. R. Boaretto, T. L. Prado, U. Feudel, and S. R. Lopes. Phase-locking intermittency induced by dynamical heterogeneity in networks of thermosensitive neurons. *Chaos: An Interdisciplinary Journal of Nonlinear Science*, 31(8):083121, 2021.
- [38] J L Hindmarsh and R M Rose. A model of neuronal bursting using three coupled first order differential equations. *Proceedings of the royal society of London B: biological sciences*, 221(1222):87–102, 1984.
- [39] Eugene M Izhikevich. *Dynamical systems in neuroscience*. MIT press, 2007.
- [40] Everton S. Medeiros, Rene O. Medrano-T, Iberê L. Caldas, and Ulrike Feudel. Boundaries of synchronization in oscillator networks. *Physical Review E*, 98(3):030201, 2018.
- [41] Everton S. Medeiros, Rene O. Medrano-T, Iberê L. Caldas, Tamás Tél, and Ulrike Feudel. State-dependent vulnerability of synchronization. *Physical Review E*, 100(5):052201, 2019. Publisher: American Physical Society.
- [42] S. Smale. A Mathematical Model of Two Cells Via Turing’s Equation. In *The Hopf Bifurcation and Its Applications*, pages 354–367. Springer New York, 1976.
- [43] George Datseris and Alexandre Wagemakers. Effortless estimation of basins of attraction. *Chaos: An Interdisciplinary Journal of Nonlinear Science*, 32(2):023104, 2022.

- [44] Helena E. Nusse, James A. Yorke, and Eric J. Kostelich. Dynamics: Numerical Explorations, Accompanying Computer Program Dynamics. *Applied Mathematical Sciences*, 1994.
- [45] Merten Stender and Norbert Hoffmann. bSTAB: an open-source software for computing the basin stability of multi-stable dynamical systems. *Nonlinear Dynamics*, pages 1–18, 2021.
- [46] George Datseris, Kalel Luiz Rossi, and Alexandre Wagemakers. Framework for global stability analysis of dynamical systems. *Chaos: An Interdisciplinary Journal of Nonlinear Science*, 33(7):073151, 2023.
- [47] Roberto C. Budzinski, Alexandra N. Busch, Samuel Mestern, Erwan Martin, Luisa H. B. Liboni, Federico W. Pasini, Ján Mináč, Todd Coleman, Wataru Inoue, and Lyle E. Muller. An exact mathematical description of computation with transient spatiotemporal dynamics in a complex-valued neural network. *Communications Physics*, 7(1):239, 2024.
- [48] Daniel Koch, Akhilesh Nandan, Gayathri Ramesan, and Aneta Koseska. Biological computations: Limitations of attractor-based formalisms and the need for transients. *Biochemical and Biophysical Research Communications*, 720:150069, 2024.
- [49] Akhilesh Nandan, Abhishek Das, Robert Lott, and Aneta Koseska. Cells use molecular working memory to navigate in changing chemoattractant fields. *eLife*, 11:e76825, 2022.
- [50] Emmanuelle Tognoli and J. A.Scott Kelso. The Metastable Brain. *Neuron*, 81(1):35–48, 2014.
- [51] B. A. W. Brinkman, H. Yan, A. Maffei, I. M. Park, A. Fontanini, J. Wang, and G. La Camera. Metastable dynamics of neural circuits and networks. *Applied Physics Reviews*, 9(1):011313, 2022.
- [52] Lauren M. Jones, Alfredo Fontanini, Brian F. Sadacca, Paul Miller, and Donald B. Katz. Natural stimuli evoke dynamic sequences of states in sensory cortical ensembles. *Proceedings of the National Academy of Sciences*, 104(47):18772–18777, 2007.
- [53] Giancarlo La Camera, Alfredo Fontanini, and Luca Mazzucato. Cortical computations via metastable activity. *Current Opinion in Neurobiology*, 58:37–45, 2019.
- [54] Peter beim Graben, Antonio Jimenez-Marin, Ibai Diez, Jesus M. Cortes, Mathieu Desroches, and Serafim Rodrigues. Metastable Resting State Brain Dynamics. *Frontiers in Computational Neuroscience*, 13:62, 2019.
- [55] Michael Dellnitz and Robert Preis. Symbolic and Numerical Scientific Computation, Second International Conference, SNSC 2001, Hagenberg, Austria, September 12–14, 2001. Revised Papers. *Lecture Notes in Computer Science*, pages 183–209, 2003.
- [56] Gary Froyland. Statistically optimal almost-invariant sets. *Physica D: Nonlinear Phenomena*, 200(3-4):205–219, 2005.

- [57] Strogatz. *Nonlinear Dynamics and Chaos*. Studies in nonlinearity. Westview, 2002.
- [58] Anant Kant Shukla, T R Ramamohan, and S Srinivas. A new analytical approach for limit cycles and quasi-periodic solutions of nonlinear oscillators: the example of the forced Van der Pol Duffing oscillator. *Physica Scripta*, 89(7):075202, 2014.
- [59] John H. Argyris, Gunter Faust, Maria Haase, and Rudolf Friedrich. *An Exploration of Dynamical Systems and Chaos*. Springer Berlin, Heidelberg, 2 edition, 2015.
- [60] John Milnor. On the concept of attractor. *Communications in Mathematical Physics*, 99(2):177–195, 1985.
- [61] Robert L.V. Taylor. Attractors: Nonstrange to Chaotic. *SIAM Undergraduate Research Online*, 4:72–80, 2011. Publisher: Society for Industrial & Applied Mathematics (SIAM).
- [62] Henk Broer and Floris Takens. *Dynamical Systems and Chaos*. Applied Mathematical Sciences. 2011.
- [63] Jorge V. José and Eugene J. Saletan. *Classical Dynamics: A Contemporary Approach*. Cambridge University Press, Cambridge, 1998.
- [64] Paul Glendinning. *Stability, Instability And Chaos: An Introduction To The Theory Of Nonlinear Differential Equations (cambridge Texts In Applied Mathematics)*. Cambridge Texts in Applied Mathematics. Cambridge University Press, Cambridge [England], 1 edition, 1994.
- [65] Yuri A. Kuznetsov. Elements of Applied Bifurcation Theory. *Applied Mathematical Sciences*, 2004.
- [66] D. Koch, A. Nandan, G. Ramesan, I. Tyukin, A. Gorban, and A. Koseska. Ghost Channels and Ghost Cycles Guiding Long Transients in Dynamical Systems. *Physical Review Letters*, 133(4):047202, 2024.
- [67] Björn Sandstede. Constructing dynamical systems having homoclinic bifurcation points of codimension two. *Journal of Dynamics and Differential Equations*, 9(2):269–288, 1997.
- [68] Ed Bullmore and Olaf Sporns. Complex brain networks: graph theoretical analysis of structural and functional systems. *Nature Reviews Neuroscience*, 10(3):186–198, 2009.
- [69] Pietro Landi, Henintsoa O. Minoarivelo, Åke Brännström, Cang Hui, and Ulf Dieckmann. Complexity and stability of ecological networks: a review of the theory. *Population Ecology*, 60(4):319–345, 2018.
- [70] D J Watts and S H Strogatz. Collective dynamics of 'small-world' networks. *Nature*, 393(6684):440–442, 1998.
- [71] Yoshiki Kuramoto. *Chemical Oscillations, Waves, and Turbulence*, volume 19 of *Springer Series in Synergetics*. Springer Berlin Heidelberg, Berlin, Heidelberg, 1984.

- [72] Richard Taylor. There is no non-zero stable fixed point for dense networks in the homogeneous Kuramoto model. *Journal of Physics A: Mathematical and Theoretical*, 45(5):055102, 2012.
- [73] Adilson E. Motter, Seth A. Myers, Marian Anghel, and Takashi Nishikawa. Spontaneous synchrony in power-grid networks. *Nature Physics*, 9(3):191–197, 2013.
- [74] Jennifer A. Dunne, Richard J. Williams, and Neo D. Martinez. Food-web structure and network theory: The role of connectance and size. *Proceedings of the National Academy of Sciences*, 99(20):12917–12922, 2002.
- [75] Patrick Crotty, Dan Schult, and Ken Segall. Josephson junction simulation of neurons. *Physical Review E*, 82(1):011914, 2010.
- [76] Micha Nixon, Moti Friedman, Eitan Ronen, Asher A. Friesem, Nir Davidson, and Ido Kanter. Synchronized Cluster Formation in Coupled Laser Networks. *Physical Review Letters*, 106(22):223901, 2011.
- [77] F Varela, J P Lachaux, E Rodriguez, and J Martinerie. The brainweb: phase synchronization and large-scale integration. *Nature Reviews Neuroscience*, 2(4):229–239, 2001.
- [78] Dirk Witthaut, Frank Hellmann, Jürgen Kurths, Stefan Kettemann, Hildegard Meyer-Ortmanns, and Marc Timme. Collective nonlinear dynamics and self-organization in decentralized power grids. *Reviews of Modern Physics*, 94(1):015005, 2022.
- [79] Yoshiki Kuramoto. Self-entrainment of a population of coupled non-linear oscillators. *International Symposium on Mathematical Problems in Theoretical Physics. Lecture Notes in Physics*, 39:420–422, 1975.
- [80] Adrián Ponce-Alvarez, Gustavo Deco, Patric Hagmann, Gian Luca Romani, Dante Mantini, and Maurizio Corbetta. Resting-State Temporal Synchronization Networks Emerge from Connectivity Topology and Heterogeneity. *PLOS Computational Biology*, 11(2):e1004100, 2015.
- [81] Joana Cabral, Etienne Hugues, Olaf Sporns, and Gustavo Deco. Role of local network oscillations in resting-state functional connectivity. *Neuroimage*, 57(1):130–139, 2011.
- [82] B. D. Josephson. Coupled Superconductors. *Reviews of Modern Physics*, 36(1):216–220, 1964.
- [83] Milos Marek and Ivan Stuchl. Synchronization in two interacting oscillatory systems. *Biophysical Chemistry*, 3(3):241–248, 1975.
- [84] John C. Neu. Chemical Waves and the Diffusive Coupling of Limit Cycle Oscillators. *SIAM Journal on Applied Mathematics*, 36(3):509–515, 1979.
- [85] M G Rosenblum, A S Pikovsky, and J Kurths. Phase synchronization of chaotic oscillators. *Physical Review Letters*, 76(11):1804–1807, 1996.
- [86] Réka Albert and Albert-László Barabási. Statistical mechanics of complex networks. *Reviews of Modern Physics*, 74(1):47–97, 2002.

- [87] Mark D. Humphries and Kevin Gurney. Network ‘Small-World-Ness’: A Quantitative Method for Determining Canonical Network Equivalence. *PLoS ONE*, 3(4):e2051, 2008.
- [88] Qawi K. Telesford, Karen E. Joyce, Satoru Hayasaka, Jonathan H. Burdette, and Paul J. Laurienti. The Ubiquity of Small-World Networks. *Brain Connectivity*, 1(5):367–375, 2011.
- [89] Jeffrey L. Rogers and Luc T. Wille. Phase transitions in nonlinear oscillator chains. *Physical Review E*, 54(3):R2193–R2196, 1996.
- [90] Mikail Rubinov, Rolf J F Ypma, Charles Watson, and Edward T Bullmore. Wiring cost and topological participation of the mouse brain connectome. *Proceedings of the National Academy of Sciences of the United States of America*, 112(32):10032–10037, 2015.
- [91] H. Hong, M. Y. Choi, and Beom Jun Kim. Synchronization on small-world networks. *Physical Review E*, 65(2):1–5, 2002.
- [92] Dane Taylor, Per Sebastian Skardal, and Jie Sun. Synchronization of Heterogeneous Oscillators Under Network Modifications: Perturbation and Optimization of the Synchrony Alignment Function. *SIAM Journal on Applied Mathematics*, 76(5):1984–2008, 2016.
- [93] Lluís Arola-Fernández, Sergio Faci-Lázaro, Per Sebastian Skardal, Emanuel-Cristian Boghiu, Jesús Gómez-Gardeñes, and Alex Arenas. Emergence of explosive synchronization bombs in networks of oscillators. *Communications Physics*, 5(1):264, 2022.
- [94] R. C. Budzinski, B. R. R. Boaretto, T. L. Prado, R. L. Viana, and S. R. Lopes. Synchronous patterns and intermittency in a network induced by the rewiring of connections and coupling. *Chaos: An Interdisciplinary Journal of Nonlinear Science*, 29(12):123132, 2019.
- [95] Per Sebastian Skardal and Alex Arenas. Higher order interactions in complex networks of phase oscillators promote abrupt synchronization switching. *Communications Physics*, 3(1):218, 2020.
- [96] Hyunsuk Hong, Jaegon Um, and Hyunggyu Park. Link-disorder fluctuation effects on synchronization in random networks. *Physical Review E - Statistical, Nonlinear, and Soft Matter Physics*, 87(4):1–5, 2013.
- [97] Christopher Rackauckas and Qing Nie. DifferentialEquations.jl – A Performant and Feature-Rich Ecosystem for Solving Differential Equations in Julia. *Journal of Open Research Software*, 5(1):15, 2016.
- [98] Jeff Bezanson, Alan Edelman, Stefan Karpinski, and Viral B Shah. Julia: A fresh approach to numerical computing. *SIAM Review*, 59(1):65–98, 2017.
- [99] John D Hunter. Matplotlib: A 2D Graphics Environment. *Computing in science & engineering*, 9(3):90–95, 2007.

- [100] George Datseris, Jonas Isensee, Sebastian Pech, and Tamás Gál. DrWatson: the perfect sidekick for your scientific inquiries. *Journal of Open Source Software*, 5(54):2673, 2020.
- [101] Karel Rossi. Repository for dynamical malleability code. *Github Repository*, 2022.
- [102] Georgi S. Medvedev. Small-world networks of Kuramoto oscillators. *Physica D: Nonlinear Phenomena*, 266:13–22, 2014.
- [103] Nicole Carlson, Dong-Hee Kim, and Adilson E. Motter. Sample-to-sample fluctuations in real-network ensembles. *Chaos: An Interdisciplinary Journal of Nonlinear Science*, 21(2):025105, 2011.
- [104] Hyunsuk Hong, Hyunggyu Park, and Lei-Han Tang. Anomalous Binder Cumulant and Lack of Self-Averageness in Systems with Quenched Disorder. *Journal of the Korean Physical Society*, 49(5):L1885–L1889, 2006.
- [105] Steven H. Strogatz and Renato E. Mirollo. Phase-locking and critical phenomena in lattices of coupled nonlinear oscillators with random intrinsic frequencies. *Physica D: Nonlinear Phenomena*, 31(2):143–168, 1988.
- [106] Jordan G Brankov, Daniel M Danchev, and Nicholai S Tonchev. *Theory of Critical Phenomena in Finite-Size Systems*. World Scientific, 2000.
- [107] Eric J. Hildebrand, Michael A. Buice, and Carson C. Chow. Kinetic Theory of Coupled Oscillators. *Physical Review Letters*, 98(5):054101, 2007.
- [108] K. Binder. Finite size effects on phase transitions. *Ferroelectrics*, 73(1):43–67, 1987.
- [109] Per Sebastian Skardal, Dane Taylor, and Jie Sun. Optimal Synchronization of Complex Networks. *Physical Review Letters*, 113(14):144101, 2014.
- [110] Markus Brede. Synchrony-optimized networks of non-identical Kuramoto oscillators. *Physics Letters, Section A: General, Atomic and Solid State Physics*, 372(15):2618–2622, 2008.
- [111] R. Carareto, F. M. Orsatti, and J. R.C. Piqueira. Optimized network structure for full-synchronization. *Communications in Nonlinear Science and Numerical Simulation*, 14(6):2536–2541, 2009.
- [112] Lubos Buzna, Sergi Lozano, and Albert Díaz-Guilera. Synchronization in symmetric bipolar population networks. *Physical Review E*, 80(6):066120, 2009.
- [113] Didier Sornette. *Critical Phenomena in Natural Sciences, Chaos, Fractals, Self-organization and Disorder: Concepts and Tools*. Springer Series in Synergetics. 2006.
- [114] Shai Wiseman and Eytan Domany. Lack of self-averaging in critical disordered systems. *Physical Review E*, 52(4):3469–3484, 1995.
- [115] M E Newman and D J Watts. Scaling and percolation in the small-world network model. *Physical Review E*, 60(6 Pt B):7332–7342, 1999.

- [116] Victor Buenda, Pablo Villegas, Raffaella Burioni, and Miguel A. Muoz. The broad edge of synchronization: Griffiths effects and collective phenomena in brain networks. *Philosophical Transactions of the Royal Society A*, 380(2227):20200424, 2022.
- [117] Pablo Villegas, Paolo Moretti, and Miguel A. Muñoz. Frustrated hierarchical synchronization and emergent complexity in the human connectome network. *Scientific Reports*, 4(1):5990, 2014.
- [118] G Tononi, O Sporns, and G M Edelman. A measure for brain complexity: relating functional segregation and integration in the nervous system. *Proceedings of the National Academy of Sciences*, 91(11):5033–5037, 1994.
- [119] Giulio Tononi and Gerald M. Edelman. Consciousness and Complexity. *Science*, 282(5395):1846–1851, 1998.
- [120] Gustavo Deco, Giulio Tononi, Melanie Boly, and Morten L. Kringelbach. Rethinking segregation and integration: contributions of whole-brain modelling. *Nature Reviews Neuroscience*, 16(7):430–439, 2015.
- [121] Andrew A Fingelkurts and Alexander A Fingelkurts. Timing in cognition and EEG brain dynamics: discreteness versus continuity. *Cognitive Processing*, 7(3):135–162, 2006.
- [122] Cheng-yu T. Li, Mu-ming Poo, and Yang Dan. Burst Spiking of a Single Cortical Neuron Modifies Global Brain State. *Science*, 324(5927):643–646, 2009.
- [123] Lyle Muller, Ján Mináč, and Tung T. Nguyen. Algebraic approach to the Kuramoto model. *Physical Review E*, 104(2):L022201, 2021.
- [124] Roberto C. Budzinski, Tung T. Nguyen, Jacqueline Doàn, Ján Mináč, Terrence J. Sejnowski, and Lyle E. Muller. Geometry unites synchrony, chimeras, and waves in nonlinear oscillator networks. *Chaos*, 32(3):031104, 2022.
- [125] Edward J. Hancock and Georg A. Gottwald. Model reduction for Kuramoto models with complex topologies. *Physical Review E*, 98(1):012307, 2018.
- [126] Ulrike Feudel, Alexander N. Pisarchik, and Kenneth Showalter. Multistability and tipping: From mathematics and physics to climate and brain - Minireview and preface to the focus issue. *Chaos*, 28(3):33501, 2018.
- [127] Yu Meng, Ying-Cheng Lai, and Celso Grebogi. The fundamental benefits of multiplexity in ecological networks. *Journal of the Royal Society Interface*, 19(194):20220438, 2022.
- [128] Laura N. Driscoll, Krishna Shenoy, and David Sussillo. Flexible multitask computation in recurrent networks utilizes shared dynamical motifs. *Nature Neuroscience*, 27(7):1349–1363, 2024.
- [129] Shai Pilosof, Mason A. Porter, Mercedes Pascual, and Sonia Kéfi. The multilayer nature of ecological networks. *Nature Ecology & Evolution*, 1(4):0101, 2017.
- [130] Goran Söhl, Stephan Maxeiner, and Klaus Willecke. Expression and functions of neuronal gap junctions. *Nature Reviews Neuroscience*, 6(3):191–200, 2005.

- [131] Michael V.L Bennett and R.Suzanne Zukin. Electrical Coupling and Neuronal Synchronization in the Mammalian Brain. *Neuron*, 41(4):495–511, 2004.
- [132] Tomislav Stankovski, Tiago Pereira, Peter V. E. McClintock, and Aneta Stefanovska. Coupling functions: Universal insights into dynamical interaction mechanisms. *Reviews of Modern Physics*, 89(4):045001, 2017.
- [133] Alessandro Loppini, Matthias Braun, Simonetta Filippi, and Morten Gram Pedersen. Mathematical modeling of gap junction coupling and electrical activity in human β -cells. *Physical Biology*, 12(6):066002, 2015.
- [134] Thomas B. Kepler, Eve Marder, and L. F. Abbott. The Effect of Electrical Coupling on the Frequency of Model Neuronal Oscillators. *Science*, 248(4951):83–85, 1990.
- [135] Bernd Blasius, Amit Huppert, and Lewi Stone. Complex dynamics and phase synchronization in spatially extended ecological systems. *Nature*, 399(6734):354–359, 1999.
- [136] Everton S. Medeiros, Ulrike Feudel, and Anna Zakharova. Asymmetry-induced order in multilayer networks. *Physical Review E*, 104(2):024302, 2021.
- [137] Guofu Liang, Hanbo Niu, and Yan Li. A multi-species approach for protected areas ecological network construction based on landscape connectivity. *Global Ecology and Conservation*, 46:e02569, 2023.
- [138] Alexander Sadykov and Keith D. Farnsworth. Model of two competing populations in two habitats with migration: Application to optimal marine protected area size. *Theoretical Population Biology*, 142:114–122, 2021.
- [139] Mahtab Mehrabbeik, Sajad Jafari, Riccardo Meucci, and Matjaž Perc. Synchronization and multistability in a network of diffusively coupled laser models. *Communications in Nonlinear Science and Numerical Simulation*, 125:107380, 2023.
- [140] Ekkehard Ullner, Alexei Zaikin, Evgenii I. Volkov, and Jordi García-Ojalvo. Multistability and Clustering in a Population of Synthetic Genetic Oscillators via Phase-Repulsive Cell-to-Cell Communication. *Physical Review Letters*, 99(14):148103, 2007.
- [141] Ekkehard Ullner, Aneta Koseska, Jürgen Kurths, Evgenii Volkov, Holger Kantz, and Jordi García-Ojalvo. Multistability of synthetic genetic networks with repulsive cell-to-cell communication. *Physical Review E*, 78(3):031904, 2008.
- [142] T. Yanagita, T. Ichinomiya, and Y. Oyama. Pair of excitable FitzHugh-Nagumo elements: Synchronization, multistability, and chaos. *Physical Review E*, 72(5):056218, 2005.
- [143] Aneta Koseska, Evgeny Volkov, and Jürgen Kurths. Oscillation quenching mechanisms: Amplitude vs. oscillation death. *Physics Reports*, 531(4):173–199, 2013.
- [144] Michael F Crowley and Irving R Epstein. Experimental and theoretical studies of a coupled chemical oscillator: phase death, multistability and in-phase and out-of-phase entrainment. *The Journal of Physical Chemistry*, 93(6):2496–2502, 1989.

- [145] Olaf Sporns, Siegfried Roth, and Friedrich Franz Seelig. Chaotic dynamics of two coupled biochemical oscillators. *Physica D: Nonlinear Phenomena*, 26(1-3):215–224, 1987.
- [146] D.G. Aronson, E.J. Doedel, and H.G. Othmer. An analytical and numerical study of the bifurcations in a system of linearly-coupled oscillators. *Physica D: Nonlinear Phenomena*, 25(1-3):20–104, 1987.
- [147] Arnab Mondal, Argha Mondal, Sanjeev Kumar Sharma, Ranjit Kumar Upadhyay, and Chris G. Antonopoulos. Spatiotemporal characteristics in systems of diffusively coupled excitable slow–fast FitzHugh–Rinzel dynamical neurons. *Chaos: An Interdisciplinary Journal of Nonlinear Science*, 31(10):103122, 2021.
- [148] Gerrit Ansmann, Klaus Lehnertz, and Ulrike Feudel. Self-induced switchings between multiple space-time patterns on complex networks of excitable units. *Physical Review X*, 6(1):011030, 2016.
- [149] Alexander Pogromsky, Torkel Glad, and Henk Numeijer. On diffusion driven oscillations in coupled dynamical systems. *International Journal of Bifurcation and Chaos*, 9(04):629–644, 1999.
- [150] L.M. Kocarev and P.A. Janjic. On Turing instability in two diffusely coupled systems. *IEEE Transactions on Circuits and Systems I: Fundamental Theory and Applications*, 42(10):779–784, 1995.
- [151] Eddie Nijholt, Tiago Pereira, Fernando C. Queiroz, and Dmitry Turaev. Chaotic Behavior in Diffusively Coupled Systems. *Communications in Mathematical Physics*, 401(3):2715–2756, 2023.
- [152] Everton Medeiros, Rene Medrano-T, Ibere Caldas, and Ulrike Feudel. The impact of chaotic saddles on the synchronization of complex networks of discrete-time units. *Journal of Physics: Complexity*, 2(3):035002, 2021.
- [153] Max Contreras, Everton S. Medeiros, Anna Zakharova, Philipp Hövel, and Igor Franović. Scale-free avalanches in arrays of FitzHugh–Nagumo oscillators. *Chaos: An Interdisciplinary Journal of Nonlinear Science*, 33(9):093106, 2023.
- [154] Everton S. Medeiros, Oleh Omel’chenko, and Ulrike Feudel. Transient chimera states emerging from dynamical trapping in chaotic saddles. *Chaos: An Interdisciplinary Journal of Nonlinear Science*, 33(9):093130, 2023.
- [155] C. Morris and H. Lecar. Voltage oscillations in the barnacle giant muscle fiber. *Biophysical Journal*, 35(1):193–213, 1981.
- [156] Bard Ermentrout. *Simulating, Analyzing, and Animating Dynamical Systems*. Society for Industrial and Applied Mathematics, 2002.
- [157] George Datseris. DynamicalSystems.jl: A Julia software library for chaos and nonlinear dynamics. *Journal of Open Source Software*, 3(23):598, 2018. Publisher: The Open Journal.
- [158] Simon Danisch and Julius Krumbiegel. Makie.jl: Flexible high-performance data visualization for Julia. *Journal of Open Source Software*, 6(65):3349, 2021.

- [159] Kalel L. Rossi. Repository MultistabilityThroTrapping. *Github Repository*, 2024.
- [160] Nadezhda Semenova, Tatyana Vadivasova, and Vadim Anishchenko. Mechanism of solitary state appearance in an ensemble of nonlocally coupled Lozi maps. *The European Physical Journal Special Topics*, 227(10-11):1173–1183, 2018.
- [161] Patrycja Jaros, Serhiy Brezetsky, Roman Levchenko, Dawid Dudkowski, Tomasz Kapitaniak, and Yuri Maistrenko. Solitary states for coupled oscillators with inertia. *Chaos: An Interdisciplinary Journal of Nonlinear Science*, 28(1):011103, 2018.
- [162] E. Rybalova, V. S. Anishchenko, G. I. Strelkova, and A. Zakharova. Solitary states and solitary state chimera in neural networks. *Chaos: An Interdisciplinary Journal of Nonlinear Science*, 29(7):071106, 2019.
- [163] Rico Berner, Alicja Polanska, Eckehard Schöll, and Serhiy Yanchuk. Solitary states in adaptive nonlocal oscillator networks. *The European Physical Journal Special Topics*, 229(12-13):2183–2203, 2020.
- [164] Leonhard Schülen, Maria Mikhailenko, Everton S. Medeiros, and Anna Zakharova. Solitary states in complex networks: impact of topology. *The European Physical Journal Special Topics*, 231(22-23):4123–4130, 2022.
- [165] J. Tyson and S. Kauffman. Control of mitosis by a continuous biochemical oscillation: Synchronization; spatially inhomogeneous oscillations. *Journal of Mathematical Biology*, 1(4):289–310, 1975.
- [166] J. E. Truscott and J. Brindley. Ocean Plankton Populations As Excitable Media. *Bulletin of Mathematical Biology*, 56(5):981–998, 1994.
- [167] Diego Contreras, Alain Destexhe, Terrence J. Sejnowski, and Mircea Steriade. Control of Spatiotemporal Coherence of a Thalamic Oscillation by Corticothalamic Feedback. *Science*, 274(5288):771–774, 1996.
- [168] Mircea Steriade, David A. McCormick, and Terrence J. Sejnowski. Thalamocortical Oscillations in the Sleeping and Aroused Brain. *Science*, 262(5134):679–685, 1993.
- [169] Michel Jouvet. What does a cat dream about? *Trends in Neurosciences*, 2:280–282, 1979.
- [170] James F. A. Poulet and Carl C. H. Petersen. Internal brain state regulates membrane potential synchrony in barrel cortex of behaving mice. *Nature*, 454(7206):881–885, 2008.
- [171] Christoph M. Michel and Thomas Koenig. EEG microstates as a tool for studying the temporal dynamics of whole-brain neuronal networks: A review. *NeuroImage*, 180(Pt B):577–593, 2017.
- [172] Dimitri Van De Ville, Juliane Britz, and Christoph M. Michel. EEG microstate sequences in healthy humans at rest reveal scale-free dynamics. *Proceedings of the National Academy of Sciences*, 107(42):18179–18184, 2010.

- [173] D. Lehmann, H. Ozaki, and I. Pal. EEG alpha map series: brain micro-states by space-oriented adaptive segmentation. *Electroencephalography and Clinical Neurophysiology*, 67(3):271–288, 1987.
- [174] L Mazzucato, G La Camera, and A Fontanini. Expectation-induced modulation of metastable activity underlies faster coding of sensory stimuli. *Nature Neuroscience*, 22(5):787–796, 2019.
- [175] Stefano Recanatesi, Ulises Pereira-Obilinovic, Masayoshi Murakami, Zachary Mainen, and Luca Mazzucato. Metastable attractors explain the variable timing of stable behavioral action sequences. *Neuron*, 2021.
- [176] M Abeles, H Bergman, I Gat, I Meilijson, E Seidemann, N Tishby, and E Vaadia. Cortical activity flips among quasi-stationary states. *Proceedings of the National Academy of Sciences*, 92(19):8616–8620, 1995.
- [177] E Seidemann, I Meilijson, M Abeles, H Bergman, and E Vaadia. Simultaneously recorded single units in the frontal cortex go through sequences of discrete and stable states in monkeys performing a delayed localization task. *The Journal of Neuroscience*, 16(2):752–768, 1996.
- [178] Daniel Jercog, Alex Roxin, Peter Barthó, Artur Luczak, Albert Compte, and Jaime de la Rocha. UP-DOWN cortical dynamics reflect state transitions in a bistable network. *eLife*, 6:e22425, 2017.
- [179] Artur Luczak, Peter Barthó, Stephan L. Marguet, György Buzsáki, and Kenneth D. Harris. Sequential structure of neocortical spontaneous activity in vivo. *Proceedings of the National Academy of Sciences*, 104(1):347–352, 2007.
- [180] Ofer Mazor and Gilles Laurent. Transient Dynamics versus Fixed Points in Odor Representations by Locust Antennal Lobe Projection Neurons. *Neuron*, 48(4):661–673, 2005.
- [181] T Sasaki, N Matsuki, and Y Ikegaya. Metastability of Active CA3 Networks. *Journal of Neuroscience*, 27(3):517–528, 2007.
- [182] George A. Mashour, Pieter Roelfsema, Jean-Pierre Changeux, and Stanislas Dehaene. Conscious Processing and the Global Neuronal Workspace Hypothesis. *Neuron*, 105(5):776–798, 2020.
- [183] Stanislas Dehaene and Jean-Pierre Changeux. Ongoing Spontaneous Activity Controls Access to Consciousness: A Neuronal Model for Inattentional Blindness. *PLoS Biology*, 3(5):e141, 2005.
- [184] Andrew E Hudson, Diany Paola Calderon, Donald W Pfaff, and Alex Proekt. Recovery of consciousness is mediated by a network of discrete metastable activity states. *Proceedings of the National Academy of Sciences of the United States of America*, 111(25):9283–9288, 2014.
- [185] D Popa, A T Popescu, and D Pare. Contrasting Activity Profile of Two Distributed Cortical Networks as a Function of Attentional Demands. *Journal of Neuroscience*, 29(4):1191–1201, 2009.

- [186] Marco de Curtis and Massimo Avoli. Initiation, Propagation, and Termination of Partial (Focal) Seizures. *Cold Spring Harbor Perspectives in Medicine*, 5(7):a022368, 2015.
- [187] Laura M. J. Fernandez and Anita Lüthi. Sleep Spindles: Mechanisms and Functions. *Physiological Reviews*, 100(2):805–868, 2020.
- [188] Valeria C. Caruso, Jeff T. Mohl, Christopher Glynn, Jungah Lee, Shawn M. Willett, Azeem Zaman, Akinori F. Ebihara, Rolando Estrada, Winrich A. Freiwald, Surya T. Tokdar, and Jennifer M. Groh. Single neurons may encode simultaneous stimuli by switching between activity patterns. *Nature Communications*, 9(1):2715, 2018.
- [189] Liam Lang, Giancarlo La Camera, and Alfredo Fontanini. Temporal progression along discrete coding states during decision-making in the mouse gustatory cortex. *PLOS Computational Biology*, 19(2):e1010865, 2023.
- [190] Andrew A. Fingelkurs and Alexander A. Fingelkurs. Information flow in the brain: Ordered sequences of metastable states. *Information (Switzerland)*, 8(1):1–9, 2017.
- [191] Federico Cavanna, Martina G. Vilas, Matías Palmucci, and Enzo Tagliazucchi. Dynamic functional connectivity and brain metastability during altered states of consciousness. *NeuroImage*, 180(Pt B):383–395, 2018.
- [192] Jordi Fonollosa, Emre Neftci, and Mikhail Rabinovich. Learning of Chunking Sequences in Cognition and Behavior. *PLOS Computational Biology*, 11(11):e1004592, 2015.
- [193] Gustavo Deco and Morten L. Kringelbach. Metastability and Coherence: Extending the Communication through Coherence Hypothesis Using A Whole-Brain Computational Perspective. *Trends in Neurosciences*, 39(3):125–135, 2016.
- [194] Enzo Olivieri and Maria Eulália Vares. *Large Deviations and Metastability*. Encyclopedia of Mathematics and its Applications. Cambridge University Press, Cambridge, 2005.
- [195] Herbert B. Callen. *Thermodynamics and an Introduction to Thermostatistics*. Wiley, 2 edition, 1991.
- [196] James A. Yorke and Ellen D. Yorke. Metastable chaos: The transition to sustained chaotic behavior in the Lorenz model. *Journal of Statistical Physics*, 21(3):263–277, 1979.
- [197] Rory G. Townsend, Selina S. Solomon, Spencer C. Chen, Alexander N.J. Pietersen, Paul R. Martin, Samuel G. Solomon, and Pulin Gong. Emergence of Complex Wave Patterns in Primate Cerebral Cortex. *The Journal of Neuroscience*, 35(11):4657–4662, 2015.
- [198] Michael Wenzel, Jordan P Hamm, Darcy S Peterka, and Rafael Yuste. Acute Focal Seizures Start As Local Synchronizations of Neuronal Ensembles. *The Journal of Neuroscience*, 39(43):8562–8575, 2019.

- [199] Akira Sakurai, Arianna N. Tamvacakis, and Paul S. Katz. Recruitment of Polysynaptic Connections Underlies Functional Recovery of a Neural Circuit after Lesion. *eNeuro*, 3(4), 2016.
- [200] Misha Rabinovich, Ramon Huerta, and Gilles Laurent. Transient Dynamics for Neural Processing. *Science*, 321(5885):48–50, 2008.
- [201] Peter Ashwin and Marc Timme. When instability makes sense. *Nature*, 436(7047):36–37, 2005.
- [202] Eve Marder and Dirk Bucher. Central pattern generators and the control of rhythmic movements. *Current Biology*, 11(23):R986–R996, 2001.
- [203] A Babloyantz and A Destexhe. Low-dimensional chaos in an instance of epilepsy. *Proceedings of the National Academy of Sciences*, 83(10):3513–3517, 1986.
- [204] Lyle Muller, Giovanni Piantoni, Dominik Koller, Sydney S Cash, Eric Halgren, and Terrence J Sejnowski. Rotating waves during human sleep spindles organize global patterns of activity that repeat precisely through the night. *eLife*, 5:e17267, 2016.
- [205] Ichiro Tsuda. Hypotheses on the functional roles of chaotic transitory dynamics. *Chaos: An Interdisciplinary Journal of Nonlinear Science*, 19(1):015113, 2009.
- [206] Friston and J. Karl. Transients, metastability, and neuronal dynamics. *NeuroImage*, 5(2):164–171, 1997.
- [207] K J Friston. The labile brain. II. Transients, complexity and selection. *Philosophical Transactions of the Royal Society of London. Series B, Biological Sciences*, 355(1394):237–252, 2000.
- [208] James A Roberts, Leonardo L Gollo, Romesh G Abeysuriya, Gloria Roberts, Philip B Mitchell, Mark W Woolrich, and Michael Breakspear. Metastable brain waves. *Nature Communications*, 10(1):1056, 2019.
- [209] Gustavo Deco, Morten L. Kringelbach, Viktor K. Jirsa, and Petra Ritter. The dynamics of resting fluctuations in the brain: Metastability and its dynamical cortical core. *Scientific Reports*, 7(1):3095, 2017.
- [210] Miguel Aguilera, Manuel G. Bedia, and Xabier E. Barandiaran. Extended neural metastability in an embodied model of sensorimotor coupling. *Frontiers in Systems Neuroscience*, 10(SEP):76, 2016.
- [211] Luca Mazzucato, Alfredo Fontanini, and Giancarlo La Camera. Dynamics of multi-stable states during ongoing and evoked cortical activity. *Journal of Neuroscience*, 35(21):8214–8231, 2015.
- [212] Valentin S. Afraimovich, Mehmet K. Muezzinoglu, and Mikhail I. Rabinovich. Long-range Interactions, Stochasticity and Fractional Dynamics, Dedicated to George M. Zaslavsky (1935–2008). *Nonlinear Physical Science*, pages 133–175, 2010.

- [213] Thomas H. Alderson, Arun L. W. Bokde, J. A. Scott Kelso, Liam Maguire, and Damien Coyle. Metastable neural dynamics underlies cognitive performance across multiple behavioural paradigms. *Human Brain Mapping*, 41(12):3212–3234, 2020.
- [214] Won Hee Lee and Sophia Frangou. Linking functional connectivity and dynamic properties of resting-state networks. *Scientific Reports*, 7(1):16610, 2017.
- [215] František Váša, Murray Shanahan, Peter J. Hellyer, Gregory Scott, Joana Cabral, and Robert Leech. Effects of lesions on synchrony and metastability in cortical networks. *NeuroImage*, 118:456–467, 2015.
- [216] Peter J. Hellyer, Murray Shanahan, Gregory Scott, Richard J.S. Wise, David J. Sharp, and Robert Leech. The control of global brain dynamics: Opposing actions of frontoparietal control and default mode networks on attention. *Journal of Neuroscience*, 34(2):451–461, 2014.
- [217] Shruti Naik, Arpan Banerjee, Raju S. Bapi, Gustavo Deco, and Dipanjan Roy. Metastability in Senescence. *Trends in Cognitive Sciences*, 21(7):509–521, 2017. Publisher: Elsevier Current Trends.
- [218] Mikhail I. Rabinovich, Ramón Huerta, Pablo Varona, and Valentin S. Afraimovich. Transient cognitive dynamics, metastability, and decision making. *PLoS Computational Biology*, 4(5):1000072, 2008.
- [219] Gerhard Werner. Metastability, criticality and phase transitions in brain and its models. *BioSystems*, 90(2):496–508, 2007.
- [220] David Bhowmik and Murray Shanahan. Metastability and Inter-Band Frequency Modulation in Networks of Oscillating Spiking Neuron Populations. *PLoS ONE*, 8(4):e62234, 2013.
- [221] Hudson and E. Andrew. Metastability of neuronal dynamics during general anesthesia: Time for a change in our assumptions? *Frontiers in Neural Circuits*, 11:58, 2017.
- [222] Tommaso Gili, Valentina Ciullo, and Gianfranco Spalletta. Metastable States of Multiscale Brain Networks Are Keys to Crack the Timing Problem. *Frontiers in Computational Neuroscience*, 12:75, 2018.
- [223] Andrew A. Fingelkurts and Alexander A. Fingelkurts. Operational architectonics of the human brain biopotential field: Towards solving the mind-brain problem. *Brain and Mind*, 2(3):261–296, 2001. ISSN: 13891987 Publication Title: Brain and Mind.
- [224] Emmanuelle Tognoli and J. A. Scott Kelso. Enlarging the scope: grasping brain complexity. *Frontiers in Systems Neuroscience*, 8:122, 2014.
- [225] Steven L Bressler and J A Scott Kelso. Coordination dynamics in cognitive neuroscience. *Frontiers in Neuroscience*, 10:397, 2016.
- [226] Kelso and J. A. Scott. Multistability and metastability: Understanding dynamic coordination in the brain. *Philosophical Transactions of the Royal Society B: Biological Sciences*, 367(1591):906–918, 2012.

- [227] Peter J. Hellyer, Gregory Scott, Murray Shanahan, David J. Sharp, and Robert Leech. Cognitive Flexibility through Metastable Neural Dynamics Is Disrupted by Damage to the Structural Connectome. *The Journal of Neuroscience*, 35(24):9050–9063, 2015.
- [228] Andrew A Fingelkarts and Alexander A Fingelkarts. Brain-Mind Operational Architectonics Imaging: Technical and Methodological Aspects. *The Open Neuroimaging Journal*, 2:73–93, 2008.
- [229] Edward Ott. *Chaos in Dynamical Systems*. Cambridge University Press, Cambridge, U.K, 2nd edition edition, 2022.
- [230] Mikail Khona and Ila R. Fiete. Attractor and integrator networks in the brain. *Nature Reviews Neuroscience*, 23(12):744–766, 2022.
- [231] Peter Hänggi, Peter Talkner, and Michal Borkovec. Reaction-rate theory: fifty years after Kramers. *Reviews of Modern Physics*, 62(2):251–341, 1990.
- [232] F. T. Arecchi, R. Badii, and A. Politi. Generalized multistability and noise-induced jumps in a nonlinear dynamical system. *Physical Review A*, 32(1):402–408, 1985.
- [233] Suso Kraut, Ulrike Feudel, and Celso Grebogi. Preference of attractors in noisy multistable systems. *Physical Review E*, 59(5):5253–5260, 1999.
- [234] Suso Kraut and Ulrike Feudel. Multistability, noise, and attractor hopping: The crucial role of chaotic saddles. *Physical Review E*, 66(1):015207, 2002.
- [235] Suso Kraut and Ulrike Feudel. Enhancement of noise-induced escape through the existence of a chaotic saddle. *Physical Review E*, 67(1):4, 2003.
- [236] Gary Froyland and Michael Dellnitz. Detecting and Locating Near-Optimal Almost-Invariant Sets and Cycles. *SIAM Journal on Scientific Computing*, 24(6):1839–1863, 2003.
- [237] Gary Froyland and Kathrin Padberg. Almost-invariant sets and invariant manifolds — Connecting probabilistic and geometric descriptions of coherent structures in flows. *Physica D: Nonlinear Phenomena*, 238(16):1507–1523, 2009.
- [238] Gary Froyland and Oliver Junge. Robust FEM-Based Extraction of Finite-Time Coherent Sets Using Scattered, Sparse, and Incomplete Trajectories. *SIAM Journal on Applied Dynamical Systems*, 17(2):1891–1924, 2018.
- [239] Kunihiko Kaneko and Ichiro Tsuda. Chaotic itinerancy. *Chaos*, 13(3):926, 2003.
- [240] Peter Hanggi. Escape from a metastable state. *Journal of Statistical Physics*, 42(1-2):105–148, 1986.
- [241] Peter Ashwin, Ozkan Karabacak, and Thomas Nowotny. Criteria for robustness of heteroclinic cycles in neural microcircuits. *The Journal of Mathematical Neuroscience*, 1(1):13, 2011.
- [242] Thomas Nowotny and Mikhail I Rabinovich. Dynamical Origin of Independent Spiking and Bursting Activity in Neural Microcircuits. *Physical Review Letters*, 98(12):128106, 2007.

- [243] M. Rabinovich, A. Volkovskii, P. Lecanda, R. Huerta, H. D. I. Abarbanel, and G. Laurent. Dynamical Encoding by Networks of Competing Neuron Groups: Winnerless Competition. *Physical Review Letters*, 87(6):068102, 2001.
- [244] Mikhail I Rabinovich, Valentin S Afraimovich, Christian Bick, and Pablo Varona. Information flow dynamics in the brain. *Physics of life reviews*, 9(1):51–73, 2012.
- [245] Mikhail I. Rabinovich, Pablo Varona, Irma Tristan, and Valentin S. Afraimovich. Chunking dynamics: heteroclinics in mind. *Frontiers in Computational Neuroscience*, 8:22, 2014.
- [246] Hildegard Meyer-Ortmanns. Heteroclinic networks for brain dynamics. *Frontiers in Network Physiology*, 3:1276401, 2023.
- [247] Celso Grebogi, Edward Ott, Filipe Romeiras, and James A. Yorke. Critical exponents for crisis-induced intermittency. *Physical Review A*, 36(11):5365–5380, 1987.
- [248] B. R. R. Boaretto, R. C. Budzinski, K. L. Rossi, T. L. Prado, S. R. Lopes, and C. Masoller. Discriminating chaotic and stochastic time series using permutation entropy and artificial neural networks. *Scientific Reports*, 11(1):15789, 2021.
- [249] Celso Grebogi, Edward Ott, and James A. Yorke. Crises, sudden changes in chaotic attractors, and transient chaos. *Physica D: Nonlinear Phenomena*, 7(1-3):181–200, 1983.
- [250] P. Manneville and Y. Pomeau. Intermittency and the Lorenz model. *Physics Letters A*, 75(1-2):1–2, 1979.
- [251] Yves Pomeau and Paul Manneville. Intermittent transition to turbulence in dissipative dynamical systems. *Communications in Mathematical Physics*, 74(2):189–197, 1980.
- [252] Everton S. Medeiros, Iberê L. Caldas, Murilo S. Baptista, and Ulrike Feudel. Trapping Phenomenon Attenuates the Consequences of Tipping Points for Limit Cycles. *Scientific Reports*, 7(1):42351, 2017.
- [253] Daniel Koch, Akhilesh Nandan, Gayathri Ramesan, and Aneta Koseska. Beyond fixed points: transient quasi-stable dynamics emerging from ghost channels and ghost cycles. *arXiv*, 2023.
- [254] David Sussillo and Omri Barak. Opening the Black Box: Low-Dimensional Dynamics in High-Dimensional Recurrent Neural Networks. *Neural Computation*, 25(3):626–649, 2013.
- [255] J. A. S. Kelso and G. C. DeGuzman. An Intermittency Mechanism for Coherent and Flexible Brain and Behavioral Function. In *Tutorials in Motor Neuroscience*, pages 305–310. Springer Netherlands, 1991.
- [256] Ying-Cheng Lai and Tamás Tél. *Transient Chaos: Complex Dynamics on Finite-TIME Scales*. Applied Mathematical Sciences. Springer New York, NY, 2009.

- [257] Keegan Keplinger and Renate Wackerbauer. Transient spatiotemporal chaos in the Morris-Lecar neuronal ring network. *Chaos: An Interdisciplinary Journal of Nonlinear Science*, 24(1):013126, 2014.
- [258] Jacopo Lafranceschina and Renate Wackerbauer. Impact of weak excitatory synapses on chaotic transients in a diffusively coupled Morris-Lecar neuronal network. *Chaos: An Interdisciplinary Journal of Nonlinear Science*, 25(1):013119, 2015.
- [259] Harrison Hartle and Renate Wackerbauer. Transient chaos and associated system-intrinsic switching of spacetime patterns in two synaptically coupled layers of Morris-Lecar neurons. *Physical Review E*, 96(3):032223, 2017.
- [260] Vitaliy Kaminker and Renate Wackerbauer. Alternating activity patterns and a chimeralike state in a network of globally coupled excitable Morris-Lecar neurons. *Chaos: An Interdisciplinary Journal of Nonlinear Science*, 29(5):053121, 2019.
- [261] Peter Ashwin, Jorge Buescu, and Ian Stewart. Bubbling of attractors and synchronisation of chaotic oscillators. *Physics Letters A*, 193(2):126–139, 1994.
- [262] Edward Ott and John C. Sommerer. Blowout bifurcations: the occurrence of riddled basins and on-off intermittency. *Physics Letters A*, 188(1):39–47, 1994.
- [263] N Platt, E A Spiegel, and C Tresser. On-off intermittency: A mechanism for bursting. *Physical Review Letters*, 70(3):279–282, 1993.
- [264] J. F. Heagy, N. Platt, and S. M. Hammel. Characterization of on-off intermittency. *Physical Review E*, 49(2):1140–1150, 1994.
- [265] P W Hammer, N Platt, S M Hammel, J F Heagy, and B D Lee. Experimental observation of on-off intermittency. *Physical Review Letters*, 73(8):1095–1098, 1994.
- [266] A. Čenys, A. N. Anagnostopoulos, and G. L. Bleris. Symmetry between laminar and burst phases for on-off intermittency. *Physical Review E*, 56(3):2592–2596, 1997.
- [267] Alexander Hramov, Alexey A. Koronovskii, I. S. Midyanovskaya, E. Sitnikova, and C. M. van Rijn. On-off intermittency in time series of spontaneous paroxysmal activity in rats with genetic absence epilepsy. *Chaos: An Interdisciplinary Journal of Nonlinear Science*, 16(4):043111, 2006.
- [268] Peter Ashwin, Eurico Covas, and Reza Tavakol. Transverse instability for non-normal parameters. *Nonlinearity*, 12(3):563–577, 1999.
- [269] Peter Ashwin, Eurico Covas, and Reza Tavakol. Influence of noise on scalings for in-out intermittency. *Physical Review E*, 64(6):066204, 2001.
- [270] Arindam Saha and Ulrike Feudel. Characteristics of in-out intermittency in delay-coupled FitzHugh-Nagumo oscillators. *The European Physical Journal Special Topics*, 227(10-11):1205–1219, 2018.
- [271] Arindam Saha and Ulrike Feudel. Extreme events in FitzHugh-Nagumo oscillators coupled with two time delays. *Physical Review E*, 95(6):062219, 2017.

- [272] J. L. Perez Velazquez, Houman Khosravani, Andres Lozano, Berj. L. Bardakjian, Peter L. Carlen, and Richard Wennberg. Type III intermittency in human partial epilepsy. *European Journal of Neuroscience*, 11(7):2571–2576, 1999.
- [273] Mathieu Desroches, John Guckenheimer, Bernd Krauskopf, Christian Kuehn, Hinke M. Osinga, and Martin Wechselberger. Mixed-Mode Oscillations with Multiple Time Scales. *SIAM Review*, 54(2):211–288, 2012.
- [274] Horacio G. Rotstein. Mixed-Mode Oscillations in Single Neurons. In Jaeger Dieter and Jung Ranu, editors, *Encyclopedia of Computational Neuroscience*, Encyclopedia of Computational Neuroscience, pages 1–9. Springer New York, NY, 2014.
- [275] David M Fox, Horacio G Rotstein, and Farzan Nadim. Bursting in neurons and small networks. In Dieter Jaeger and Ranu Jung, editors, *Encyclopedia of computational neuroscience*, pages 455–469. Springer New York, New York, NY, 2015.
- [276] H A Swadlow and A G Gusev. The impact of 'bursting' thalamic impulses at a neocortical synapse. *Nature Neuroscience*, 4(4):402–408, 2001.
- [277] J. L. Hindmarsh and R. M. Rose. A model of neuronal bursting using three coupled first order differential equations. *Proceedings of the Royal Society of London. Series B. Biological Sciences*, 221(1222):87–102, 1984.
- [278] Rajat Karnatak, Gerrit Ansmann, Ulrike Feudel, and Klaus Lehnertz. Route to extreme events in excitable systems. *Physical Review E*, 90(2):022917, 2014.
- [279] John M Beggs and Dietmar Plenz. Neuronal avalanches in neocortical circuits. *Journal of neuroscience*, 23(35):11167–11177, 2003.
- [280] Mauricio Girardi-Schappo. Brain criticality beyond avalanches: open problems and how to approach them. *Journal of Physics: Complexity*, 2(3):031003, 2021.
- [281] Freeman and J. Walter. Evidence from human scalp electroencephalograms of global chaotic itinerancy. *Chaos: An Interdisciplinary Journal of Nonlinear Science*, 13(3):1067–1077, 2003.
- [282] Ichiro Tsuda. Chaotic itinerancy and its roles in cognitive neurodynamics. *Current Opinion in Neurobiology*, 31:67–71, 2015.
- [283] Junji Ito, Andrey R. Nikolaev, and Cees van Leeuwen. Dynamics of spontaneous transitions between global brain states. *Human Brain Mapping*, 28(9):904–913, 2007.
- [284] Levin Kuhlmann, Klaus Lehnertz, Mark P. Richardson, Björn Schelter, and Hitzen P. Zaveri. Seizure prediction — ready for a new era. *Nature Reviews Neurology*, 14(10):618–630, 2018.
- [285] Thorsten Rings, Mahmood Mazarei, Amin Akhshi, Christian Geier, M. Reza Rahimi Tabar, and Klaus Lehnertz. Traceability and dynamical resistance of precursor of extreme events. *Scientific Reports*, 9(1):1744, 2019.
- [286] Henning U. Voss, Jens Timmer, and Jürgen Kurths. Nonlinear dynamical system identification from uncertain and indirect measurements. *International Journal of Bifurcation and Chaos*, 14(06):1905–1933, 2004.

- [287] Steven L. Brunton, Joshua L. Proctor, and J. Nathan Kutz. Discovering governing equations from data by sparse identification of nonlinear dynamical systems. *Proceedings of the National Academy of Sciences*, 113(15):3932–3937, 2016.
- [288] M. Reza Rahini Tabar. *Analysis and Data-Based Reconstruction of Complex Nonlinear Dynamical Systems, Using the Methods of Stochastic Processes*. Understanding Complex Systems. Springer Cham, 2019.
- [289] Mehrnaz Anvari, M. Reza Rahimi Tabar, Joachim Peinke, and Klaus Lehnertz. Disentangling the stochastic behavior of complex time series. *Scientific Reports*, 6(1):35435, 2016.
- [290] Mozes Jacobs, Bingni W Brunton, Steven L Brunton, J Nathan Kutz, and Ryan V Raut. HyperSINDy: Deep Generative Modeling of Nonlinear Stochastic Governing Equations. *arXiv*, 2023.
- [291] Wang and Xiao-Jing. 50 years of mnemonic persistent activity: quo vadis? *Trends in Neurosciences*, 44(11):888–902, 2021.
- [292] Rodrigo Laje and Dean V Buonomano. Robust timing and motor patterns by taming chaos in recurrent neural networks. *Nature Neuroscience*, 16(7):925–933, 2013.
- [293] Akhilesh Nandan and Aneta Koseska. Non-asymptotic transients away from steady states determine cellular responsiveness to dynamic spatial-temporal signals. *PLOS Computational Biology*, 19(8):e1011388, 2023.
- [294] Dean V. Buonomano and Wolfgang Maass. State-dependent computations: spatiotemporal processing in cortical networks. *Nature Reviews Neuroscience*, 10(2):113–125, 2009.
- [295] Gabriel B. Benigno, Roberto C. Budzinski, Zachary W. Davis, John H. Reynolds, and Lyle Muller. Waves traveling over a map of visual space can ignite short-term predictions of sensory input. *Nature Communications*, 14(1):3409, 2023.
- [296] Roberto C Budzinski, Alexandra N Busch, Samuel Mestern, Erwan Martin, Luisa H B Liboni, Federico W Pasini, Ján Mináč, Todd Coleman, Wataru Inoue, and Lyle E Muller. An exact mathematical description of computation with transient spatiotemporal dynamics in a complex-valued neural network. *arXiv*, 2023.
- [297] Luisa H B Liboni, Roberto C Budzinski, Alexandra N Busch, Sindy Löwe, Thomas A Keller, Max Welling, and Lyle E Muller. Image segmentation with traveling waves in an exactly solvable recurrent neural network. *arXiv*, 2023.
- [298] K. L. Rossi. Repository for metastability. *GitHub repository*, 2023. <https://github.com/ComplexNetworks-jl/MetastableDynamics>.
- [299] Hiroaki Ishii, Hirokazu Fujisaka, and Masayoshi Inoue. Breakdown of chaos symmetry and intermittency in the double-well potential system. *Physics Letters A*, 116(6):257–263, 1986.
- [300] Lorenz and N. Edward. Deterministic Nonperiodic Flow. *Journal of the Atmospheric Sciences*, 20(2):130–141, 1963.

- [301] Kathleen T. Alligood, Tim D. Sauer, and James A. Yorke. *Chaos: An Introduction to Dynamical Systems*. Textbooks in Mathematical Sciences. Springer Berlin Heidelberg, Berlin, Heidelberg, 1996.
- [302] Steven Strogatz. *Sync: The Emerging Science of Spontaneous Order*. Hyperion Press, 2003.
- [303] Peter J. Menck, Jobst Heitzig, Norbert Marwan, and Jürgen Kurths. How basin stability complements the linear-stability paradigm. *Nature Physics*, 9(2):89–92, 2013.
- [304] Hana Krakovská, Christian Kuehn, and Iacopo P Longo. Resilience of dynamical systems. *European Journal of Applied Mathematics*, pages 1–46, 2023.
- [305] Alan Hastings, Karen C. Abbott, Kim Cuddington, Tessa Francis, Gabriel Gellner, Ying-Cheng Lai, Andrew Morozov, Sergei Petrovskii, Katherine Scranton, and Mary Lou Zeeman. Transient phenomena in ecology. *Science*, 361(6406), 2018.
- [306] A. M. Turing. On Computable Numbers, with an Application to the Entscheidungsproblem. *Proceedings of the London Mathematical Society*, s2-42(1):230–265, 1937.
- [307] George S. Boolos, John P. Burgess, and Richard C. Jeffrey. *Computability and Logic*. Cambridge University Press, 5 edition, 2007.
- [308] Claire M. Postlethwaite, Peter Ashwin, and Matthew Egbert. A Continuous Time Dynamical Turing Machine. *IEEE Transactions on Neural Networks and Learning Systems*, PP(99):1–13, 2024.
- [309] Saurabh Vyas, Matthew D. Golub, David Sussillo, and Krishna V. Shenoy. Computation Through Neural Population Dynamics. *Annual Review of Neuroscience*, 43(1):249–275, 2020.
- [310] Peter Ashwin and Claire Postlethwaite. Excitable networks for finite state computation with continuous time recurrent neural networks. *Biological Cybernetics*, 115(5):519–538, 2021.
- [311] Peter Ashwin, Muhammed Fadera, and Claire Postlethwaite. Network attractors and nonlinear dynamics of neural computation. *Current Opinion in Neurobiology*, 84:102818, 2024.

Acknowledgments

Doing a PhD is not trivial (no citation needed here, I think). It is made possible not just from one's own hard work, but with help and support from many others.

To start, the PhD was possible due to financial support from the German Academic Exchange Foundation (DAAD, in german). I am very thankful for the opportunity to do all this work with their warm support. In this sense, I am also grateful to the University of Oldenburg for the structures provided that allowed me to work.

Moving from the material to the intellectual and personal support, I am extremely grateful to Prof. Ulrike Feudel, my supervisor for all of these years! We had a lot of fun, and I learned so much from her. On top of the specific knowledge of the area, I think maybe the most important skill she developed on me was the ability to refine a thought and rigorously develop an idea until you are confident about it. On top of all the actual science we made, I find it amazing how many conferences I had the opportunity to participate in, and how many people I met - a lot of this I owe to Ulrike's support. In a similar vein I also want to deeply thank my friend and collaborator, Prof. (yes, Prof!) Everton Medeiros. Maybe without even noticing, he also taught me so much. He was a crucial aid in making this whole process a lot more fun and exciting - with, of course, better science. I will always remember this fondly - as will I remember his legendary goal from the corner of the pitch in Spiekeroog. Football's loss is academia's gain. Finally, since my Bachelor's I've always been able to count on my friends and collaborators Roberto Budzinski and Bruno Boaretto. I've counted on them for endless scientific discussions, arguments about how something should be written on a paper, and motivation. All of this always with a really nice and fun atmosphere.

Moving more to the emotional (and personal still) support, I am above all thankful to my mom and my sister for just about everything. Moving abroad is not easy - for anyone involved - but their unwavering love, warmth, and understanding made it all happen! This extends to my whole family, in fact.

Friends are also a crucial ingredient to a nice life. And in this I also have had the luck to count on some amazing figures. I will only name some - their egos will have to be satisfied. In no particular order I want to thank from the bottom of my heart Jakob and Bianca Weik, Maira Theisen, Gabriel Gubert, Lucas Pollyceno, Carlos Martins, Alexandre Camargo, Rafa Jakuboski, Joao Paludo, Marcos Sato, George Datseris, Bryony Hobden, Patryk Bielski, Luis Gustavo, and Deoclecio Valente - and many others I equally love but, come on, the list is already too big.

Finally, I mentioned I met a lot of amazing people doing science, some of whom I already mentioned. For all the discussions, support, and fun, I want to especially thank Klaus Lehnertz, Lyle Muller, Peter Ashwin, Aneta Koseska, Vyacheslav Kruglov, Ryan Deeley, Jordan Gault, and Jan Freund.

Eidesstattliche Erklärung

Hiermit versichere ich, dass ich diese Dissertation selbstständig verfasst habe und nur die hier angegebenen Hilfsmittel und Quellen benutzt habe. Zudem versichere ich, dass diese Dissertation weder in ihrer Gesamtheit noch in Teilen einer anderen Hochschule zur Begutachtung in einem Promotionsverfahren vorliegt oder vorgelegen hat. Bis auf die angegebenen Teilpublikationen, ist diese Arbeit noch nicht veröffentlicht worden. Die Leitlinien guter wissenschaftlicher Praxis an der Carl von Ossietzky Universität Oldenburg wurden befolgt. Für dieses Promotionsvorhaben wurden keine kommerziellen Vermittlungs- oder Beratungsdienste in Anspruch genommen.



Oldenburg, den 05.11.2024
Kalel Luiz Rossi